Quantification of microtubule stutters: dynamic instability behaviors that are strongly associated with catastrophe

Shant M. Mahserejian[a,b,†,*], Jared P. Scripture[c,†], Ava J. Mauro[c,d,*], Elizabeth J. Lawrence[e], Erin M. Jonasson[c,f], Kristopher S. Murray[c], Jun Li[a], Melissa Gardner[g], Mark Alber[a,h], Marija Zanic[e,i,j], and Holly V. Goodson[c,*]

[a]Department of Applied and Computational Mathematics and Statistics and [c]Department of Chemistry and Biochemistry, University of Notre Dame, Notre Dame, IN 46556; [b]Pacific Northwest National Laboratory, Richland, WA 99352; [d]Department of Mathematics and Statistics, University of Massachusetts Amherst, Amherst, MA 01003; [e]Department of Cell and Developmental Biology, Vanderbilt University, Nashville, TN 37240; [f]Department of Natural Sciences, Saint Martin's University, Lacey, WA 98503; [g]Department of Genetics, Cell Biology, and Development, University of Minnesota, Minneapolis, MN 55455; [h]Department of Mathematics, University of California, Riverside, Riverside, CA 92521; [i]Department of Chemical and Biomolecular Engineering, Vanderbilt University, Nashville, TN 37235; [j]Department of Biochemistry, Vanderbilt University, Nashville, TN 37205

ABSTRACT **Microtubules (MTs) are cytoskeletal fibers that undergo dynamic instability (DI), a remarkable process involving phases of growth and shortening separated by stochastic transitions called catastrophe and rescue. Dissecting DI mechanism(s) requires first characterizing and quantifying these dynamics, a subjective process that often ignores complexity in MT behavior. We present a Statistical Tool for Automated Dynamic Instability Analysis (STADIA) that identifies and quantifies not only growth and shortening, but also a category of intermediate behaviors that we term "stutters." During stutters, the rate of MT length change tends to be smaller in magnitude than during typical growth or shortening phases. Quantifying stutters and other behaviors with STADIA demonstrates that stutters precede most catastrophes in our in vitro experiments and dimer-scale MT simulations, suggesting that stutters are mechanistically involved in catastrophes. Related to this idea, we show that the anticatastrophe factor CLASP2γ works by promoting the return of stuttering MTs to growth. STADIA enables more comprehensive and data-driven analysis of MT dynamics compared with previous methods. The treatment of stutters as distinct and quantifiable DI behaviors provides new opportunities for analyzing mechanisms of MT dynamics and their regulation by binding proteins.**

Monitoring Editor
Claire Walczak
Indiana University

Received: Jun 2, 2020
Revised: Nov 1, 2021
Accepted: Jan 5, 2022

This article was published online ahead of print in MBoC in Press (http://www.molbiolcell.org/cgi/doi/10.1091/mbc.E20-06-0348) on February 2, 2022.

*Address correspondence to: Shant M. Mahserejian (shant.mahserejian@pnnl.gov), Ava J. Mauro (avamauro@bu.edu), Holly V. Goodson (hgoodson@nd.edu).
†Co–first authors.

Abbreviations used: DI, dynamic instability; fps, frames per second; GDP, guanosine diphosphate; GTP, guanosine triphosphate; k, number of clusters; MT, microtubule; MTBP, microtubule binding protein; PF, protofilament; STADIA, Statistical Tool for Automated Dynamic Instability Analysis; TIRF, total internal reflection fluorescence.

1. INTRODUCTION

Microtubules (MTs) are protein-based biological polymers that have a central role in fundamental eukaryotic processes including cellular organization, chromosome separation during cell division, and intracellular transport (Goodson and Jonasson, 2018). Crucial to the function of MTs in these processes is a well-known behavior termed dynamic instability (DI), where the polymers switch stochastically between periods of growth and shortening as seen in traditional MT length-history plots (Figure 1, A and B) (Mitchison and Kirschner, 1984; Desai and Mitchison, 1997). Accurate quantification of MT DI behavior is essential for understanding its significance and mechanism and also for investigating the activities of DI-regulating proteins and pharmaceutical agents (e.g., chemotherapy drugs, fungicides).

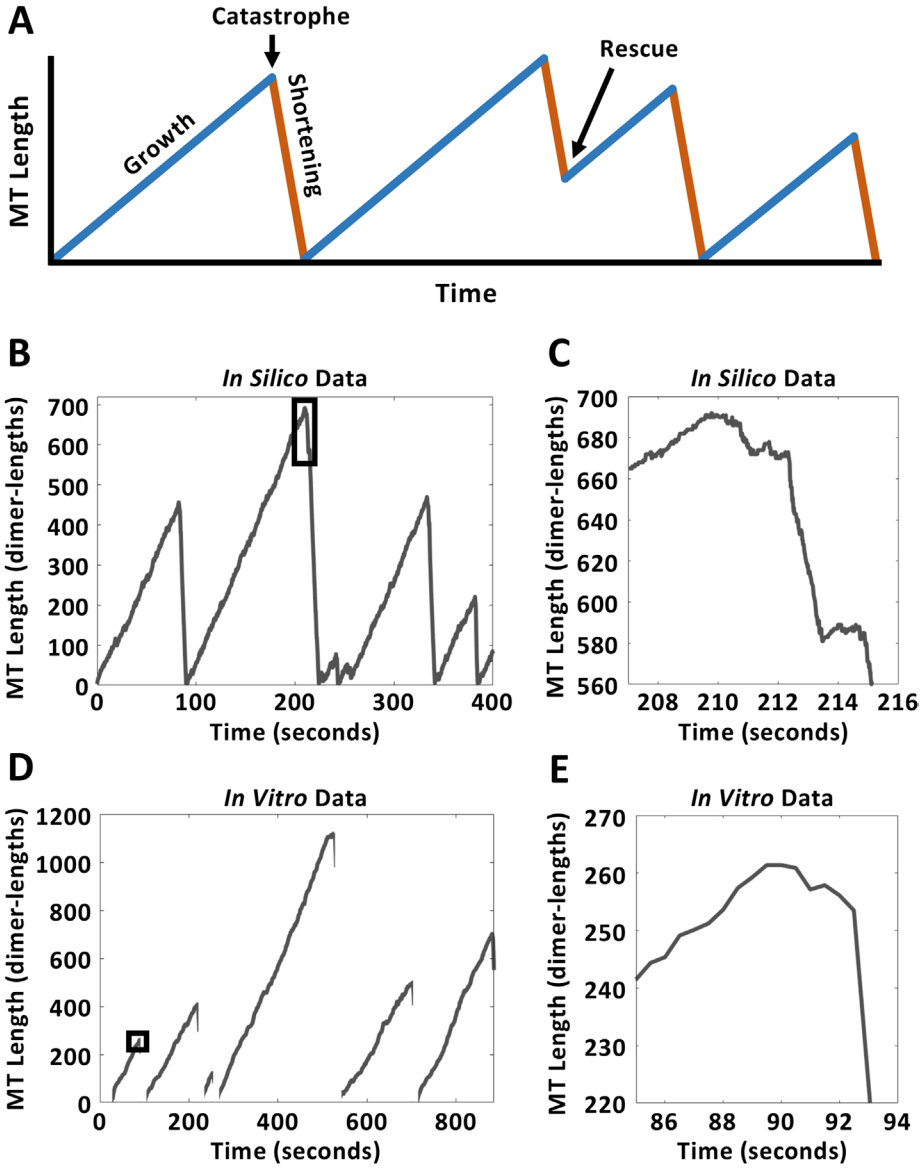

FIGURE 1: Qualitative examples of MT behaviors that do not fit the two-state (growth-shortening) framework. (A) An illustration of the classically recognized two-state representation of dynamic instability (DI), in which behavior is classified as either growth or shortening phases, with instantaneous transitions known as catastrophe and rescue events. (B, D) Zoomed-out length-history plots of simulation data (B, dimer-scale 13-protofilament model, temporal resolution of ~1650 dimer-scale events per second per MT, *Materials and Methods* Section 5.2) and experimental data (D, temporal resolution of 2 frames per second, note that depolymerizations were not tracked in their entirety in these experiments, *Materials and Methods* Section 5.1). Black rectangles in B and D indicate the zoomed-in portions shown in C and E, respectively. (C, E) Closer inspection of transitions shows ambiguous behavior that cannot clearly be categorized as either growth or shortening.

1.1. Traditional DI measurements

Traditionally, MTs have been treated as two-state polymers; that is, MTs have been considered to be either growing or shortening, with abrupt, instantaneous transitions called catastrophes and rescues between these two phases (Figure 1, A, B, and D). In this framework, MT behavior is characterized by four quantities called DI parameters (Walker *et al.*, 1988):

- V_{growth}—velocity of growth, commonly measured as the mean of the growth rates as averaged over the set of growth phases
- V_{short}—velocity of shortening, commonly measured as the mean of the shortening rates as averaged over the set of shortening phases
- F_{cat}—frequency of catastrophe, commonly measured as the number of catastrophes (transitions from growth to shortening) per time in growth
- F_{res}—frequency of rescue, commonly measured as the number of rescues (transitions from shortening to growth) per time in shortening

The specific procedures for measuring these DI parameters have varied among research groups, but methods typically begin with the user specifying the minimal values (i.e., thresholds) of length change, time duration, and/or velocity required for recognizing phases of growth and shortening; sometimes pauses are also allowed, as discussed more below in Section 1.2. Then the length-history plot is partitioned into growth and shortening segments (Figures 1A and 2, A and B). The endpoints of the segments are assumed to correspond to the events of catastrophe and rescue, and the slopes of the segments provide the growth or shortening velocities. In other words, the velocity of an individual growth or shortening phase is typically determined as the slope of a line drawn between the points of catastrophe and rescue (e.g., Zanic, 2016).

1.2. Limitations of common methods for quantifying dynamic instability

While determination of DI parameters as described above is a standard way to quantify MT behavior (see, e.g., Portran *et al.*, 2017; Zwetsloot *et al.*, 2018; Kapoor *et al.*, 2019, for recent examples), there are aspects of MT behavior that are not captured using this approach. First, it has long been recognized that both growth and shortening rates are variable. This variability occurs both with and without MT binding proteins (MTBPs), and it is observed both within and between individual growth phases and similarly for shortening phases (e.g., Gildersleeve *et al.*, 1992; Pedigo and Williams, 2002; Schek *et al.*, 2007; Lawrence *et al.*, 2018). Spectral analysis of such variability in growth and shortening rates has suggested that the two-state (growth and shortening) model approximation agrees well with experimentally observed MT behavior when frequencies in the length-history data are analyzed at timescales longer than ~1 min but underestimates the observed variability at timescales shorter than ~1 min (Odde *et al.*, 1996). These observations raise the concern that DI analysis methods that categorize an entire period between nucleation (or rescue) and catastrophe as a single growth or shortening phase could cause functionally significant details of MT behavior to be missed.

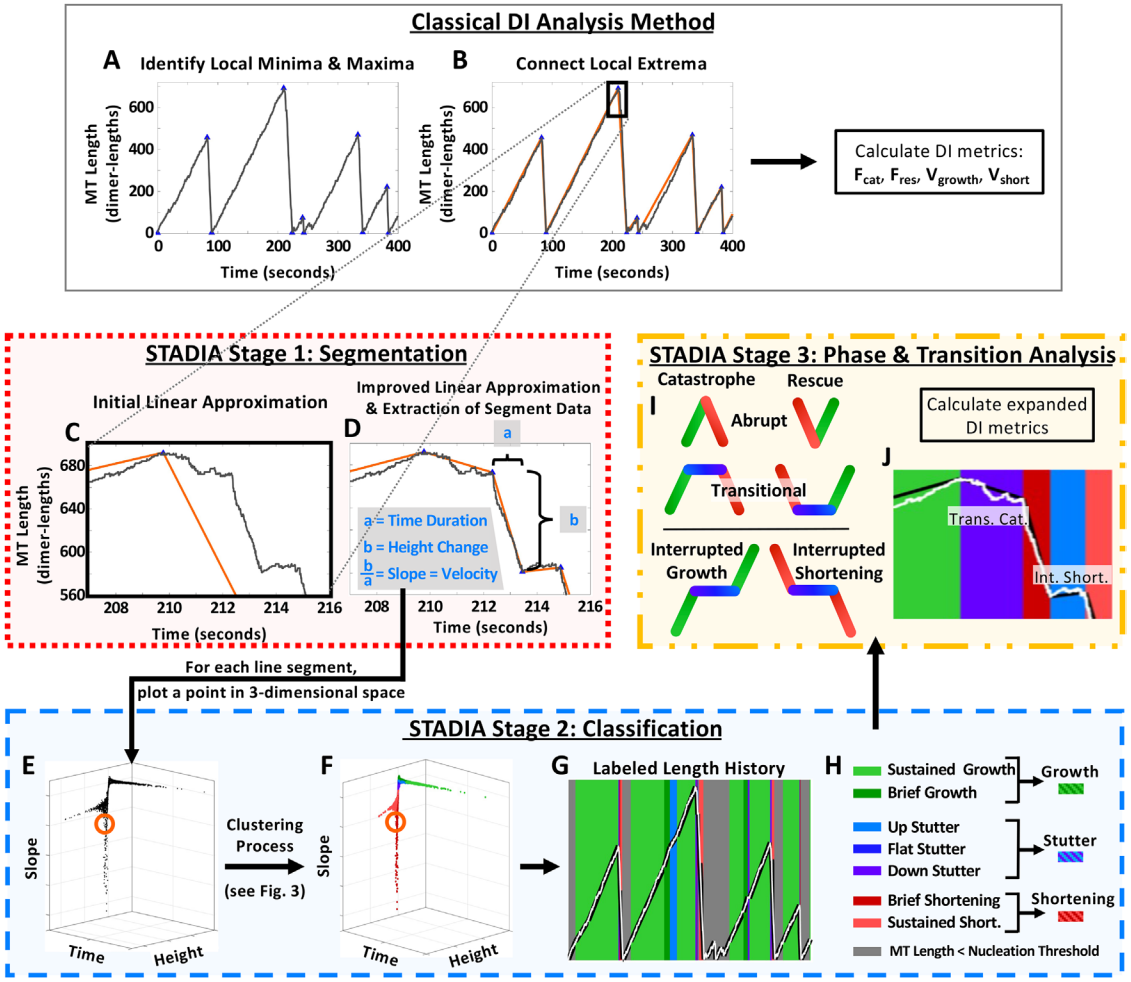

FIGURE 2: Comparison of classical DI analysis method and STADIA. Classical DI analysis method (A, B): Major peaks and valleys (blue triangles) are first identified (A), and these are defined as catastrophes and rescues (or nucleation events), respectively. Each period from a nucleation event or rescue to a catastrophe is defined as a growth phase, and each period from a catastrophe to a complete depolymerization or rescue is defined to be a shortening phase (B). Then, V_{growth} and V_{short} are calculated from the slopes of straight line segments plotted between the transitions (B, orange lines) or alternatively, from regression lines fitted to the data points in each period. F_{cat} and F_{res} are calculated from the number of catastrophes or rescues divided by the total time in growth or shortening, respectively. STADIA (C–J): An initial approximation of inputted length-history data is produced by connecting major peaks and valleys with line segments (C, similar to classical methods). STADIA then iteratively adds segment endpoints to improve the approximation (D, this iterative process is regulated by user-defined parameters Maximum Error Tolerance and Minimum Segment Duration). The time duration, height change, and slope (velocity) of each line segment are measured (D) and visualized as a point in 3-dimensional space (E). The orange circles in (E, F) denote the approximate location of the data point corresponding the example line segment in (D). The line segments are grouped into "clusters" (see Figure 3), as indicated by the colors in the plots (F, G, J; key in left column of H). The clusters are named and grouped into larger behavior classes based on their average features (e.g., average slope) (H). STADIA then identifies multiple types of transitions (I), allowing the calculation of various metrics including (and expanding beyond) the traditional V_{growth}, V_{short}, F_{cat}, and F_{res}. In (G, J), the white lines represent the raw length-history data, and the black lines represent the line segment approximation. Results Section 2.2 contains a more thorough overview of STADIA's analysis procedure, and full details are provided in *Materials and Methods* Sections 5.4–5.6.

Second, pauses, attenuation phases, and other intermediate states have been observed in experiments and proposed in models, but the way these behaviors have been identified and defined has varied. Pauses are commonly observed in vivo (e.g., Sammak and Borisy, 1988; Schulze and Kirschner, 1988; Waterman-Storer and Salmon, 1997; Gierke *et al.*, 2010; Kamath *et al.*, 2010; Applegate *et al.*, 2011). Pauses have also been observed in vitro in the presence of MTBPs (e.g., Moriwaki and Goshima, 2016), cell extracts (e.g., Keller *et al.*, 2008), and drugs (e.g., Toso *et al.*, 1993), and occasionally for purified tubulin (e.g., Walker *et al.*, 1988). Recognition of states other than growth and shortening has led various authors to consider theoretical three- or four-state models in which the additional states are pauses or an intermediate state (Odde *et al.*, 1995; Tran *et al.*, 1997; Jánosi *et al.*, 2002; Maly, 2002; Keller *et al.*, 2008; Smal *et al.*, 2010; Blackwell *et al.*, 2017). Thus, it is clear that many researchers are interested in methods for identifying states beyond growth and shortening in data and the inclusion of such states in the development of theory. However,

there is not a general consensus on how these states should be defined.

In particular, as noted in Section 1.1, identification of growth, shortening, and pause phases in length-history data frequently relies on fixed thresholds for velocity, length change, and/or time duration. For example, it has been common to require a length-change threshold of at least 0.5 microns to recognize a growth or shortening phase, but the exact way in which this threshold was applied to data has varied among research groups (e.g., compare Sammak and Borisy, 1988; Dhamodharan and Wadsworth, 1995; Rusan *et al.*, 2001; Kamath *et al.*, 2010; and Fees *et al.*, 2017). Others have used combinations of thresholds on the speed of length change (e.g., in pixels per frame or microns per minute), length change itself, and/or number of data points involved (e.g., compare Panda *et al.*, 1996; Gierke *et al.*, 2010; Kiris *et al.*, 2010; Matov *et al.*, 2010; Yenjerla *et al.*, 2010; Mahrooghy *et al.*, 2015; and Moriwaki and Goshima, 2016). It is important to be aware that thresholds have differed between analyses, because it is well-established (but perhaps not widely recognized) that thresholds can have dramatic effects on measurements of MT dynamics (e.g., Odde *et al.*,1996; Gierke *et al.*, 2010; Matov *et al.*, 2010; Smal *et al.*, 2010; Prahl *et al.*, 2014; Guo *et al.*, 2018).

Finally, recent improvements in imaging technology have enabled acquisition of MT DI data with both high temporal and high spatial resolution, which allows for the possibility of analyzing length-history data at finer scales (e.g., Maurer *et al.*, 2014; Andrecka *et al.*, 2016; Mickolajczyk *et al.*, 2019). These data have verified the intrinsic variability of MT behavior. They have also demonstrated that both growth and shortening phases can include significant time periods (e.g., a few seconds in duration or longer) during which the growth or shortening velocity slows significantly (Figure 1, C and E; see also Maurer *et al.*, 2014; Duellberg *et al.*, 2016a,b; Rickman *et al.*, 2017). These slowdown periods likely overlap with pauses discussed above, though it is important to note that "bona fide" pauses are often considered to be time periods "during which no polymerization or depolymerization occurs" (Gierke *et al.*, 2010) and so are separable from periods of slowed growth or shortening, at least in principle.

Significantly, these slowdown periods can also occur in association with catastrophe (Maurer *et al.*, 2014; Duellberg *et al.*, 2016a,b; see also predictions based on simulations in Margolin *et al.*, 2012), making it difficult to determine with reasonable precision where transitions between phases begin and end. To illustrate this problem, consider the zoomed-out length-history plots that are typically used for DI analysis (Figure 1, B and D). Examination of these plots can make the task of determining when transitions occur look trivial. However, the zoomed-in views made possible by high-resolution data acquisition (Figure 1, C and E) demonstrate the difficulty of identifying the points of transition and/or categorizing DI behaviors.

Thus, many researchers have recognized that MT DI behavior is more complex than a simple two-state system of growth and shortening with abrupt transitions. The four traditional DI parameters (V_{growth}, V_{short}, F_{cat}, and F_{res}) would be sufficient to quantify such a two-state system but are not sufficient to quantify all aspects of observed MT DI as discussed above. One previous approach to dealing with the existence of slowdown periods has been to exclude them from quantification of DI parameters, because including these slowdown periods in either growth or shortening phases would reduce the magnitude of measured values of V_{growth} and V_{short} (e.g., Rickman *et al.*, 2017). However, entirely excluding these behaviors from analysis could result in the loss of information critical for understanding the mechanisms of phase transitions or their regulation by MTBPs. Furthermore, although previous publications have quantified some aspects of the slowdown periods (e.g., time durations [Maurer *et al.,* 2014]), none of these to our knowledge have presented a set of velocities and transition frequencies that expands beyond the traditional four DI parameters. Capturing and quantifying behaviors in addition to growth and shortening would be a key step toward further dissecting the recognized variations in growth and shortening rates, improving the precision of DI metrics, and elucidating mechanisms of DI.

To study MT dynamics more comprehensively than is possible with standard DI approaches, we developed the Statistical Tool for Automated Dynamic Instability Analysis (STADIA), an automated tool that uses established statistical methods to characterize and quantify MT behavior without prior assumptions about the number or characteristics of the behaviors detected. As shown in the *Results* below, STADIA can be used with both simulation- and experiment-generated data, and it is compatible with a wide range of data acquisition rates.

1.3. Summary of conclusions

Applying STADIA to in silico and in vitro MT length-history data demonstrated the prevalence of a category of intermediate behaviors that we propose calling "stutters." Stutters share similar characteristics with each other and are distinguishable from typical growth and shortening. The primary distinguishing factor is that during stutters the overall rate of change in MT length is markedly smaller in magnitude compared with the velocities of classically recognized growth and shortening phases. Stutters are also distinguishable from pauses in that during true pauses "no polymerization or depolymerization occurs" (Gierke *et al.*, 2010). In contrast, during stutters dimer-scale dynamics continue, and during most stutters measurable length changes do occur although at slower velocities than during typical growth and shortening. Stutters, as recognized and quantified by STADIA, overlap with previously observed behaviors such as precatastrophe slowdowns (e.g., Maurer *et al.,* 2014) and events that have been called "pauses" despite length changes occurring (e.g., Kamath *et al.,* 2010; Matov *et al.,* 2010; Guo *et al.,* 2018). The relationship of our results to previous work is further covered in *Discussion* Section 3.3.

Analysis of length-history data using STADIA leads to two major observations regarding the relationship between stutters and catastrophes:

- Stutters precede most catastrophes in our in vitro control and in silico data sets.
- The MT stabilizing protein CLASP2γ reduces catastrophe in vitro by increasing the fraction of stutters that return to growth rather than entering shortening phases. Specifically, CLASP2γ reduces the frequency of growth-to-stutter-to-shortening (which we term transitional catastrophe) and increases the frequency of growth-to-stutter-to-growth (which we term interrupted growth).

These results indicate that STADIA is able to recognize and quantify behaviors that are missed by classical methods of analyzing MT length-history data. Furthermore, these results suggest that stutters play a mechanistically significant role in the process of catastrophe. We conclude that identification of stutters as distinct from growth, shortening, or pause warrants their future inclusion in DI analyses and serves as a necessary step forward in gaining a better understanding of MTs, their dynamics, and their regulation by MTBPs.

2. RESULTS

For ease of navigation and to allow readers to focus on the information that is most relevant to them, we have divided the Results below into six sections. Section 2.1 introduces the in vitro and in silico data sets used in this work. Section 2.2 provides a general overview of our new tool, STADIA. Sections 2.3, 2.4, and 2.5 present the results of using STADIA to analyze our data sets. More specifically, in Section 2.3, we use STADIA to identify and characterize MT behaviors, including a category of intermediate behaviors that we term "stutters." In Section 2.4, we use STADIA to quantify characteristics of the behaviors identified in Section 2.3. This quantification includes studying the relationship between stutters and phase transitions, which shows that stutters are strongly associated with catastrophe. In Section 2.5, we further test the functional significance of stutters in catastrophe and demonstrate the utility of STADIA in studying MTBPs. More specifically, we use STADIA to analyze the dynamics of in vitro MTs growing in the presence of the anticatastrophe factor CLASP2γ, thus examining for the first time its effect on stutters. In Section 2.6, we test the effects of varying the values of STADIA's input parameters and demonstrate the robustness of the conclusions drawn in Sections 2.3–2.5.

2.1. Data sets used in this work: in vitro and in silico

In the analysis below (Sections 2.3–2.6), we used STADIA to analyze length-history data sourced from both laboratory experiments (in vitro) and computational simulations (in silico). We provide a brief overview of the data sets here, with additional information in *Materials and Methods* Sections 5.1 and 5.2.

We analyzed two in vitro data sets: a control with purified tubulin + EB1 and a treatment data set with purified tubulin + EB1 + CLASP2γ. The data sets were obtained using total internal reflection fluorescence (TIRF) microscopy with images taken at 2 frames per second (fps). A subset of the experimental data used here was previously analyzed using other methods (in Lawrence *et al.*, 2018). The in vitro data sets enabled us to test STADIA on data from physical experiments and to test STADIA's utility in analyzing the effects of a MTBP on DI behavior.

The in silico data set was obtained using our dimer-scale 13-protofilament (PF) kinetic Monte Carlo model of MT dynamics (Margolin *et al.*, 2012). The model simulates attachment/detachment of tubulin dimers to/from PFs, formation/breaking of lateral bonds between dimers in neighboring PFs, and hydrolysis converting GTP-bound dimers to GDP-bound dimers. The values of kinetic rate constants governing these biochemical events are input by the user. The observed DI behavior is an emergent property that arises as a consequence of the dimer-scale events. The input parameters for the model were tuned based on experimental measurements from Walker *et al*. (1988). The MT length-history data outputted by the simulation have spatial resolution at the scale of individual tubulin dimers (8 nm in length) and temporal resolution at the scale of the biochemical events described above (>1000 events per second per MT for the parameters used here).

Including the in silico data in our analysis is useful for several reasons. First, our in silico data allow us to test STADIA on a data set that has quantitatively different DI behavior as compared with the in vitro data sets. Note that the in silico data are not intended to replicate any numerical values from the in vitro data sets used here. Rather, using STADIA on quantitatively different data sets provides a test of the generality of the qualitative conclusions that we draw. Further, the detection of stutters in the in silico data demonstrates that stutters can arise as an emergent property of the dimer-scale biochemical events described above. Additionally, because the in silico data are recorded at the scale of the addition and loss of individual tubulin dimers, the in silico data have higher resolution than is currently possible in in vitro experiments. Therefore, comparison of the in silico and in vitro data sets demonstrates that STADIA is able to process data from a wide range of spatial and temporal resolutions. Relatedly, the high temporal resolution makes the in silico data set ideal for testing the robustness of STADIA to changes in data acquisition rates, because the full-resolution in silico data can be compared with data with imposed slower acquisition rates (Section 2.6).

2.2. STADIA: a novel tool for characterizing and quantifying MT dynamics

2.2.1. Goals of STADIA. To meet the goal of identifying, categorizing, and quantifying the range of MT behaviors in length-history data more precisely than with previous methods, we created STADIA. Specific aims for the development of STADIA were that it have the following attributes: 1) Automated to create a consistent and reproducible method with minimal user input; 2) Impartial such that it does not presuppose that MT dynamics are restricted to two states (i.e., limited to growth and shortening); 3) Adaptive to handle data from systems with qualitatively and quantitatively different DI behaviors (e.g., different types of tubulin and/or the presence of MTBPs); 4) Compatible with classical DI analysis, enabling comparison to and continuity with previous work; 5) Capable of analyzing data from a range of spatial and temporal resolutions (e.g., from computational simulations or laboratory experiments). The features of STADIA that collectively satisfy these goals are described in the remainder of Section 2.2.

2.2.2. Brief summary of STADIA. STADIA's analysis procedure consists of three major stages: segmentation, classification, and phase and transition analysis. In the segmentation stage, STADIA approximates inputted length-history data with a series of straight-line segments that are connected to each other at their endpoints (Figure 2, C and D) and then measures characteristics of each line segment (Figure 2D). In the classification stage, STADIA uses the characteristics of the line segments from the segmentation stage (Figure 2, E and F) to identify how many distinguishable DI behaviors exist in the set of line segments and then groups line segments into named DI behaviors (Figure 2H). For visualization purposes, color labels corresponding to the named behaviors from the classification stage are applied to each line segment in the length-history approximation (Figure 2G). In the phase and transition analysis stage, STADIA measures aggregate phase metrics (e.g., total time in growth) as well as the frequencies of various transitions beyond typical catastrophe and rescue (Figure 2I). These three stages are summarized here in Sections 2.2.3–2.2.5, with more details provided in *Materials and Methods* Section 5.5. Limitations of STADIA and guidance for users are also discussed in *Materials and Methods* Section 5.6.

2.2.3. Segmentation stage. The first step in the segmentation stage is to generate an initial approximation of inputted length-history data by identifying major peaks and valleys (Figure 2C), similar to more classical DI analysis methods (Figure 2, A and B). However, unlike classical methods, STADIA does not go directly from this step to calculating DI parameters. Instead, to improve the initial linear approximation, STADIA implements an iterative process to add new segment endpoints, which mark where the MT velocity changes as shown in Figure 2D. The user regulates how closely the segments approximate the raw data through the values of two input parameters: 1) the maximum error allowed between the line segments and

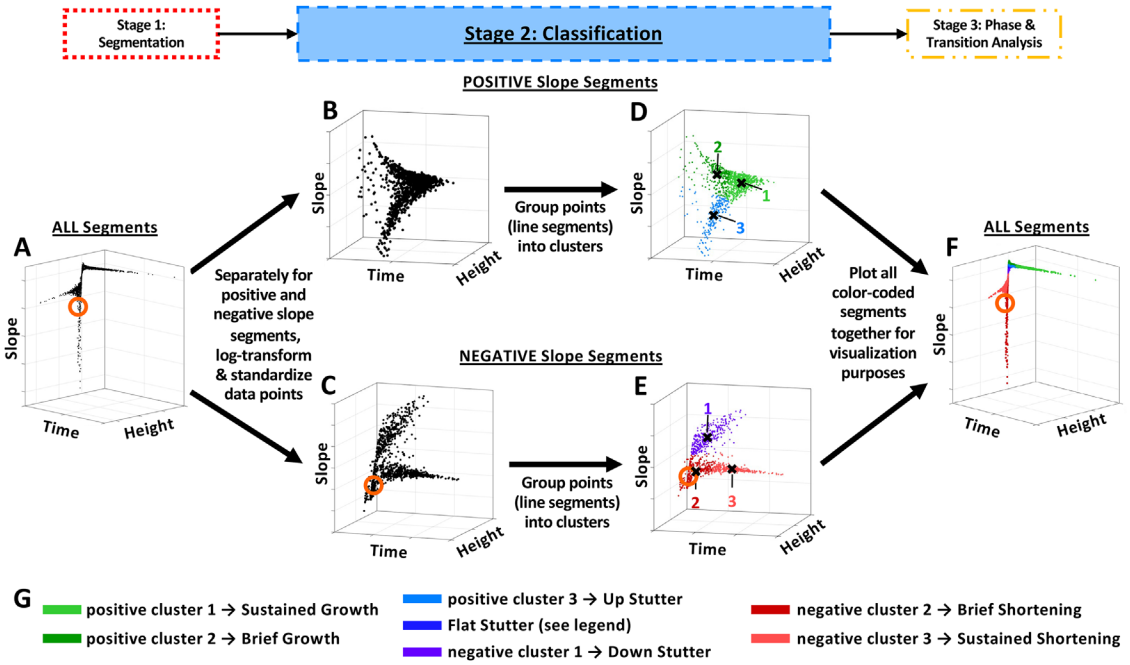

FIGURE 3: Overview of the clustering process in the Classification Stage of STADIA. As shown in Figure 2C–D, STADIA begins by approximating inputted length-history data with a series of line segments. For each line segment, three features are measured: time duration, height change, and slope (Figure 2D). Using these three features, a data point corresponding to each line segment is plotted in 3-dimensional space (A, replotted from Figure 2E). The orange circles in (A, C, E, F) denote the approximate location of the data point corresponding the example line segment in Figure 2D. Then, line segments that share similar values of time duration, length change, and slope (i.e., data points that are near each other in the 3-dimensional space) are grouped together into "clusters". As initial preparation for this grouping process, segments with slopes that are very near zero are identified by user-defined thresholds and assigned to one group (called "flat stutters"; see Section 5.5.2.1 for more information). In the next step of the process, applied separately to the remaining positive and negative slope segments (B,C), STADIA uses established statistical methods (described in Box 1 and *Materials and Methods* Sections 5.4.3 and 5.5.2.2) to determine the number of distinguishable clusters and then to assign each line segment to a cluster (D, E). After the segments are grouped into clusters, the average features (e.g., average slope) of the segments in each cluster are used to label each cluster with a named DI behavior (G).

the raw length-history data at each timepoint; 2) the minimum time duration for any line segment. Together these two parameters enable the user to avoid overfitting or underfitting the data relative to the scale of the dynamics the user wishes to study. As demonstrated in Section 2.6, proper tuning of these parameters enables STADIA to be compatible with data sets that have a wide range of temporal resolutions.

Note that the segmentation process imposes no restrictions on the slope of the segments and makes no assumptions about the number or type of behaviors present. These attributes are in contrast to the more traditional DI analysis methods described above, which use thresholds (e.g., on length change or velocity) to seek out segments corresponding to predefined behaviors (e.g., growth, shortening, pauses).

Effectively, the approximation produced by the segmentation stage of STADIA resembles the raw data more closely (Figure 2D) than does the approximation from classical methods (Figure 2, A–C). In particular, there are two fundamental differences between the segmentations resulting from classical methods and Stage 1 of STADIA. First, an individual segment of growth or shortening as identified by classical methods (Figure 2, A and B) may be identified as multiple segments of various slopes in the STADIA analysis (Figure 2D). Second, STADIA's refined approximation identifies segments of shallower slope that are not separated out from longer growth and shortening segments in classical methods.

2.2.4. Classification stage. This stage identifies the number of behavior types observed in the output from the segmentation stage and bins similar segments into behavior classes. To do this, STADIA measures three key features of each line segment (namely length change, time duration, and velocity; Figure 2D) and then plots a data point corresponding to each line segment in three-dimensional (3-D) space (Figure 2E). Line segments that share similar values of the three features (i.e., data points that are near each other in the 3-D space) are grouped into "clusters." STADIA uses established statistical methods (Box 1) to determine the optimal number of distinguishable clusters and to assign each line segment to a cluster (Figures 2F and 3). Note that this clustering step avoids assuming that any cluster corresponds to a predetermined DI phase/behavior.

After the line segments are assigned to clusters, the average features (e.g., average slope) of the segments in each cluster are used to assign each cluster to a named DI behavior (Figure 3G). Clusters containing segments with similar slopes are "bundled" into DI phase/behavior classes (Figure 2H). In particular, clusters of shallow-slope segments are bundled into "stutters," clusters of steep positive slope segments are bundled into "growth," and clusters of steep negative slope segments are bundled into "shortening."

2.2.5. Phase and transition analysis stage. For each cluster identified in the classification stage, STADIA calculates the following metrics: total number of segments (counts obtained from the piecewise linear approximation) in each cluster, percent time spent in each

Box 1:
For interested readers, Box 1 summarizes how established statistical methods are used in the clustering step of STADIA's Classification Stage (more details in *Materials and Methods* Sections 5.4.3 and 5.5.2.2).

We first note that STADIA can be run in two modes: Diagnostic Mode (used to inform the number of distinguishable clusters in the data set), and Automated Mode (used for performing full DI analysis after Diagnostic Mode work is complete). Automated Mode performs all three stages: segmentation, classification, and phase and transition analysis (Figure 2, C–I; workflow diagram in Supplemental Figure S1.1). Diagnostic Mode stops after a modified version of the classification stage.

The clustering process, applied separately to the positive slope segments and the negative slope segments, uses an established algorithm called *k*-means clustering (Macqueen, 1967; Lloyd, 1982). *K*-means groups together data points that share similar characteristics, that is, data points that are near each other in a relevant feature space (in our case, the log-transformed and standardized 3-D space defined by segment time duration, height change, and slope [Figure 3, B–E]).

The *k*-means algorithm requires that the number of clusters, *k*, be provided in advance. The value of *k* is informed by running STADIA in Diagnostic Mode. When run in Diagnostic Mode, STADIA repeats the *k*-means clustering process with the value of *k* set equal to each integer from 1 to 12. For each of these *k*-values, STADIA calculates a measurement called the gap statistic, which quantifies how well the data can be separated into *k* many clusters (Tibshirani *et al.*, 2001). Analysis of the gap statistic data from Diagnostic Mode as well as visual examination of the clusters plotted in the feature space (Supplemental Figures S1.4 and S1.5) informs the choice of the optimal *k*-value, which the user then inputs into Automated Mode.

cluster, percent height change corresponding to each cluster and average velocity of each cluster. These metrics can also be calculated for each of the larger bundled phase/behavior classes (i.e., growth, shortening, stutters.

Next, STADIA examines the chronological occurrences of the phases in the length-history data to identify all examples of transitions to/from growth and shortening, with or without stutters. Specifically, STADIA automatically categorizes the following types of phase transitions (Figure 2, I and J):

- "Abrupt Catastrophe": growth ➔ shortening directly
- "Abrupt Rescue": shortening ➔ growth directly
- "Transitional Catastrophe": growth ➔ stutter ➔ shortening
- "Transitional Rescue": shortening ➔ stutter ➔ growth
- "Interrupted Growth": growth ➔ stutter ➔ growth
- "Interrupted Shortening": shortening ➔ growth ➔ shortening

Similar chronological orderings of phases have previously been considered with pauses in experiments performed in the presence of cell extracts (Keller *et al.*, 2008).

After identifying all occurrences of the above transitions, STADIA calculates the frequency of each type of transition (see *Materials and Methods* Section 5.5.3 for formulas). For continuity with previous methods, the traditional transition frequencies can be calculated: the total catastrophe frequency, F_{cat}, is the sum of the frequencies of abrupt and transitional catastrophes, and the total rescue frequency, F_{res}, is the sum of the frequencies of abrupt and transitional rescues.

The STADIA process as outlined here enables extraction of traditional DI parameters as well as information about more complex behaviors and transitions. STADIA thus characterizes and quantifies MT dynamics without predefined assumptions about the number of behaviors or their defining attributes.

2.3. MT behaviors identified and characterized using STADIA

2.3.1. STADIA identifies multiple types of behavior within the groups of positive and negative slope segments. If MT growth and shortening each corresponded to one behavior (with variation), one would expect that the positive slope line segments from the approximation of the length-history plot would all fall into one cluster (i.e., one group of line segments); similarly, all the negative slope segments would be expected to fall into one cluster.

Contrary to these expectations, STADIA identified three clusters within the positive slope segment data of each data set (i.e., the in silico data set and the in vitro control and CLASP2γ data sets; Supplemental Figure S1.4). Examination of the characteristics of the three clusters shows that they can be described as follows (Figure 4, A–C, and Supplemental Figures S1.4, B, D, F, and H, and S1.8, A and B):

- segments with steep slopes and long time durations (positive slope cluster 1);
- segments with steep slopes and short time durations (positive slope cluster 2);
- segments with shallow slopes and short time durations (positive slope cluster 3).

Similarly, when analyzing the negative slope segments from the in silico data, STADIA identified three clusters (Supplemental Figure S1.5, A–D), which have the following characteristics (Figure 4, D and F, and Supplemental Figures S1.5, B and D, and S1.8, C and D):

- segments with shallow slopes and short time durations (negative slope cluster 1);
- segments with steep slopes and short time durations (negative slope cluster 2);
- segments with steep slopes and long time durations (negative slope cluster 3).

For technical reasons, the in vitro data sets contain the beginnings of shortening phases (Figure 1D), but not full depolymerizations of MTs to near-zero length as were present in the simulation data set (Figure 1B). Consistent with this information, STADIA's analysis of the in vitro negative slope segments (Figure 4E) did not find a cluster of long-time-duration segments (i.e., no cluster analogous to negative slope cluster 3 in the in silico data in Figure 4D). Nonetheless, STADIA did find evidence for two distinguishable clusters of short-duration negative-slope segments in the in vitro data: negative slope cluster 1 with shallow slope segments, and negative slope cluster 2 with steep slope segments (Figure 4, E and F, and Supplemental Figures S1.5, E–H, and S1.8, C and D). For illustration purposes, a "ghost" region was added to Figure 4E, where we expect the missing third negative slope cluster would reside if full depolymerization events had been captured in the experiments.

In summary, our simulations and experiments lead to a similar conclusion: the data argue against the idea that MT DI can be characterized as a two-state process consisting of only growth and shortening with instantaneous transitions. Instead, the results

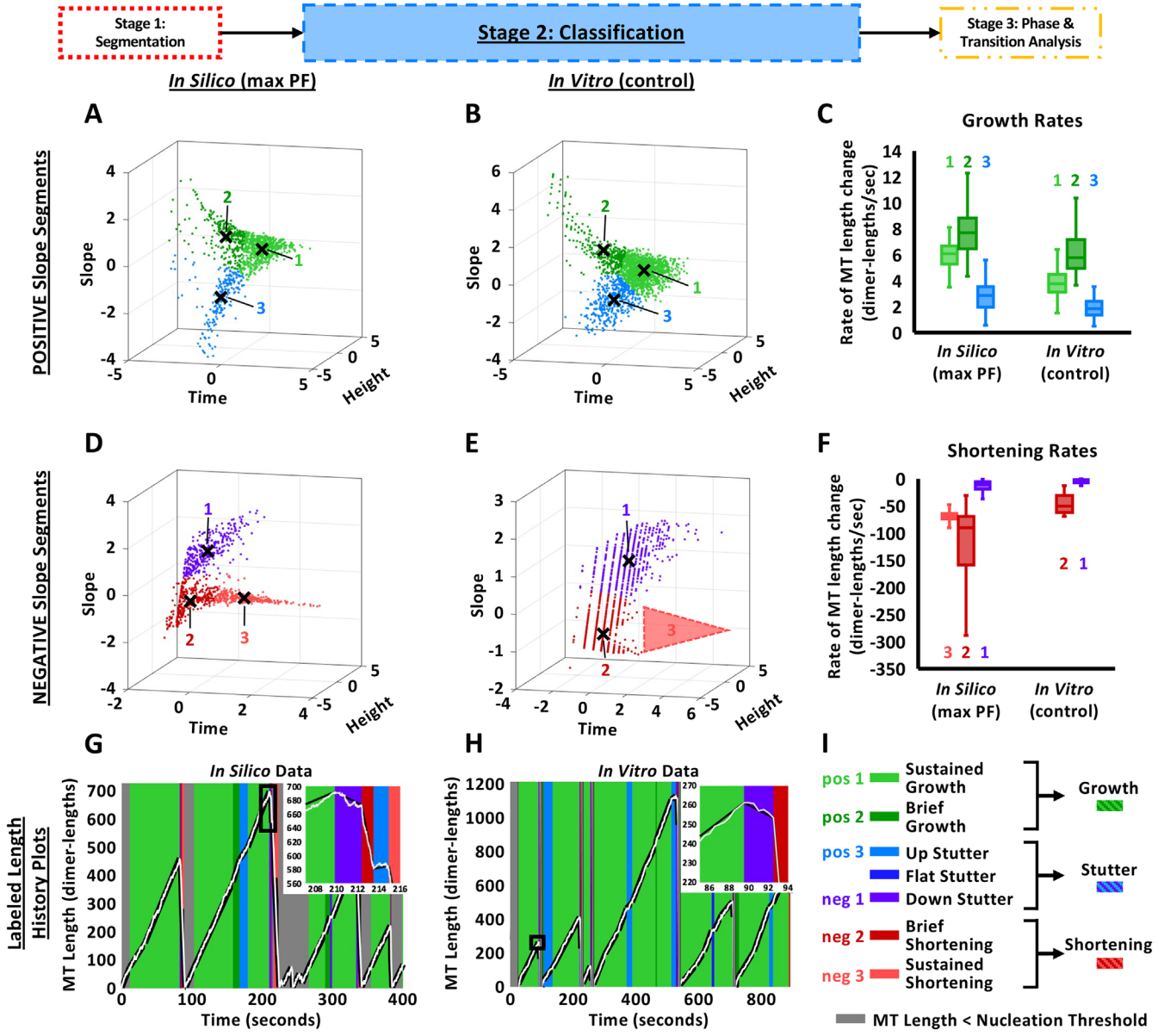

FIGURE 4: Results of STADIA's Classification analysis of in silico and in vitro datasets. (A, B, D, E) Color-coded clustering results for the in silico data (A, D) and in vitro control data (B, E); the clustering results for the in vitro CLASP2γ dataset are in Supplemental Figures S1.4 H, S1.5 H. Each data point in these plots corresponds to one line segment from the length-history approximations (see Figures 2D–F, 3). The scales of each axis reflect log-transformation and standardization of the data (see Figure 3). (C, F) Box plots of growth rates (C) and shortening rates (F) (i.e., segment slopes) for segment clusters as indicated. Outliers were excluded from the box plots (but not from the cluster plots) using the default definition in MATLAB (i.e., any value more than 1.5 times the interquartile range away from the bottom or top of the box is considered an outlier). (G, H) MT length-history plots with each segment labeled according to its assigned cluster. Zoomed-in portions of previously ambiguous length-history data are now clearly labeled (compare to Figure 1B–E). (I) Clusters with similar average slopes (panels C, F) bundled (grouped together) into larger behavior classes (see also Supplemental Figure S1.8). Notes: The raw length-history data have temporal resolution of ~1650 events per second per MT in silico and 2 frames per second in vitro. *Materials and Methods* Section 5.4.3 and Supplemental Figures S1.4, S1.5 provide justification for identifying three clusters each of positive and negative slope segments in most of our datasets (two clusters were used for the in vitro negative slope segments because complete depolymerizations to the seeds were not captured).

provide evidence for considering more complexity, including multiple types of behavior within both the positive and negative slope segments.

In the next two sections (Sections 2.3.2 and 2.3.3), we examine the average characteristics of the length-history segments in each cluster to determine how these clusters might correspond to recognizably different DI behaviors.

2.3.2. Growth and shortening phases consistent with classical DI analysis are among the multiple types of behavior identified by STADIA. Examining the average characteristics of the segments in each cluster (Figure 4, Supplemental Figure S1.8, and Table 1) shows that, for both the in silico and in vitro data, some of the clusters correspond to the well-recognized growth and shortening phases of DI. More specifically, two of the positive segment clusters

In Silico Data (Max PF Length; ~1650 events per second)						
Analysis Method	**# of Cat.**	**# of Res.**	**F_{cat} (min^{-1})**	**F_{res} (min^{-1})**	**V_{growth} (nm/s)**	**V_{short} (nm/s)**
Classical Method	355	123	0.659	2.483	46.1 ± 5.1	540.0 ± 47.9
STADIA limited to growth and shortening: *k*=1 for pos & neg	449	214	0.912	4.391	46.4 ± 18.4	530.4 ± 556.0
STADIA limited to growth, shortening, and flat stutters: *k*=1 for pos & neg	429	195	0.870	4.098	47.2 ± 17.6	547.2 ± 556.8
All behaviors identified by STADIA: *k*=3 pos, *k*=3 neg	298	75	0.660	1.944	48.0 ± 7.2 63.2 ± 19.2 22.4 ± 8.8	552.8 ± 87.2 1016.8 ± 717.6 107.2 ± 72.8

In Vitro Data - Control (2 fps)						
Analysis Method	**# of Cat.**	**# of Res.**	**F_{cat} (min^{-1})**	**F_{res}† (min^{-1})**	**V_{growth} (nm/s)**	**V_{short} (nm/s)**
Classical Method	802	40	0.717	N.D.	29.5 ± 12.7	330.1 ± 136.5
STADIA limited to growth and shortening: *k*=1 for pos & neg	856	83	0.777	N.D.	32.0 ± 24.8	216 ± 199.2
STADIA limited to growth, shortening, and flat stutters: *k*=1 for pos & neg	846	76	0.760	N.D.	32.8 ± 24.8	227.2 ± 198.4
All behaviors identified by STADIA: *k*=3 pos, *k*=2 neg	734	18	0.756	N.D.	30.4 ± 7.2 60.0 ± 44.8 15.2 ± 5.6	373.6 ± 143.2‡ 39.2 ± 25.6

In Vitro Data - CLASP2γ (2 fps)						
Analysis Method	**# of Cat.**	**# of Res.**	**F_{cat} (min^{-1})**	**F_{res}† (min^{-1})**	**V_{growth} (nm/s)**	**V_{short} (nm/s)**
Classical Method	99	62	0.500	N.D.	43.1 ± 34.4	155.1 ± 77.6
STADIA limited to growth and shortening: *k*=1 for pos & neg	142	94	0.720	N.D.	46.4 ± 41.6	96.0 ± 84.0
STADIA limited to growth, shortening, and flat stutters: *k*=1 for pos & neg	131	87	0.676	N.D.	48.0 ± 41.6	108 ± 82.4
All behaviors identified by STADIA: *k*=3 pos, *k*=2 neg	86	52	0.498	N.D.	37.6 ± 11.2 100.0 ± 57.6 16.0 ± 7.2	158.4 ± 68.8‡ 32.8 ± 17.6

Sustained Growth (positive slope cluster 1)

Brief Growth (positive slope cluster 2)

Up Stutter (positive slope cluster 3)

Sustained Shortening (negative slope cluster 3)

Brief Shortening (negative slope cluster 2)

Down Stutter (negative slope cluster 1)

TABLE 1: Comparison of DI measurements from classical two-state analysis, STADIA two-state analysis (i.e., STADIA with k = 1), and STADIA analysis with full classification. *Top row of each subtable*: classical two-state analysis method (*Materials and Methods* Section 5.3) performed by identifying only major peaks and valleys (Figure 2 A–B). *Second row of each subtable*: STADIA analysis with classification limited to two states: only growth and shortening. *Third row of each subtable*: STADIA analysis with classification limited to growth, shortening, and flat stutters. *Bottom row of each subtable*: STADIA analysis using full results of the classification stage (Figure 4; *Results* Section 2.3). All STADIA analyses used the fine-grained length-history approximation generated by the segmentation stage of STADIA (Figure 2D) but differed in the settings for the classification stage. These data show that there is general, but not exact, agreement between the analysis methods as applied to each dataset. V_{growth} and V_{short} measurements are listed as mean ± standard deviation over the set of all segments identified in each type of behavior. See Supplemental Figure S1.9 for the number of segments in each cluster from the STADIA full analysis. See *Materials and Methods* Sections 5.1.4 and 5.2.2 for the number of MTs and total observation times in each dataset.
†,‡: Because depolymerizations in the in vitro datasets were not captured in their entirety (see examples in Figure 1D), rescue frequencies are not reported (†), and negative slope segments were separated into only two clusters, yielding only two V_{short} measurements in the full STADIA analysis (‡), instead of three as seen with the in silico data.

(positive slope clusters 1 and 2 from Figure 4, A and B) have slopes (rates of length change) similar to growth rates reported in classical DI analysis (compare STADIA results in Figure 4C and Table 1 to classical analysis results in Table 1). Similarly, negative slope cluster 2 (in silico and in vitro, Figure 4, D and E) and negative slope cluster 3 (in silico, Figure 4D) have slopes similar to shortening rates reported in classical DI analysis (compare Figure 4F and Table 1). Based on this information, STADIA classifies length-history segments as "growth" if they belong to one of the clusters with a steep positive slope (positive slope cluster 1 or 2 in Figure 4, C and I) and as "shortening" if they belong to a cluster with a steep negative slope (negative slope cluster 2 or 3 in Figure 4, F and I).

The two clusters of steep positive slope segments (and of steep negative slope segments for the in silico data) differ primarily by time duration, so we refer to them as "brief" or "sustained" (Figure 4I and Supplemental Figure S1.8, B, D, and E). It is also notable that the brief growth/shortening clusters have greater variation in slope than the sustained growth/shortening clusters (Figure 4, C and F, and Supplemental Figure S1.8, A and C), which suggests that the most rapid velocities are not sustainable over long periods of time.

These observations may be evidence of different behaviors of tapered or split tips relative to the rest of the MT (e.g., as observed by Coombes *et al.*, 2013; Doodhi *et al.*, 2016; and Aher *et al.*, 2018); such structures might be able to extend or retract faster than the bulk MT lattice in the absence of lateral bonds. Future work is needed to investigate whether the differences between brief and sustained growth (or shortening) relate to tip structure.

2.3.3. STADIA detects and characterizes "stutters": a category of dynamic behaviors distinct from growth, shortening, and pause. Examination of Figure 4, A–F, shows that, in addition to clusters of segments with slopes that correspond to rates of length change seen in classical growth or shortening behaviors, STADIA also identifies clusters of segments with much shallower slopes (positive slope cluster 3 and negative slope cluster 1 in Figure 4, A–F; Table 1). Moreover, the segments in these shallow-slope clusters have time durations shorter than typical segments classified as sustained growth and sustained shortening, though typically longer than those classified as brief growth and brief shortening segments (Supplemental Figure S1.8). We term these clusters of shallow-slope segments "stutters" to convey the idea that these sections of length-history data exhibit high-frequency, low-amplitude fluctuations throughout which the overall rate of MT length change is slow from a macro-level perspective. Within the category called "stutters," we name the clusters based on their slopes (Figure 4I): "up stutters" (positive slope cluster 3), "down stutters" (negative slope cluster 1), and "flat stutters" (relatively rare near-zero slope segments identified before analyzing the positive and negative slope segments as described in the Figure 3G legend and Section 5.5.2.1).

In summary, stutters are a category of intermediate behaviors that share similar characteristics with each other and are distinguishable from typical growth and shortening. Distinguishing the various behaviors described above involved the use of segment slope, time duration, and height change, as explained in *Materials and Methods* Section 5.5. For any one of these three features individually, there is overlap between different clusters identified in the data (Figure 4, A–F, and Supplemental Figures S1.3 and S1.8). Of the three segment features, slope is the primary feature distinguishing stutters from typical growth and shortening (Figure 4C and F, and Supplemental Figure S1.8, A and C). In other words, the rate of change in MT length tends to be slower during stutters than during growth and shortening. In regard to time durations, up and down stutters, respectively, have similar or somewhat longer time durations than brief growth and shortening segments, but shorter time durations than sustained growth and shortening segments (Supplemental Figure S1.8, B and D).

2.3.4. Stutters overlap with previously observed slowdown periods but are distinguishable from pauses. Note that most stutters are distinguishable from previously identified "pauses" during which the MT neither grows nor shortens detectably (e.g., Gierke *et al.*, 2010; Yenjerla *et al.*, 2010). In contrast to pauses, MT lengths do indeed change measurably during most periods identified as stutters (for examples, see insets in Figure 4, G and H), with a net rate of change that is small but nonzero (Figure 4, C and F). In addition, it is notable that events categorized as pauses are typically described as being rare (<1% of total experiment time duration) in the absence of MT stabilizing proteins (e.g., Walker *et al.*, 1988; Moriwaki and Goshima, 2016). In contrast, stutters are relatively common, as discussed more below (Section 2.4.3 and Supplemental Figure S1.9). These observations support the conclusion that most stutters are different from events previously classified as pauses, though there is likely some overlap, particularly between the relatively rare flat stutters (Supplemental Figure S1.9) and cases where pauses were allowed to be short in duration (e.g., Walker *et al.*, 1988; Guo *et al.*, 2018). Stutters as described above likely do encompass the periods of slowed growth or shortening previously noted (but not quantified or characterized in detail) in recent DI data of in vitro MTs acquired at high spatiotemporal resolution (e.g., Maurer *et al.*, 2014; Duellberg *et al.*, 2016a,b; Rickman *et al.*, 2017; see also Margolin *et al.*, 2012). In contrast to this previous work, here we have quantified spontaneously occurring stutters and examined their relationship to other DI behaviors.

2.3.5. Negative control: two-state growth-shortening model. As a negative control to verify that the observation of stutters is not an artifact of STADIA's analysis process, we ran STADIA on length-history simulation data from a model designed to have only two states: growth and shortening. As would be expected, STADIA analysis of the length-history data from the two-state model did not identify behaviors comparable to the stutters detected in our main data sets (i.e., the dimer-scale simulation data and the in vitro data). For a description of the two-state simulations and the analysis results, please see Supplemental Material Section S4, "Negative Control: Simulations of a Two-State (Growth-Shortening) Model," and Supplemental Figures S4.1, S4.2, and S4.3.

2.4. Quantification of MT dynamics using STADIA

2.4.1. Comparison of the traditional DI parameters as measured by STADIA versus a classical DI analysis method. For each of the three data sets, Table 1 contains a comparison of results obtained using STADIA with three different sets of conditions in the classification stage to results from a classical DI analysis method (top row of each subtable; the classical analysis procedure is described in *Materials and Methods* Section 5.3). In the first set of STADIA conditions (second row), meant to approximate classical DI analysis, we restricted the classification stage of STADIA to recognizing only growth and shortening, that is, all positive slope segments were classified as growth and all negative slope segments were classified as shortening. In the next set of conditions (third row), we allowed STADIA to separate out near-zero slope segments as flat stutters but constrained the classification of the remaining positive and negative slope segments to one cluster each of growth and shortening. The final STADIA analysis (bottom row) utilized all clusters identified in the classification results in Section 2.3.

Within each data set in Table 1, the measured values of the standard DI parameters (V_{growth}, V_{short}, F_{cat}, and F_{res}) are similar across the different analysis approaches. The differences in measured values between the classical analysis and STADIA constrained to only growth and shortening occur because of differences in the segmentation. More specifically, the line-segment approximation produced by the segmentation stage of STADIA (Figure 2D) resembles the raw length-history data more closely than does the approximation from the classical method (Figure 2, A–C). Thus, STADIA can produce measurements of the traditional DI parameters but does so by using a finer linear approximation of the length-history data than the classical analysis, resulting in differences in the measured values of the DI parameters (Table 1).

2.4.2. Quantification of velocities and transition frequencies beyond the traditional DI parameters. While STADIA can provide measurements of the four traditional DI parameters that are similar to the measurements obtained from classical approaches, the multiple clusters (i.e., multiple types of behaviors) detected in the

full classification results (Section 2.3) indicate that the traditional DI parameters alone are inadequate to capture the full range of MT dynamics. Expanding beyond the traditional V_{growth} and V_{short}, the full STADIA analysis provides quantification of the intrinsic variability in growth and shortening rates by separately measuring the velocities for each cluster (Table 1, bottom row of each subtable). Expanding beyond the traditional F_{cat} and F_{res}, STADIA measures the frequencies of additional types of phase transitions (Figure 2I; Supplemental Figure S1.10).

2.4.3. MTs spend a significant fraction of time in stutters. We begin to investigate the significance of stutters by first examining the fraction of time that MTs spend in stutters. As one might expect, both in silico MTs and physical MTs spend the majority of their time in growth phases. However, in both the simulations and experiments, MTs spend a substantial amount of time in behaviors categorized as stutters. Notably, in our in silico data sets, the MTs spent more time in stutters (8%) than in shortening (6%) (Figure 5A; Supplemental Figure S1.9). The in vitro MTs spent a substantial amount of the time in stutters (Supplemental Figure S1.9), but direct comparison to time spent in shortening phases is not conclusive because depolymerizations were not fully captured. These observations indicate that stutters contribute appreciably to MT behavior as assessed in length-history plots.

2.4.4. Catastrophes are usually preceded by stutters in silico and in vitro. To investigate the functional significance of stutters, we used STADIA to examine how transitions between phases occur. More specifically, STADIA considers all possible transitions into and out of growth or shortening, with or without stutters (see Figure 2I for schematic, Figure 5, D–I, for in silico examples, Figure 6 for in vitro examples with corresponding kymographs, Figure 7, D–I, for additional in vitro examples, and Supplemental Figure S1.10 for frequencies).

Notably, in both the simulation data and the experimental control data, the majority of catastrophes involved a stutter between the growth and shortening phases (i.e., they were transitional catastrophes). In particular, 78% of the catastrophes in the simulation data were transitional (Figure 5B). A related observation in the simulation data is that almost half (44%) of stutters that occurred after a growth segment ended in catastrophe as opposed to returning to growth (i.e., they occurred as part of a transitional catastrophe as opposed to interrupted growth; Figure 5C). A similar but more dramatic association between stutters and catastrophe was observed in the in vitro control data: 86% of catastrophes involved a stutter (Figure 7A), and 75% of stutters from growth ended in a catastrophe (Figure 7B).

In contrast to catastrophes, rescues as observed in the in silico data set rarely occurred with stutters. More specifically, only 5% of in silico rescues were transitional (i.e., few rescues involved a stutter) (Figure 5B), and only 8% of stutters that occurred during shortening resulted in a rescue (Figure 5C). Because we do not have sufficient data for rescues in vitro, we cannot make strong conclusions on the correlation between stutters and rescue in physical MTs. However, these results do suggest that catastrophe and rescue are not simply the mechanistic opposites of each other.

2.5. Dissecting the effects of a MT binding protein: CLASP2γ reduces the frequency of catastrophe by increasing the prevalence of interrupted growth

To further test STADIA's utility in analyzing DI and to examine both the prevalence and the significance of stutters, we compared the control in vitro data set to the in vitro data set with the MTBP CLASP2γ, which has been previously characterized as an anticatastrophe factor (Aher *et al.*, 2018; Lawrence and Zanic, 2019). CLASP2 proteins are of interest to the biomedical community because they have been implicated in functions as diverse as kinetochore attachment (Girão *et al.*, 2020), nervous system development (Dillon *et al.*, 2017), and the insulin response (Kruse *et al.*, 2017).

Recall that the clustering results, including detection of stutters, are similar for the control and CLASP2γ data sets (Supplemental Figures S1.4 and S1.5). However, dramatic differences in the transition frequencies between the CLASP2γ data and control in vitro data were observed when these data were examined quantitatively by STADIA.

First, the overall frequency of catastrophe in the presence of CLASP2γ was significantly reduced (Figure 7C and Supplemental Figure S1.10). This observation itself is not surprising, given that previous work has shown that CLASP2γ reduces the frequency of catastrophe (e.g., Sousa *et al.*, 2007; Aher *et al.*, 2018; Lawrence *et al.*, 2018; Majumdar *et al.*, 2018). However, STADIA provides additional insight by distinguishing transitional catastrophes (growth-stutter-shortening) from abrupt catastrophes (growth-shortening). In particular, our results demonstrate that the reduction in overall catastrophe frequency was due to a large decrease in transitional catastrophe frequency, while the abrupt catastrophe frequency actually increased somewhat (Figure 7A and Supplemental Figure S1.10).

Second, CLASP2γ slightly reduced the frequency of growth-to-stutter occurrences (i.e., $F_{TransCat}$ + $F_{IntGrowth}$; Figure 7C) but not enough to account for the large decrease in transitional catastrophe frequency.

Third, and most striking, CLASP2γ increased the frequency of interrupted growth (growth-stutter-growth) (Supplemental Figure S1.10). More specifically, among transitions that began as growth-to-stutter, CLASP2γ increased the proportion of transitions that resulted in interrupted growth (growth-stutter-growth) and decreased the proportion of transitions that proceeded to transitional catastrophes (growth-stutter-shortening) (Figure 7B). This change in proportions is the factor that accounts for most of the decrease in transitional catastrophe frequency.

Taken together, these data demonstrate that STADIA analysis provides information about CLASP2γ function not supplied by traditional analysis and indicate that CLASP2γ suppresses catastrophe at least in part by enabling stuttering MTs to reenter growth (i.e., CLASP2γ tends to convert would-be transitional catastrophes into interrupted growths). This idea is supported by recent reports that MTs can withstand greater growth rate variability without undergoing catastrophe in the presence of CLASP2γ (Lawrence *et al.*, 2018; Lawrence and Zanic, 2019) and that CLASP2γ can protect against catastrophe in the presence of lagging PFs (Aher *et al.*, 2018).

2.6. Robustness of conclusions over varied values of input parameters and data acquisition rates

Note that this section assumes that readers are familiar with STADIA's analysis procedure as described in Section 2.2 and Box 1.

The results in the preceding sections led to the following main conclusions: 1) stutters (previously observed but not quantified in detail) are distinguishable from typical growth and shortening (Section 2.3); 2) stutters are strongly associated with spontaneously occurring catastrophes, both in silico and in vitro (Section 2.4.4); 3) the anticatastrophe factor CLASP2γ reduces catastrophe by increasing the fraction of stuttering microtubules that return to growth rather than entering shortening phases (Section 2.5). An important remaining question is whether these conclusions are robust to

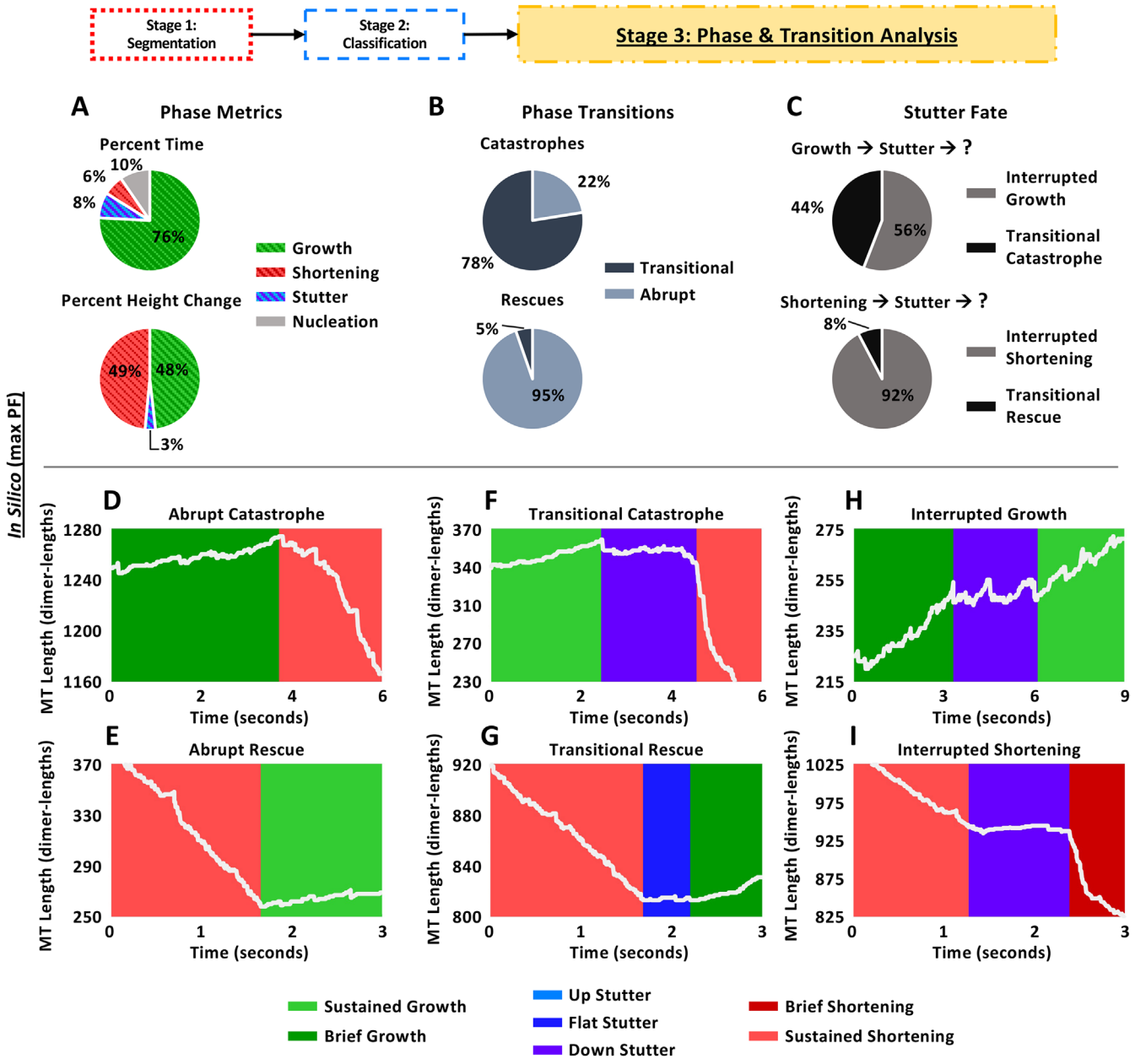

FIGURE 5: Results of STADIA's Phase and Transition Analysis of the dimer-scale in silico data. (A) Percent time spent in each class of phases/behaviors (top) and percent height (MT length) change occurring during each class of phases/behaviors (bottom). These data show that a large majority of time is spent in growth. Notably, the in silico MTs spend more time in stutters than in shortening, emphasizing the importance of studying stutter behaviors. Most height change occurs during growth and shortening phases, as expected. (B) Percentages of catastrophes (top) and rescues (bottom) that are transitional or abrupt (see Figure 2I and Section 2.2.5 for transition definitions). These data show that most catastrophes are transitional, whereas rescues are overwhelmingly abrupt. (C) Examination of stutter fate. These data show that when growth-to-stutter occurs (top), interrupted growth is slightly more likely than transitional catastrophe. However, when shortening-to-stutter occurs (bottom), interrupted shortening is much more likely than transitional rescue. (D–H) Examples of abrupt/transitional catastrophes (D, F), abrupt/transitional rescues (E, G), and interrupted growth/shortening (H, I). As noted earlier, the in silico dataset has temporal resolution of approximately 1650 events per second per MT (see *Materials and Methods* Section 5.2 for more information).

variations in the STADIA input parameters. To address this question, we performed sensitivity analyses, which are summarized here, with full details provided in Supplemental Material Sections S2 and S3.

2.6.1. STADIA input parameter sensitivity analysis. To test the effects of STADIA's input parameters, we analyzed all three data sets (i.e., in silico as well as in vitro with and without CLASP2γ), using a range of values for each of the key user-defined segmentation parameters in STADIA, namely the Minimum Segment Duration and the Maximum Error Tolerance. Directly, the values of these parameters determine how closely the segmentation stage's continuous piecewise linear approximation matches the raw length-history data inputted into STADIA. Indirectly, these parameters have downstream effects on the results of the classification stage and the

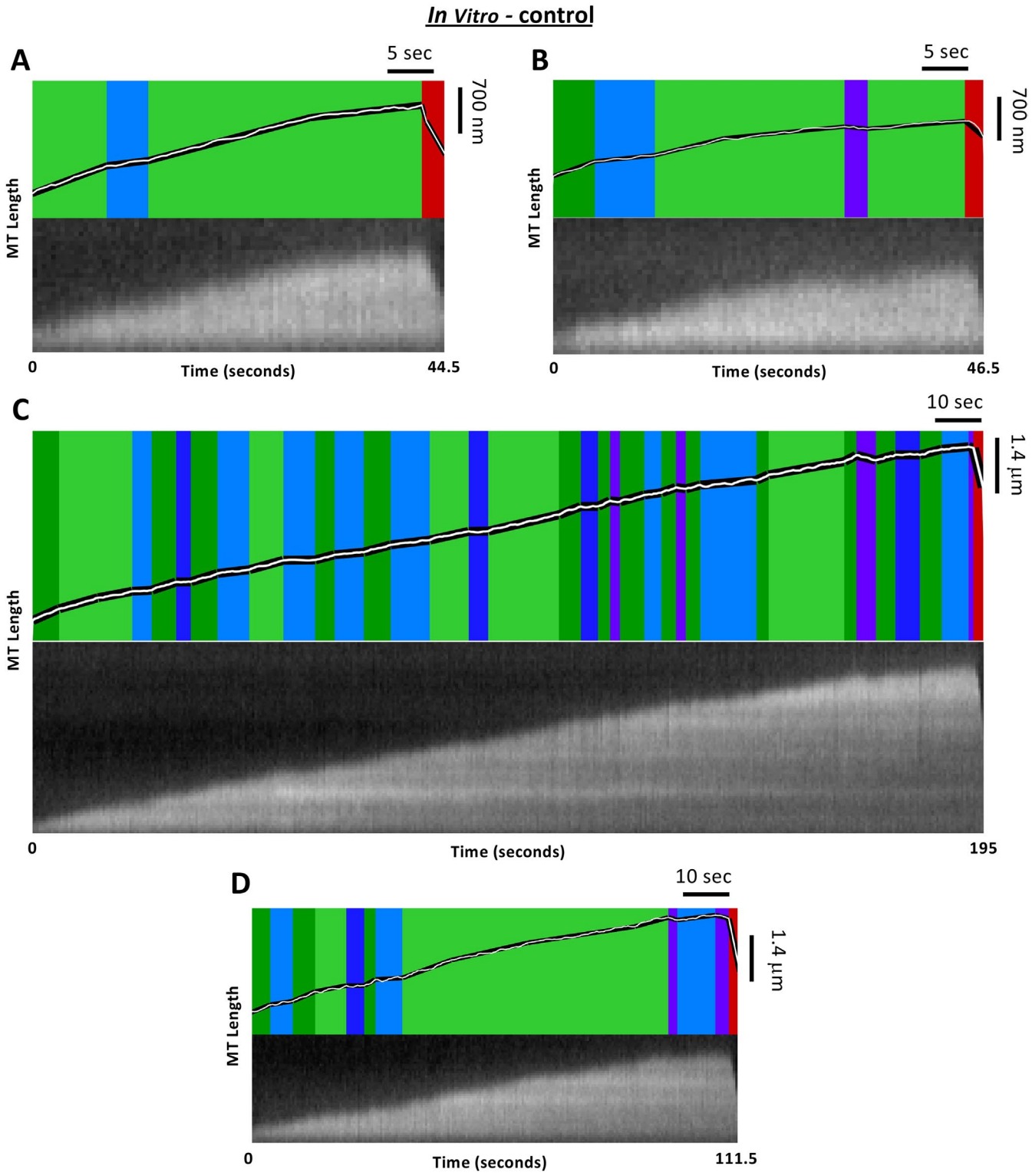

FIGURE 6: Alignment of STADIA length-history plots (top of each panel) and their corresponding kymographs (bottom of each panel) from the in vitro control dataset (with STADIA colors as in Figure 4 and scale bars as indicated). (A, B) Examples of abrupt catastrophes, where a growth phase (green) is followed directly by a shortening phase (red). (C, D) Examples of transitional catastrophes, where one or more types of stutter (blue, purple) occurs between a growth phase (green) and a shortening phase (red). Note also the numerous stutters (blue, purple) that interrupt growth phases (green). These length histories include examples of all three types of stutters that we distinguish based on slope: up stutters (light blue), flat stutters (dark blue), and down stutters (purple). The kymographs and the length-history traces inputted into STADIA were generated from the in vitro imaging data (2 fps) as described in *Materials and Methods* Section 5.1. The movies corresponding to each kymograph are provided as Supplemental Materials. Note that the movies are presented at 3.5 × real time (i.e., 3.5 × the time labeled on the kymographs and length-history plots).

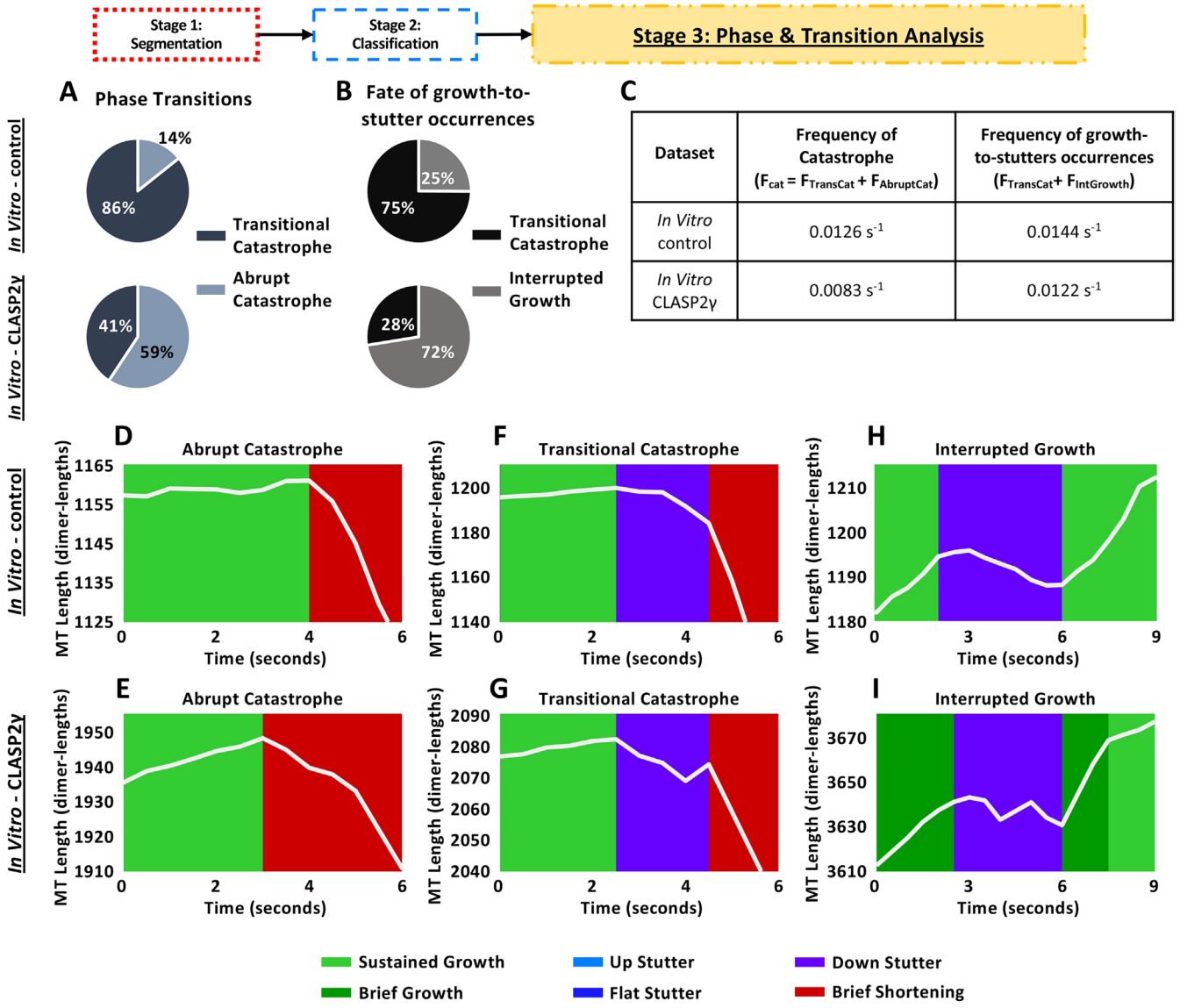

FIGURE 7: Results of STADIA's transition analysis of in vitro data (2 fps): Effect of CLASP2γ on the nature of catastrophes and the fate of stuttering MTs. See Section 2.2.5 for transition definitions. (A) The majority of catastrophes for in vitro MTs without CLASP2γ are transitional (top). However, introduction of CLASP2γ increases the fraction of catastrophes that are abrupt (bottom). (B) Most growth-to-stutter occurrences for the in vitro MTs without CLASP2γ (top) result in catastrophe. Addition of CLASP2γ (bottom) decreases the probability that a growth-to-stutter occurrence will proceed to shortening and increases the probability of returning to growth. (C) CLASP2γ decreases the overall frequency of catastrophe without greatly reducing the frequency of stutter-to-growth occurrences. Taken together (A–C), these data indicate that CLASP2γ reduces catastrophes by promoting growth following stutters. More specifically, transitions that would have been transitional catastrophes without CLASP2γ tend to become interrupted growths with CLASP2γ. (D–I) Examples of transitions as observed for the in vitro MTs both without CLASP2γ (top) and with CLASP2γ (bottom).

phase and transition analysis stage (for overview of STADIA stages, see Section 2.2, Figure 2, and Supplemental Figure S1.1). The results of the sensitivity analysis show how changes to the above input parameters impact STADIA outputs (e.g., number of behaviors detected, classification of segments as illustrated by labeled length-history plots, transition frequencies).

Briefly, results of this analysis (Supplemental Material Section S2) indicate that the three main conclusions enumerated above are indeed robust as long as the user-defined parameters are kept within ranges relevant to the scale of the dynamics being studied. In the first part of the sensitivity analysis, we examined how changing the user-defined parameters affects the number of behaviors detected (as determined by the number of clusters, i.e., *k*-values as described in Box 1 and *Materials and Methods* Sections 5.4.3 and 5.5.2.2). The results show that to detect stutter clusters, one must use spatial and temporal parameters that are sufficiently fine to distinguish the multiple behaviors detected (see the classification results in Sections 2.3.1–2.3.3) but not so fine that the analysis is affected by experimental noise or MT length fluctuations below the scale of the dynamics being studied. For our in silico data set, ideal ranges for these parameters were empirically determined to be from 15 to 25 dimer lengths (i.e., 120–200 nm) for the Maximum Error Tolerance

and 2 s or less for the Minimum Segment Duration (Supplemental Figures S2.1, S2.3, S2.5, and S2.7). For our in vitro control data set, ideal ranges were determined to be from 15 to 20 dimer lengths (120–160 nm) for the Maximum Error Tolerance and 1 s or less for the Minimum Segment Duration (Supplemental Figures S2.2, S2.4, S2.6, and S2.8). Note that while these ranges meet strict standards for detecting all of the behaviors studied, the analysis can tolerate a wider range of parameter values and still detect multiple types of behaviors including stutters within the positive and negative slope segments, thus demonstrating further robustness (see Supplemental Section S2).

In the next part of the sensitivity analysis, we examined the transition frequencies measured from running STADIA with varied values of the Minimum Segment Duration and the Maximum Error Tolerance while using the number of behaviors detected in the full classification results in Sections 2.3.1–2.3.3 (i.e., the analysis used the *k*-values selected in *Materials and Methods* Section 5.4.3). For the in silico data, both the values of the frequencies of abrupt and transitional catastrophe and the ratio between them are relatively insensitive to changes in the Maximum Error Tolerance in the range of 10–40 dimer lengths (i.e., 80–320 nm) (Supplemental Figure S2.9). Moreover, the conclusion that most catastrophes are transitional is robust for Minimum Segment Duration values of 1 s or less. However, for Minimum Segment Duration values of 1.5 s or greater, abrupt catastrophes become more common (Supplemental Figure S2.9), likely due to fewer stutters being detected and therefore fewer catastrophes being recognized as transitional. This observation is illustrated in examples of the labeled length-history plots (Supplemental Figure S2.7). Notably, the overall catastrophe frequency (the sum of abrupt and transitional) is less sensitive to changes in Minimum Segment Duration and Maximum Error Tolerance than are the abrupt and transitional catastrophe frequencies. The situation is similar, though somewhat noisier, for the in vitro data (Supplemental Figures S2.8, S2.10, and S2.11).

Significantly, the conclusion that CLASP2γ reduces catastrophe by promoting the growth of stuttering MTs is robust to changes across wide ranges of both Minimum Segment Duration and Maximum Error Tolerance (Supplemental Figures S2.10, S2.11, and S2.12). More specifically, for almost all parameter combinations tested, the presence of CLASP2γ decreased the frequency of transitional catastrophe and increased the frequency of interrupted growth relative to the in vitro control, even as the values of the frequencies themselves changed with varying the segmentation parameters (Supplemental Figures S2.10, B and C, S2.11, B and C, and S2.12, C–H). These results are particularly relevant to demonstrating STADIA's usefulness in studying the effects of MTBPs.

2.6.2. Data acquisition rate sensitivity analysis. To test the effect of varying the acquisition rate of length-history data inputted into STADIA, we took the original full-resolution in silico data set and resampled the length-history data at varied fixed data acquisition time steps (Supplemental Material Section S3). Examining a wide range of data acquisition rates is feasible because the in silico data set records every dimer-scale biochemical event (bond formation/breaking, hydrolysis; on the scale of >1000 data points per second per MT; see *Materials and Methods* Section 5.2). For comparison, frame rates in physical experiments vary from more than 100 fps (e.g., Mickolajczyk *et al.*, 2019) to fewer than 0.3 fps (e.g., Gierke *et al.*, 2010).

The resulting analysis (Supplemental Figures S3.1–S3.9) shows that the conclusion that "up stutters" exist is robust for data acquisition time steps up to 3 s, and similarly for "down stutters" at data acquisition time steps up to 1 s, assuming reasonable choices for Maximum Error Tolerance and Minimum Segment Duration (see Section 2.6.1). However, even when stutters are detected as distinct clusters, the number of stutter segments detected generally decreases for larger data acquisition time steps (i.e., slower data acquisition rates). This observation is not surprising because some stutters, particularly down stutters for the in silico data, have time durations on the order of 1 s or less (Supplemental Figure S1.8), and with frame rates slower than 1 s, such stutters would be undetectable.

Note that the in vitro data set was obtained using a frame rate of 2 fps, which was determined to be near the slower end of the range of acceptable data acquisition rates for some of the conclusions. As continued technological improvements allow physical experiments to have faster frame rates, in vitro data may tolerate a wider range of STADIA parameters (similar to the in silico data set). Significantly, short data acquisition time steps do not introduce problems (indeed, they are ideal, as seen with the full-resolution in silico data set) because the Maximum Error Tolerance and Minimum Segment Duration parameters prevent the segmentation (i.e., the continuous piecewise linear approximation) of MT length-history data from containing arbitrarily short segments.

3. DISCUSSION

Here we have presented STADIA, a data-driven, automated tool for performing DI analysis using length-history data as input. Using STADIA, we have quantified stutters and their associated transitions (Figures 4–7, Table 1, and Supplemental Figures S1.8–S1.10). Stutters are a set of dynamic behaviors that can be distinguished from typical growth or shortening; the primary differentiating factor is that stutters on average have slower rates of MT length change (Section 2.3). Stutters are also distinguishable from pauses in that a pause is typically described as a period of time when the MT neither grows nor shortens. Our analysis shows that stutters (i.e., slowdown periods, previously observed but not quantified in detail) are strongly associated with spontaneously occurring catastrophes, both in silico and in vitro (Section 2.4.4). Our STADIA analysis also indicates that the anticatastrophe factor CLASP2γ reduces catastrophe by increasing the fraction of stutters that return to growth rather than entering shortening phases (Section 2.5).

Importantly, we have shown that these results are robust across a range of STADIA parameter values (Section 2.6.1) and are compatible with data acquired across a range of temporal resolutions (Section 2.6.2). More specifically, as shown by the temporal resolution sensitivity analysis and the fact that our full-resolution simulation data set includes every subunit attachment and detachment event, STADIA is compatible with data acquired at temporal resolutions ranging from those produced by iSCAT (which can be as high as 1000 fps) to those used in TIRF experiments (e.g., 2 fps). This sensitivity analysis further shows that STADIA can also be used with data at lower temporal resolutions, but the ability to quantify stutters is reduced.

3.1. Mechanisms of stutters and implications for the process of catastrophe

What causes stutters, especially those that disrupt growth, and why are they associated with catastrophe? A fundamental component to answering this question comes from recognizing that when transitioning from growth to stutter, there is a net decrease in the number of subunits (tubulin dimers) that are incorporated into the MT per unit time. This net decrease could occur because new subunits attach to the tip less frequently than during normal growth, or because bound subunits leave the tip more frequently than during growth, or a combination of these two.

While simple stochastic fluctuations in subunit arrival or departure could potentially contribute to stutters, examination of length-history plots (Figures 4–7) suggests that the stochastic fluctuations, which occur throughout growth, shortening and stutter segments, are too short in duration to account for the sustained decrease in growth rate that occurs when going from growth to stutter. Alternatively, changes in rates of attachment and detachment could also result from changes in tip structure. However, one could argue that the rate of subunit attachment should not vary with tip structure: assuming that longitudinal bonds form first, there are always 13 landing sites for new subunits (Castle and Odde, 2013). Therefore, we suggest that stutters following growth segments likely result from a situation where an unusually large fraction of incoming subunits detach from the tip structure without being fully incorporated into the lattice (e.g., because tip taper or other structural features like the presence of GDP-tubulin make it difficult for lateral bonds to form). In other words, we suggest that stutters occur when the structure of the tip is such that the subunit detachment rate is unusually high compared with the average detachment rate during growth.

This reasoning provides a potential explanation for the correlation between stutters and catastrophe: if the fraction of incoming subunits incorporated into the lattice is smaller than during normal growth periods, the stabilizing cap of GTP-tubulin at the MT end will become smaller, the likelihood of exposing GDP-tubulin subunits will increase, and the possibility of complete cap loss (catastrophe) will rise. At present, these ideas are speculation, but future work may be able to shed light on these hypotheses (see also related discussions in VanBuren *et al.*, 2005; Howard and Hyman, 2009; Gardner *et al.*, 2011; Margolin *et al.*, 2012; Coombes *et al.*, 2013; Zakharov *et al.*, 2015; and McIntosh *et al.*, 2018).

Furthermore, the mechanisms could vary for different types of stutters. As demonstrated in the results, STADIA distinguishes up, down, and flat stutters and distinguishes stutters that occur as part of interrupted growth, interrupted shortening, transitional catastrophe, and transitional rescue. Thus, as a tool for comprehensively identifying multiple types of stutters, STADIA lays the groundwork for future mechanistic studies.

3.2. Comparison of the in silico and in vitro results

The behaviors observed in the dimer-scale simulation data and the experimental data are qualitatively similar. In particular, both types of data support the prevalence of stutters throughout length histories and the role of stutters in catastrophes. The differences in the particular numerical values of measured quantities are not surprising, because the simulation parameters were tuned in Margolin *et al.* (2012) based on an experimental data set (Walker *et al.*, 1988) different from the experimental data sets used here (a subset of which was used in Lawrence *et al.*, 2018). The qualitative similarities between the results from the different data sets provide evidence that the observed trends are not specific to one experimental preparation or one type of tubulin (e.g., 10 μM pure porcine tubulin in Walker *et al.*, 1988, vs. 12 μM bovine tubulin with EB1 and with or without CLASP2γ here and in Lawrence *et al.*, 2018). Furthermore, comparison with the negative control (two-state growth-shortening model; Supplemental Material Section S4) demonstrates that the existence of stutters in the dimer-scale simulations and the in vitro data is not manufactured by STADIA.

3.3. Relationship to previous work

3.3.1. Distinguishing stutters and previously identified pauses. Pauses have most frequently been observed in vivo (see citations in the *Introduction*) and are likely caused by MTBPs (Moriwaki and Goshima, 2016) and other factors external to the MTs themselves (e.g., reaching the cell edge [Rusan *et al.*, 2001; Komarova *et al.*, 2002]). Furthermore, in vitro pauses in the absence of drugs or MTBPs are rare (Walker *et al.*, 1988). In contrast, the observation that stutters are prevalent in both our in silico and in vitro data sets suggests that stutters are an intrinsic component of DI itself.

Gierke *et al.* (2010) have described "bona fide pauses" as phases "during which no polymerization or depolymerization occurs." Due to physical detection limits, true pauses would be indistinguishable from periods of very slow polymerization or depolymerization that do not meet the detection threshold (Gierke *et al.*, 2010). Particularly in older data sets with large thresholds (e.g., a length-change threshold of 0.5 microns), some stutters may have been considered pauses while others may not have been separated out from larger growth or shortening phases at all. With newer imaging technology, data can be obtained at higher temporal and spatial resolution (e.g., Maurer *et al.*, 2014; Duellberg et al., 2016a,b; Rickman *et al.*, 2017; Guo *et al.*, 2018; Mickolajczyk *et al.*, 2019), which can enable the distinction of stutters and pauses.

For most stutters, a measurable net length change does occur over the course of the stutter segment: up and down stutters occur much more often than flat stutters. Using this information about stutters from our results and definitions of pauses already existing in the literature, we propose the following operational criteria for distinguishing pauses and stutters: pauses are periods during which no detectable length change occurs, whereas stutters are periods during which the MT structure changes but with slower net rates of length change than typical growth and shortening phases. In data sets that contain both stutters and pauses, the current version of STADIA would classify "bona fide pauses" as flat stutters. Future work is needed to determine whether it would be meaningful to apply criteria to distinguish flat stutters, which generally have very short time durations, from pauses.

3.3.2. Previously observed behaviors that are similar to particular types of stutters. Maurer *et al.* (2014) observed short episodes of pause or slow growth before catastrophes in experiments with EB1. These precatastrophe slowdowns are analogous to transitional catastrophes in our terminology. Pauses or slowdowns before catastrophe have also been observed in cases where the catastrophe is induced by outside factors such as mechanical force (Janson and Dogterom, 2004) or reduction in tubulin concentration (Duellberg *et al.*, 2016a,b), similar to predictions based on simulations in Margolin *et al.* (2012). In contrast, the catastrophes in our data sets occur spontaneously as part of DI; in the in vitro data sets, EB1 and CLASP2γ affect the frequency of catastrophe, but the catastrophes still occur stochastically over time, as opposed to being induced by an experimenter at a particular moment.

The episodes of slow growth in Rickman *et al.* (2017) bear some similarity to stutters interrupting growth as identified by STADIA. However, the slow growth episodes of Rickman *et al.* occurred rarely (two to five occurrences; ~0.26% to ~6.1% of the time analyzed, depending on tubulin concentration). These episodes appear to correspond to the most extreme of our stutters, meaning the stutters with the longest time durations or with the most variability in length during the stutter.

Based on analysis of variability in growth rates in experimental data, Odde *et al.* (1996) proposed a model with multiple substates of growth and "near catastrophes," which are similar to stutters interrupting growth. They suggested that the largest of the "near catastrophes" may correspond to previously observed pauses and that

the smaller "near catastrophes" would not be easily detected by eye (the time between data points in their analysis was ~3 s).

Building beyond this previous work, STADIA provides a comprehensive method for detecting and quantifying multiple types of stutters and distinguishing phase transitions that include stutters from those that do not.

3.3.3. Differences between STADIA and previous segmentation/classification methods. Although STADIA identifies DI phases at a finer scale than many existing DI analysis methods, it differs from methods that simply consider individual displacements between frames and label them as growth, shortening, or pause using thresholds on the length change (e.g., Komarova *et al.*, 2002; Guo *et al.*, 2018). In contrast to such methods, STADIA identifies larger-scale segments during which a MT exhibits a consistent behavior.

Similar to STADIA, many existing time-series analysis methods that have been used in other applications (e.g., identifying runs and pauses in the transport of organelles along MTs by motor proteins [Zaliapin *et al.*, 2005]) involve a segmentation step (e.g., Zaliapin *et al.*, 2003) that is often followed by a classification step (e.g., Fu, 2011). To our knowledge, such methods have not been previously applied to MT DI data. In contrast, many DI analysis methods essentially perform classification before segmentation, by setting thresholds for classifying growth, shortening, and possibly pause or slowdown periods, and then applying the thresholds to identify segments in the data (e.g., Dhamodharan and Wadsworth, 1995; Kiris *et al.*, 2010; Fees *et al.*, 2017). Additionally, unlike existing methods that use predefined thresholds on segment features (length change, time duration, and/or slope), STADIA uses a data-driven approach to identify emergent clusters in the segment feature data (e.g., stutters have shallow slopes, but shallow is relative to the slopes of other segments in a given data set).

3.3.4. Differences between STADIA and previous phase transition analysis. In regard to phase transition analysis, several previous articles grouped their pauses with growth when defining catastrophe and rescue; by their definitions, a catastrophe is a transition from growth or pause to shortening, and a rescue is a transition from shortening to growth or pause (Dhamodharan *et al.*, 1995; Dhamodharan and Wadsworth, 1995; Panda *et al.*, 1996; Rusan *et al.*, 2001; Kamath *et al.*, 2010; Kiris *et al.*, 2010; Yenjerla *et al.*, 2010; Moriwaki and Goshima, 2016). By these definitions or analogous definitions with stutter in place of pause, an episode of interrupted shortening would be labeled as a rescue followed by a catastrophe, whereas an interrupted growth would not be distinguished from *un*-interrupted growth.

STADIA improves upon typical transition analysis by considering all possible transitions between growth, shortening, and stutters (similar to the transitions among growth, shortening, and pause that were considered in Keller *et al.*, 2008). Such transition analysis enables more in-depth investigation of the mechanisms of DI and DI-regulating proteins. For example, the observation that CLASP2γ tends to convert would-be transitional catastrophes into interrupted growths would not have been possible without a method that is able to identify transitional catastrophes and interrupted growths.

4. CONCLUSIONS

Our work has four major conclusions: 1) STADIA can quantify and examine "stutters," a previously observed category of behaviors during which MTs undergo slow rates of overall length change compared with growth or shortening phases; 2) stutters are strongly associated with catastrophe in dimer-scale in silico and TIRF-imaged in vitro data; 3) the anticatastrophe factor CLASP2γ reduces catastrophe by increasing the fraction of stutters that return to growth rather than enter shortening phases; 4) STADIA provides an improved analytical tool for quantification of MT behavior, as exemplified by the first three points. Our results concerning the detection of stutters differ from those of previous work in that STADIA comprehensively and systematically identifies all types of stutters (up stutter, flat stutter, down stutter) across length-history data and considers all possible transitions among growth, shortening, and stutters. We suggest that quantification of stutters in future DI analysis through STADIA or similar tools will enable improved analysis of MT dynamics that is more complete, precise, and reproducible. The clearer picture that results from this analysis will facilitate investigation of the mechanisms of catastrophe and rescue as well as the activities of the MTBPs that regulate these transitions.

5. MATERIALS AND METHODS

The methods are presented in the following order: Sections 5.1 and 5.2, respectively, describe the acquisition of the in vitro and in silico data sets. Section 5.3 summarizes our classical DI analysis method, used for comparison with STADIA. Section 5.4 outlines our use of STADIA to analyze the data sets in this article. Section 5.5 describes STADIA's analysis procedure in more detail than the overview in *Results* Section 2.2. Section 5.6 provides guidance for users of STADIA.

5.1. Data acquisition: in vitro microtubule experiments

The in vitro MT data were obtained from two sets of conditions: a control group (tubulin + EB1) and a group with the MTBP CLASP2γ (tubulin + EB1 + CLASP2γ). A subset of these data was previously published in Lawrence *et al.* (2018).

5.1.1. Protein preparation. His-CLASP2γ and His-EB1 were purified as previously described (Zanic *et al.*, 2013; Lawrence *et al.*, 2018). Bovine brain tubulin was purified using the high-molarity method (Castoldi and Popov, 2003). Tubulin was labeled with TAMRA and Alexa Fluor 488 (Invitrogen) according to the standard protocols, as previously described (Hyman *et al.*, 1991).

5.1.2. TIRF microscopy. Imaging was performed using a Nikon Eclipse Ti microscope with a 100×/1.49 n.a. TIRF objective; an Andor Neo sCMOS (complementary-metal–oxide–semiconductor) camera; 488- and 561- solid-state lasers (Nikon Lu-NA); a Finger Lakes Instruments HS-625 high-speed emission filter wheel; and standard filter sets. An objective heater was used to maintain the sample at 35°C. Microscope chambers were constructed as previously described (Gell *et al.*, 2010). In brief, 22 × 22 mm and 18 × 18 mm silanized coverslips were separated by strips of Parafilm to create a narrow channel for the exchange of solution (Gell *et al.*, 2010). Images were acquired using NIS-Elements (Nikon).

5.1.3. Dynamic MT assay. GMPCPP-stabilized MTs were prepared according to standard protocols (Hyman *et al.*, 1992; Gell *et al.*, 2010). Dynamic MT extensions were polymerized from surface-immobilized GMPCPP-stabilized templates as described previously (Gell *et al.*, 2010). The imaging buffer consisted of BRB80 supplemented with 40 mM glucose, 40 µg/ml glucose oxidase, 16 µg/ml catalase, 0.5 mg/ml casein, 100 mM KCl, 10 mM dithiothreitol, and 0.1% methylcellulose. Purified proteins and 1 mM GTP were added to the imaging buffer, and the solution was introduced into the imaging chamber. Dynamic MTs were grown with 12 µM Alexa 488–labeled tubulin and 200 nM EB1 with or without 400 nM CLASP2γ

and imaged at 2 fps using TIRF microscopy as described above (pixel size of 70 nm). Alexa 488–labeled tubulin was used at a ratio of 23% of the total tubulin.

5.1.4. In vitro MT length-history data. Length-history data for in vitro MTs were obtained from 30-min experiments using both a control group and a group with the stabilizing MTBP, CLASP2γ. Kymographs of dynamic microtubules (examples in Figure 6) were generated using the KymographClear macro for ImageJ, and the dynamic MT tip positions as a function of time were determined in KymographClear, using a thresholding-based, edge-detection method that can trace the microtubule tip position in kymographs with subpixel accuracy (Mangeol *et al.*, 2016). Note that long shortening phases were not well-captured by this process for technical reasons including photobleaching. Therefore, the position-time data from a given MT were broken into samples that typically consisted of a growth phase followed by an initial depolymerization and then termination of that observation (e.g., Figure 1D).

The control group data set was acquired from 68 MT seeds, from which 776 individual traces were observed. The group with CLASP2γ was acquired from 29 MT seeds, from which 85 individual traces were observed. The control group and the group with CLASP2γ yielded total time durations of more than 21 h and 3.5 h, respectively. The in vitro MT lengths were measured in nanometers and then divided by 8 nm per dimer length to convert to units of dimer lengths.

5.2. Data acquisition: in silico microtubule experiments

This section outlines the details regarding the acquisition of the dimer-scale simulation MT data, analyzed in the *Results* and in Supplemental Sections S1, S2, and S3, including information about both the model and the parameters used.

5.2.1. The computational model: stochastic model for simulating 13-protofilament MTs. The computational MT model used in this paper to generate the in silico length-history data is an updated version of the detailed, stochastic 13-PF MT model published in Margolin *et al*. (2012) and utilized in Margolin *et al.*, 2011; Gupta *et al.*, 2013; Li *et al.*, 2014; Duan *et al.*, 2017; Mauro *et al.*, 2019; Jonasson *et al.*, 2020). The model tracks the state of individual subunits (representing tubulin dimers bound to either GTP or GDP) in the entire 13-PF MT structure. The events that occur in the model are attachment/detachment of subunits to/from a PF, formation/breaking of lateral bonds between subunits in neighboring PFs, and hydrolysis of GTP subunits to GDP subunits. The values of the biochemical kinetic rate constants for each type of event are user inputs and depend on the state (GTP-bound or GDP-bound) of the subunits involved in the event. To carry out the simulation, the event that occurs at each step and the times between events are sampled using the Gillespie algorithm (Gillespie, 1976, 1977), which is a kinetic Monte Carlo algorithm. At each event, the simulation outputs the time of the event and the length of the MT. The DI behavior, including stutters, and the values of DI parameters are emergent properties that arise as a consequence of the subunit-scale events. This feature is in contrast to two-state growth-shortening DI models, where the four traditional DI parameters are inputs (e.g., negative control in Supplemental Section S4; Verde *et al.*, 1992; Dogterom and Leibler, 1993).

A key difference between the previous versions of our 13-PF MT computational model and the current implementation is strict adherence to the assumption that only one of the many possible biochemical events occurs at a time. The previous detailed-level 13-PF MT model approximated hydrolysis events by allowing several subunits to hydrolyze simultaneously after one of the other four reaction events (lateral bonding/breaking or subunit gain/loss) has occurred. Individual hydrolysis events are now considered as a possible event in the same way that the other events are handled. This modification resulted in very little change in macro-level behavior of in silico MTs, but the ability to output dedicated observations of each dimer-level event provides a more accurate representation of MT biochemistry. The overall result of the simulation is in silico MTs that exhibit macro-level DI behaviors in agreement with those observed previously (Margolin *et al.*, 2012).

5.2.2. Simulation setup and parameters. The dimer-scale kinetic parameters used in this study to simulate a 13-PF MT using the model described above were tuned in Margolin *et al*. (2012) based on in vitro DI measurements from Walker *et al*. (1988); a detailed list of parameters can be found in Supplemental Table S1.2. For the purposes of this analysis, a single MT was simulated at a constant [free tubulin] of 10 μM for 10 h of simulation time. For the kinetic parameters and tubulin concentration used here, approximately 1650 subunit-scale reaction events occurred per second on average over the course of the simulation.

To generate the length-history data passed into STADIA, we used either the max PF length (i.e., the length of the longest of the 13 PFs) or the mean PF length (i.e., the mean of the 13-PF lengths) as the length of the MT. Comparisons of results using the mean or max PF length are shown in Supplemental Figures S1.4, S1.5, S1.6, S1.9, and S1.10. The clustering profiles in Supplemental Figure S1.4 show better agreement with the in vitro data used here when using the max PF length instead of the mean PF length. Thus, all the in silico results are presented for the max PF length unless otherwise indicated. Each dimer has a length of 8 nm. The max and mean PF lengths are both reported in units of dimer lengths; this is not the same as the number of dimers in the MT, which would be 13 times the mean PF length.

5.3. Classical DI analysis

For purposes of comparison to STADIA, we used our implementation of classical DI analysis, a custom program written in MATLAB and described in the Supplemental Methods of Jonasson *et al.* (2020). Briefly, this method segments growth and shortening phases by first identifying major peaks and valleys in the length-history data using the MATLAB function "findpeaks." Then the ascent to each major peak is classified as a growth segment, and the descent from the peak is classified as a shortening segment. Each major peak is classified as a catastrophe, where the end of growth and the start of shortening are identified as occurring at the same time point. A major valley is classified as a rescue only if the MT length at the time of the major valley is greater than or equal to a user-defined value called the "minimum rescue length," in which case the end of shortening and the start of growth are identified as the same point. For a major valley that occurs below the minimum rescue length, the end of shortening can be identified as an earlier point in time than the start of growth, in which case the time between these points would correspond to a nucleation period near the MT seed (see Supplemental Methods of Jonasson *et al.*, 2020, for additional details).

For the classical DI analysis in this paper, the minimum prominence for major peaks (i.e., minimum height change between a major peak and the nearest major valley) in the classical method was set equal to the same value that we used for the Maximum Error Tolerance in STADIA (Supplemental Table S1.1). The minimum peak

height and the minimum rescue length in the classical method were each set equal to the sum of the values of the Nucleation Height Threshold plus the Maximum Error Tolerance in STADIA (Supplemental Table S1.1).

In the classical method results shown in Table 1, the V_{growth} and V_{short} calculations relied on linear regressions fitted to each growth or shortening segment. V_{growth} was calculated as the arithmetic mean of the slopes of the regression lines for all growth segments whose linear regression had an R^2 value of at least 95%. V_{short} was calculated in the same manner using the shortening segments. F_{cat} was calculated as the total number of catastrophes divided by the total time spent in growth phases. Similarly, F_{res} was calculated as the total number of rescues divided by the total time spent in shortening phases. Note that linear regressions and R^2 values are used here in our classical analysis but not in STADIA.

5.4. Using STADIA for the analyses in this article

5.4.1. Data input and preprocessing. The simulation data (Section 5.2) were inputted into STADIA as one long length-history time series from an individual MT. For each of the two in vitro data sets (Section 5.1), individual length-history traces (which typically consisted of a growth phase followed by the beginning of a shortening phase; e.g., Figure 1D) were inputted from multiple MTs recorded over shorter periods of observation. As described below (Section 5.5.1.1), when multiple length-history traces are inputted into STADIA, STADIA "stitches" the traces into a single time-series representation, but with separators between the traces to avoid artifactually introducing rescues, catastrophes, or any other transitions. Thus, for our inputted in vitro data, STADIA automatically stitched all of the traces for all of the MTs within each experiment into a single time-series representation (one with CLASP2γ and one without).

5.4.2. Input parameter values (Supplemental Table S1.1). In both Diagnostic and Automated Modes, STADIA analysis requires that the user provide values for the following five user-defined parameters: Minimum Segment Duration, Maximum Error Tolerance, Nucleation Height Threshold, Maximum Height Change Magnitude for Flat Stutters, and Maximum Slope Magnitude for Flat Stutters. The role of each of these parameters in STADIA is further described in Sections 5.5.1 and 5.5.2.1 below.

The Minimum Segment Duration and Maximum Error Tolerance parameters regulate the accuracy of the continuous piecewise linear approximations. For all analyses in the main text and Supplemental Material Section S1, they were set to the following values: Minimum Segment Duration = 0.5 s; Maximum Error Tolerance = 20 dimer lengths. These segmentation parameters were varied over a range of values in Supplemental Material Sections S2 and S3 for the purposes of the sensitivity analysis, which is summarized in Section 2.6.

The Nucleation Height Threshold sets the minimum MT length required for further DI analysis. Segments where the MT length is entirely below the Nucleation Height Threshold are classified as "nucleation" at the beginning of the classification stage and then omitted from analysis thereafter. For all analyses in this article, we set the Nucleation Height Threshold to 75 dimer lengths.

STADIA identifies a segment as a flat stutter if the absolute value of its net height change is less than the user-input Maximum Height Change Magnitude for Flat Stutters and/or the absolute value of its slope is less than the Maximum Slope Magnitude for Flat Stutters. In our analyses, we set the Maximum Height Change Magnitude for Flat Stutters to 3 dimer lengths and the Maximum Slope Magnitude for Flat Stutters to 0.5 dimer lengths/second.

5.4.3. Determination of the number of clusters (i.e., values of k) for k-means clustering. In Automated Mode, STADIA requires that the user provide the number of clusters (i.e., values of *k*) for the *k*-means clustering step. As discussed more in Section 5.5.2, the value of *k* is set separately for the positive and negative slope line segments of each length-history data set and is informed by first running STADIA in Diagnostic Mode. Briefly, the Diagnostic Mode of STADIA outputs gap statistic plots and cluster plots (Supplemental Figures S1.4 and S1.5), which provide information that aids in choosing the optimal number of clusters (i.e., *k*-values) to input into Automated Mode. The gap statistic is a quantity that is calculated at each possible value of *k* to provide a measure of how well the data can be described by *k* clusters. Though there are various ways to interpret gap statistic plots, one rule of thumb is to choose the *k*-value corresponding to the first local maximum of the gap statistic plot (Maechler, 2021) (see also Tibshirani *et al.*, 2001; Hastie *et al.*, 2009, for related information). However, because these plots can have ambiguities, visual examination of the gap statistic plots and cluster plots is useful for interpreting the results in the context of the particular application and thus determining an appropriate number of clusters.

In our analyses of the Diagnostic Mode outputs for each data set, the *k*-value corresponding to the first local maximum of the gap statistic plot was usually chosen as the optimal number of clusters. In particular, for the simulation data, we chose $k = 3$ for each of the positive and negative slope segment groups, as indicated by the first local maximum of the gap statistic plots (Supplemental Figures S1.4C and S1.5C). However, the situation was more complicated for the in vitro data. First, for the negative slope segments in each in vitro data set, we chose $k = 2$, consistent with the first local maximum of the gap statistic plots (Supplemental Figure S1.5, E and G); as discussed in *Results* Section 2.3.1, $k = 2$ for negative slope segments was appropriate for these data sets (in contrast to the $k = 3$ for negative slope segments in the in silico data set) because full depolymerizations to the seed were not captured in the in vitro data sets for technical reasons. For the positive slope segments in the in vitro CLASP2γ data set, we chose $k = 3$, again consistent with the first local maximum of the gap statistic plot (Supplemental Figure S1.4G). However, for positive slope segments in the in vitro control data set, we chose the second local maximum ($k = 3$) instead of the first local maximum ($k = 1$) based on qualitative inspection of the cluster profiles (Supplemental Figure S1.4, E and F). More specifically, the cluster profile for the in vitro control positive slope segments (Supplemental Figure S1.4F) displays three appendages, similar to the cluster profiles for the positive slope segments in the in vitro CLASP2γ data set (Supplemental Figure S1.4H) and the in silico data set (Supplemental Figure S1.4D), where the gap statistic plots indicate $k = 3$ (Supplemental Figure S1.4, C and G).

After choosing the *k*-values based on the results of running STADIA in Diagnostic Mode, we inputted these *k*-values into Automated Mode to perform the full STADIA analysis.

5.5. STADIA'S analysis procedure

This section provides an in-depth description of the three major stages of STADIA analysis (Segmentation, Classification, and Phase and Transition Analysis; Figure 2; Supplemental Figure S1.1). For readers interested in a shorter overview of STADIA's analysis procedure, please see *Results* Section 2.2.

5.5.1. Segmentation stage. In the segmentation stage, STADIA takes MT length-history data and generates a continuous piecewise linear approximation of the MT length-history plot (Figure 2, A–D). The approximation is a series of straight-line segments (i.e., the

approximation is "piecewise linear"), where the endpoint of each line segment coincides with the start point of the next line segment (i.e., there are no discontinuities in the approximation). The segmentation stage includes a preprocessing step that prepares the user's length-history data for input into STADIA and a postprocessing step that prepares the results of the segmentation stage for classification.

5.5.1.1. Preprocessing of input length-history data. As an initial step, STADIA automatically formats the inputted MT length-history data into a single time series of length-history data points. MT length-history data can be inputted into STADIA either as a long-time observation of a single MT (possible with simulations) or as a series of length histories of multiple MTs (common with experimental data). In the latter case, STADIA automatically connects, or "stitches," the data from multiple MTs (with separators in between) into a single time-series representation of MT length-history data (e.g., Figure 1D). Note that special treatment of the stitching separator between observations allows STADIA to avoid misclassification of stitch boundaries as transitions. This preprocessing step allows STADIA to conduct analysis for both simulation data and experimental data in a similar and consistent manner.

5.5.1.2. Segmentation process. STADIA takes the single time-series length-history graph produced by the preprocessing step and performs segmentation as an adaptive, iterative process. As described in this section, how closely the segmentation fits the length-history plot is regulated by two user-defined parameters: Maximum Error Tolerance and Minimum Segment Duration.

The segmentation process begins by identifying major peaks and valleys (i.e., local extrema) in MT length-history data using the "findpeaks" function in MATLAB. The "findpeaks" function uses inputs of minimum peak prominence (i.e., minimum vertical distance between a major peak and nearest major valley) and minimum peak height. The values that STADIA uses for the minimum peak prominence and the minimum peak height in "findpeaks" are the same values, respectively, as the user-input values of the Maximum Error Tolerance and the Nucleation Height Threshold.

Consecutive extrema are connected by line segments to form an initial linear approximation of the length-history data (Figure 2C). An initial list of vertices is defined by these peaks and valleys.

New vertices are added to mark the locations where the MT length crosses the user-input Nucleation Height Threshold, generally chosen to be near the lower limit of observation in experimental conditions. When a MT crosses from below to above the threshold (i.e., a growing MT), the vertex is added at the last data point less than or equal to the Nucleation Height Threshold. When a MT crosses from above to below the threshold (i.e., a shortening MT), the vertex is added at the first data point less than or equal to the Nucleation Height Threshold. At the classification stage described below (Section 5.5.2), segments that are entirely below the Nucleation Height Threshold are excluded from further analysis because these segments are generally not experimentally detectable (note that in our in vitro data sets none of the tracked lengths are below the nucleation threshold).

Then, the iterative process seeks to include new vertices to define line segment endpoints. This improves the approximation accuracy by constructing a continuous piecewise linear approximation that satisfies the user-defined parameters of Maximum Error Tolerance and Minimum Segment Duration mentioned above (Figure 2D). Note that the segmentation algorithm implemented in STADIA is similar, but not identical, to the "top-down" category of algorithms reviewed in Keogh *et al*. (2001).

STADIA's segmentation algorithm can be explained in the following steps:

1. Let $\{x^1, x^2, \ldots, x^N\}$ represent the initial list of vertices (i.e., segment endpoints), where x^1 and x^N are the first and last points of the length-history data, respectively, and $\{x^2, \ldots, x^{N-1}\}$ are the consecutive peaks, valleys, and nucleation threshold points described above.
2. For any $i = 1, \ldots, N-1$, define the ith region as the interval between the consecutive pair of initial vertices, x^i and x^{i+1}. Construct a line segment with endpoints as $x_1^i = x^i$ and $x_2^i = x^{i+1}$ such that the vertices corresponding to the ith region are $\{x_1^i, \cdots, x_M^i\}$, where initially $M = 2$, but we seek to grow this list in the following steps.
3. For $j = 1 \ldots, M-1$, consider the jth line segment in the ith region defined by x_j^i and x_{j+1}^i. Calculate the error (absolute value of the difference) between this line segment and the corresponding points in the original length-history data.
   - If the maximum error is greater than the user-defined Maximum Error Tolerance, then the error condition is not satisfied, and an additional data point needs to be included in the vertex list. Proceed to step 4.
   - If the maximum error from this segment is less than the user-defined Maximum Error Tolerance, then the error condition is satisfied for the jth line segment in the ith region. Proceed to step 6.
4. Define the data point where the greatest error occurs in step 3 as x_{new}^i
   - If x_{new}^i violates the user-defined Minimum Segment Duration, attempt to choose the closest point in the length-history data that would satisfy both the Maximum Error Tolerance and Minimum Segment Duration.
5. Include the newly identified vertex into the list of vertices for the ith region. This will require reindexing to preserve ordering. For example, for the first new vertex added to the ith region, the original single segment in the ith region is now broken into two segments, and the list of vertices corresponding to the ith region is now defined as

   $$\{x_1^i, x_2^j, x_3^j\} = \{x_1^i, x_{new}^i, x_2^j\}$$

   where the vertex list on the right side is indexed according to the preceding iteration and the updated vertex list on the left side replaces the list defined in step 2, such that $x_j^i < x_{j+1}^i$ for all $j = 1, \ldots, 1, M-1$.
6. Repeat steps 3–5 until the error condition is satisfied without adding more vertices into the ith region.
7. Repeat steps 2–6 for all $i \leq N-1$.

The final result is a continuous piecewise linear approximation of the inputted length-history data set (excerpts of the full length-history approximation are illustrated in Figure 2D, orange lines, and Figure 2, G and J, black lines). The vertices of the piecewise linear approximations provide line segments with endpoints at moments where significant changes in slope occur in length-history plots. Thus, the activity covered by each segment between endpoints represents a consistent period of MT length-history behavior that can be identified as belonging to a DI phase in the classification stage.

5.5.1.3. Justification for segmentation method. To create a more accurate approximation of MT length-history data as compared with more classical methods that identify segment endpoints only at peaks and valleys (Figure 2, A–C), STADIA employs the iterative approach described above in Section 5.5.1.2 to create an improved continuous piecewise linear approximation of the MT length-history data. The resulting approximation satisfies the user-defined Maximum Error Tolerance and Minimum Segment Duration (Figure 2D). We chose this approach because it provides a simple method for identifying points that may not necessarily be peaks or valleys, but where a change from one sustained MT behavior to another occurs. Through the Maximum Error Tolerance choice, the user is able to regulate the accuracy of the linear approximation. Through the Minimum Segment Duration choice, the user is able to perform the analysis of MT length-history data at the desired timescale. An assumption of performing segmentation in this manner is that MT behavior follows a linear trend at the timescale being analyzed. Finally, we note that this segmentation method in STADIA produces a *continuous* piecewise linear approximation, whereas some other segmentation methods produce *discontinuous* approximations (e.g., Zaliapin *et al.*, 2003).

5.5.1.4. Postprocessing to prepare for classification. For each line segment from the continuous piecewise linear approximation, STADIA measures the slope, time duration, and height change of the segment (Figure 2D); this set of measurements provides a 3-D feature space where the segments reside (Figure 2E).

5.5.1.5. Justification for using all three of slope, time duration, and height change in the classification feature space. Mathematically, knowing the values of any two of the segment variables (time duration, height change, and slope) provides sufficient information to calculate the value of the remaining third variable. However, we use all three variables in the clustering step because some data points that are well separated in the 3-D space would become indistinguishable for all practical purposes if only two of the variables were used (Supplemental Figures S1.2 and S1.3). Additionally, which data points become indistinguishable would depend on which pair of variables was used (time duration and height change, time duration and slope, or height change and slope).

The slope = height/time surface (Supplemental Figures S1.2A and S1.3E) could be parameterized with only two variables in a way that would maintain the separation present in the 3-D space. However, these two new variables would be some combination of the original three variables, and these combinations would not necessarily have clear physical meanings. We therefore chose to use all three of the basic variables (time duration, height change, and slope) to maintain a more direct connection to the biology.

The inclusion of nonlinear combinations of variables (i.e., interaction terms) is not uncommon in statistics (e.g., Rawlings *et al.*, 1998; Karaca-Mandic *et al.*, 2012; Matuschek and Kliegl, 2018). Additional combinations of our three basic variables as well as other variables may be worth exploring in future work that aims to further dissect MT length-history behaviors. For the purposes of the present work, the three basic variables are sufficient for verifying the existence of distinguishable clusters within the positive and negative slope groups.

5.5.2. Classification stage. The purpose of the classification stage in STADIA is to group the segments from the segmentation stage into subsets that share similar attributes. In the classification procedures, each segment from the approximation of the MT length-history data is represented as a point in the 3-D space generated by segment time duration, height change, and slope (Figure 2, D and E). The classification stage is where differences arise between the two modes of STADIA: Diagnostic Mode aids the user in selecting the number of clusters to use but ends after the clustering step, which is described below in Section 5.5.2.2; Automated Mode requires that the number of clusters be provided as input but performs all other stages of the analysis.

5.5.2.1. Classification first steps—identification of nucleation segments and flat stutters. First, segments that are entirely below the user-input Nucleation Height Threshold described above (Section 5.5.1.2) are classified as "nucleation." These nucleation segments are excluded from further analysis and therefore are excluded from the 3-D plots of segment features (e.g., Figure 3).

Next, STADIA identifies any segments that satisfy either or both of the following criteria:

- the absolute value of the segment's net height change is less than the user-input Maximum Height Change Magnitude for Flat Stutters;
- the absolute value of the segment's slope is less than the Maximum Slope Magnitude for Flat Stutters.

These near-flat segments clearly lack the qualities characteristic of traditionally recognized growth or shortening and thus already qualify as a subset of points that share attributes different from the remaining points requiring classification. Therefore, STADIA assigns them into a class labeled "flat stutters."

We remark that in comparison to the up stutters and down stutters that are identified by the next step of classification (Section 5.5.2.2), flat stutters are relatively rare, in terms of both number of segments and total time spent in each type of segment (Supplemental Figure S1.9). Thus, flat stutters account for only a small share of all stutter behaviors detected.

Removing flat stutters from the rest of the collection of points creates a clear boundary between points that represent positive and negative slope segments. However, we do not simply label the remaining segments as growth and shortening. Instead, further analysis is warranted for two reasons. First, attempting to execute the rest of the classification procedures on the positive and negative slope segments together fails to produce conclusive results (Supplemental Figure S1.6), suggesting that the positive and negative groups should be analyzed separately. Second, complex geometric structures of distinguishable appendages observed in both the positive and negative slope point groups (Figure 3, B and C) suggest that multiple types of behaviors are present within each subset.

5.5.2.2. k-means clustering step of the classification stage. To continue the classification stage, STADIA takes the segments that are now segregated into positive and negative slope line segments and analyzes them using *k*-means clustering (Macqueen, 1967; Lloyd, 1982), where the number of clusters, the *k*-value, is suggested by the gap statistic (Tibshirani *et al.*, 2001).

Justification for using k-means clustering. As an unsupervised clustering algorithm commonly used in machine learning, *k*-means does not require prior knowledge of the characteristics of the clusters to be found in order for the algorithm to identify boundaries that separate them. Rather, *k*-means groups together data points that share similar characteristics (i.e., data points that are near each other in a relevant feature space). The *k*-means algorithm also has

the advantages of its ease of use and interpretability. Ideal data sets for *k*-means have globularly shaped clusters (i.e., each cluster would follow a Gaussian distribution). Although the clusters resulting from our data are not Gaussian per se, *k*-means still provides an objective methodology to find substructures in the overall data structure. The observation that *k*-means enables us to identify and quantify stutters (behaviors that have been noted previously but not quantified in detail) indicates that it provides a useful methodology for categorization and quantification of MT behavior.

Preprocessing of segment data for input into k-means clustering. *k*-means clustering uses Euclidean distance (i.e., straight-line distance) between points in the feature space (3-D space for our data) as the primary measurement in its algorithm to classify data. Therefore, all features should exist on the same scale to give each feature equal weight in the *k*-means classification process. To meet this requirement, the segment features (slope, height change, and time duration values) are transformed by first being log-scaled and then standardized with respect to each feature's statistics (i.e., by subtracting the mean and dividing by the SD) (Figure 3, B and C). Scaling and standardizing the data in this way is a common practice for analysis utilizing *k*-means clustering (Hastie *et al*., 2009).

Determining appropriate number of clusters for each data set. As noted in Section 2.2.1, one of the goals for STADIA development was that it be impartial in determining the number of behaviors exhibited by MTs, thus avoiding any assumptions about MT dynamics being restricted to two behaviors (i.e., only growth and shortening). The *k*-value (i.e., number of clusters to use in *k*-means) is determined for positive and negative slope segments separately and is informed by running the Diagnostic Mode of STADIA.

Though various approaches exist for determining the *k*-value with which to perform the clustering (reviewed by Pham *et al*., 2005; Steinley, 2006), STADIA utilizes a quantity called the gap statistic, which is calculated at each potential value of *k* (Supplemental Figures S1.4 and S1.5, left column) (Tibshirani *et al*., 2001). The gap statistic aids in answering the question, "what number of clusters results in the best separation between the clusters?" More technically, the gap statistic measures the within-cluster dispersion compared with a null reference distribution.

When examining the values of the gap statistic at different values of *k* to seek the optimal number of clusters that best separates the data, higher values of the gap statistic indicate better separation between clusters. However, a significant increase in the value of the gap statistic is generally considered necessary to justify using an additional cluster. Tibshirani *et al*. (2001) formalized this idea with the following criterion: choose the smallest value of *k* such that

$$\text{Gap}(k) \geq \text{Gap}(k+1) - \text{one standard error of Gap}(k+1).$$

In words, this criterion means choose the smallest value of *k* such that the value of the gap statistic does not increase by more than one standard error when going to the next value of *k*. Other possible criteria include choosing the first local maximum of the gap statistic plot or the smallest *k*-value such that the gap value is within one standard error of the first local maximum (Hastie *et al*., 2009; Maechler, 2021). Depending on the particular data set, the different criteria may yield the same *k*-value as each other or different *k*-values.

The Diagnostic Mode of STADIA outputs the *k*-value chosen by the Tibshirani *et al*. (2001) criterion. However, when choosing *k*-values to input into Automated Mode, it is also recommended for the user to examine the gap statistic plots and cluster profiles (Supplemental Figures S1.4 and S1.5) to check how well the number of clusters suggested by the gap statistic describes the data set qualitatively. For example, in some cases, qualitative inspection of the data may suggest that the second local maximum of the gap statistic plot describes the data better than the first local maximum (e.g., as seen in Supplemental Figure S1.4. E and F).

Measuring the gap statistic in Diagnostic Mode. For the purposes of informing the optimal *k*-value for use in *k*-means clustering, the Diagnostic Mode of STADIA repeats the clustering procedure for each potential value of *k* ranging from 1 through 12, using 100 random starts for each value (a single run of *k*-means clustering does not necessarily converge to a global optimum, so multiple starts are required to determine optimal centroid locations). Using the clustering results at each *k*-value, STADIA measures the value of the gap statistic for each value of *k* (Supplemental Figures S1.4 and S1.5).

k-means clustering in Automated Mode. As noted above, the purpose of *k*-means clustering is to group together data points that share similar characteristics (i.e., data points that are near each other in the feature space of segment slope, height change, and time duration). Once the optimal number of clusters is determined for both positive and negative slope segments using the Diagnostic Mode of STADIA, the user inputs these *k*-values and runs STADIA in Automated Mode. In Automated Mode, STADIA performs *k*-means clustering, on the positive and negative slope segments separately, using 500 random starts. Centroid locations that attain the lowest sum of squared distances between the centroids and each point in their respective clusters are chosen for further analysis. The chosen centroid locations are indicted by x-symbols in the cluster plots (e.g., Figure 3, D and E).

5.5.2.3. Phase/behavior bundling step of the classification stage. After *k*-means clustering is performed on the log-transformed and standardized data, the resulting cluster assignments are applied to the original segment data (i.e., the data before applying log-transformation and standardization; Supplemental Figure S1.7). Statistics such as average slopes, average time duration, and average height change are calculated for each cluster (slopes in Figure 4, C and F; slopes and time durations in Supplemental Figure S1.8) and then utilized for naming the clusters (Figure 3G). Clusters with similar average slopes are bundled together to form larger groups, which we refer to as "phase classes" or "behavior classes" (Figures 2H and 4I). Groups of clusters with large positive slopes are classified as growth, while those with large negative slopes are classified as shortening. The remaining clusters with segment slopes considerably smaller in magnitude (i.e., flatter) are grouped into the category of behaviors called "stutters" (along with the "flat stutters," which were separated out before the clustering process).

At this point, every segment identified during the segmentation stage has been classified as growth, shortening, stutter, or nucleation. Applying these phase class labels to each segment in the length-history plot is illustrated in Figure 2, G and J.

5.5.3. Phase and transition analysis stage. After classifying segments into clusters and then bundling the clusters into larger phase/behavior classes as described above (Section 5.5.2), classical methods of calculating DI metrics are adapted to account for stutters in addition to growth and shortening.

5.5.3.1. Phase analysis. For each cluster, STADIA calculates the average velocity of the segments in the cluster (Table 1, bottom row of each subtable). STADIA also calculates the following cluster attributes (Supplemental Figure S1.9):

- total number of segments (counts obtained from the piecewise linear approximation) in each cluster,
- percent time spent in each cluster $= \left(\frac{\text{sum of segment time durations in cluster}}{\text{total time of data set}} \times 100\% \right)$,
- and percent height change corresponding to each cluster $= \left(\frac{\text{sum of segment height change magnitudes in cluster}}{\text{sum of all segment height change magnitudes}} \times 100\% \right)$.

These attributes can be determined for each of the larger phase/behavior classes (i.e., growth, shortening, stutters) by combining the measurements for the clusters in each class (Figure 5A).

5.5.3.2. Transition analysis. Transition frequencies are calculated in a manner similar to what has been done classically. However, when considering stutters in addition to growth and shortening, there are additional transitions to quantify (Figure 2I). In particular, it is necessary to determine whether catastrophes and rescues are or are not directly preceded by stutters. Catastrophes and rescues are identified as either abrupt (occurring without detectable stutters) or transitional (occurring via a stutter) (Figures 5–7). Additionally, our analysis quantifies interrupted growth (growth → stutter → growth) (Figures 5H, 6, and 7, H and I) and interrupted shortening (shortening → stutter → shortening) (Figure 5I).

As mentioned above in Section 5.5.2.1, MTs shorter than the user-defined Nucleation Height Threshold are considered to be in "nucleation" phases. Transitions into or out of nucleation phases are not analyzed by the current version of STADIA because such MTs would be difficult to detect in experiments, and their behavior might be influenced by proximity to the seed.

In agreement with what has been done in classic DI analyses, frequencies of catastrophe and rescue are calculated as the ratio of the number of catastrophe or rescue events to the total time spent in growth or shortening, respectively (Table 1). For the additional types of transitions identified by STADIA (Figure 2I), the frequencies are calculated in a similar manner: the frequency of each type of transition out of growth or shortening is calculated as the ratio of the number of transition events of that type to the total time spent in growth or shortening, respectively (Supplemental Figure S1.10). More specifically,

$$F_{\text{AbruptCatastrophe}} = \frac{\text{\# of abrupt catastrophes}}{\text{total time spent in growth}},$$

$$F_{\text{TransitionalCatastrophe}} = \frac{\text{\# of transitional catastrophes}}{\text{total time spent in growth}},$$

$$F_{\text{InterruptedGrowth}} = \frac{\text{\# of growth interruptions}}{\text{total time spent in growth}},$$

$$F_{\text{AbruptRescue}} = \frac{\text{\# of abrupt rescues}}{\text{total time spent in shortening}},$$

$$F_{\text{TransitionalRescue}} = \frac{\text{\# of transitional rescues}}{\text{total time spent in shortening}},$$

$$F_{\text{InterruptedShortening}} = \frac{\text{\# of shortening interruptions}}{\text{total time spent in shortening}}.$$

The total F_{cat} equals $F_{\text{AbruptCatastrophe}} + F_{\text{TransitionalCatastrophe}}$ (Figure 7C; Supplemental Figure S1.10), and the total F_{res} equals $F_{\text{AbruptRescue}} + F_{\text{TransitionalRescue}}$ (Supplemental Figure S1.10). Similarly, the total frequency of growth-to-stutter transitions equals $F_{\text{TransitionalCatastrophe}} + F_{\text{InterruptedGrowth}}$ (Figure 7C), and the total frequency of shortening-to-stutter transitions equals $F_{\text{TransitionalRescue}} + F_{\text{InterruptedShortening}}$.

5.6. Guidance for users: expectations for input data and effect of thresholds

STADIA is ideally intended for use on data sets with moderate or high temporal resolution, for example, at least 2 fps. For lower resolution data sets, we suggest that STADIA will provide more systematic analysis than manual methods, but the resolution of the data themselves will be a limiting factor in what conclusions can be supported.

We expect that the most common difficulty will be obtaining a total amount of data that is large enough for effective clustering during the classification stage. The clustering process performs better as the amount of data increases; more specifically, determining the optimal number of clusters and assigning segments to the appropriate cluster is done more accurately when there are more data points in the segment feature space (e.g., Figure 3). The total time duration of MT length-history data required will generally be on the order of hours, not minutes. To determine whether one has a sufficient quantity of data, we recommend two possible tests. First, users should examine the error bars in the gap statistic plots generated by Diagnostic Mode; if the error bars are too large to conclusively choose an optimal *k*-value, then more data may be needed. Second, we suggest that users run STADIA on their entire data set and on half of their data set; if both cases yield similar clustering results, this indicates that the user has a sufficient quantity of data. If one has an insufficient amount of data for effective clustering, STADIA can still be used to perform segmentation, detection of flat stutters with user-defined parameters, and clustering with $k = 1$ (one cluster each for positive and negative slope segments), because these analyses do not depend on the number of data points in the feature space; on the contrary, the number of data points in the feature space depends on the number of segments in the segmentation. However, DI metrics resulting from sparse data sets should be treated with caution.

As one specific example of the amount of data needed, in the in silico results presented here, we used 10 h of simulation time to ensure that enough segments were generated for effective clustering. Testing different total time durations of data yielded consistent results for simulations that ran for 7.5 h or longer when using STADIA in Diagnostic Mode. However, using significantly shorter length-history data sets (e.g., 2.5 h) did not provide acceptable clustering results. On the other hand, if the number of clusters (i.e., *k*-values) is preestablished (e.g., from a similar but larger data set), then STADIA can be used in Automated Mode to calculate DI metrics from significantly fewer data (e.g., at least 2.5 h).

It is important for users to be aware that the values of inputted thresholds will affect the numerical values of results of STADIA (as well as any other DI analysis method; e.g., Odde *et al.*, 1996; Gierke *et al.*, 2010; Matov *et al.*, 2010; Smal *et al.*, 2010; Prahl *et al.*, 2014; Guo *et al.*, 2018). For examples of the effects of changing these values, see the analyses with varied values of the Minimum Segment Duration and Maximum Error Tolerance in STADIA and the data acquisition rate of the length-history data as shown in Supplemental Sections S2 and S3. We recommend that users try at least a few different values of thresholds to test the strength of any conclusions they draw. In articles using STADIA, users should report the values

of the input parameters that they use in STADIA, in addition to reporting the resolution of their measurements, quantity of data, and values of any other relevant quantities.

At the segmentation stage, users should examine the piecewise linear approximation to ensure that the approximation is not overfitting or underfitting the raw data. The user's choices for the values of the Minimum Segment Duration and Maximum Error Tolerance determine how closely the piecewise linear approximation will fit the raw length-history data. When choosing the values of these thresholds, the user should take into account the resolution and noise level of their data as well as the timescale of the dynamics that the user wishes to study. For example, there are small-amplitude stochastic fluctuations that occur within growth, shortening, and stutter segments; if the user is studying phases at a scale similar to what we study in this article, which is a larger scale than the small-amplitude fluctuations, then the Minimum Segment Duration and Maximum Error Tolerance should not be so small as to pick up these fluctuations.

Note that for certain combinations of the Minimum Segment Duration and Maximum Error Tolerance, STADIA will produce "irreconcilable errors." These errors occur because it is not always possible to satisfy both the Minimum Segment Duration and the Maximum Error Tolerance. In such cases, STADIA outputs a warning to the user for each error. Such errors are most likely to occur if the user has chosen a long Minimum Segment Duration with a small Maximum Error Tolerance. The specific values of Minimum Segment Duration and Maximum Error Tolerance that result in irreconcilable errors will depend on the particular data set being analyzed. If such errors occur, the user should either change the parameter values or recognize that some segments of the piecewise linear approximation will not meet the input criteria.

If the user is aiming to identify one set of input parameter values or a small number of parameter sets that are ideal for their particular data set, then we recommend that the user choose input parameter values that minimize the number of irreconcilable errors. Our parameter sensitivity analysis (Section 2.6 and Supplemental Material Sections S2 and S3) indicates that the number of irreconcilable errors is more sensitive to the Maximum Error Tolerance than to the Minimum Segment Duration. For our in silico data set, the percentage of segments that have irreconcilable errors has a local minimum at Maximum Error Tolerance = 20 dimer lengths. The percentage of segments that have irreconcilable errors is also low for Maximum Error Tolerance > 40 dimer lengths but is very high for Maximum Error Tolerance < 15 dimer lengths. If the user is performing a parameter sensitivity analysis with a large range of parameter values (similar to the range used in Supplemental Material Sections S2 and S3), then the user should be aware that some parameter combinations may result in a large number of irreconcilable errors.

For further instructions on how to use the STADIA MATLAB code, we refer readers to Patel *et al*. (2020). Note that the input parameter called the "Minimum Segment Duration" here was referred to as the "minimum time step" in Patel *et al*. (2020).

Software and data availability

STADIA software (MATLAB code) and tutorials can be downloaded from GitHub (https://github.com/GoodsonLab/STADIA/). Data analyzed in this paper are available from the authors upon request.

ACKNOWLEDGMENTS

This work was supported by National Science Foundation (NSF) grants MCB-1244593 to H.V.G. and M.A., MCB-1817966 to H.V.G., and MCB-1817632 to E.M.J., National Institutes of Health (NIH) grant R35GM119552 to M.Z., and National Institutes of Health Integrated Biological Systems Training in Oncology training grant T32CA119925 to E.J.L. M.Z. also acknowledges the Searle Scholars Program. Portions of the work were also supported by funding from the University of Massachusetts Amherst (A.J.M.), NSF-GFRP DGE-1313583 (K.S.M.), and a fellowship from the Dolores Zohrab Liebmann Fund (S.M.M.). We thank the members of the Goodson laboratory and the Chicago Cytoskeleton community for their insightful discussions.

REFERENCES

Aher A, Kok M, Sharma A, Steinmetz MO, Dogterom M, Akhmanova A (2018). CLASP suppresses microtubule catastrophes through a single TOG Domain. Dev Cell 46, 40–58.

Andrecka J, Arroyo JO, Lewis K, Cross RA, Kukura P (2016). Label-free imaging of microtubules with sub-Nm precision using interferometric scattering microscopy. Biophys J 110, 214–217.

Applegate KT, Besson S, Matov A, Bagonis MH, Jaqaman K, Danuser G (2011). PlusTipTracker: quantitative image analysis software for the measurement of microtubule dynamics. J Struct Biol 176, 168–184.

Blackwell R, Sweezy-Schindler O, Edelmaier C, Gergely ZR, Flynn PJ, Montes S, Crapo A, Doostan A, McIntosh JR, Glaser MA, *et al*. (2017). Contributions of microtubule dynamic instability and rotational diffusion to kinetochore capture. Biophys J 112, 552–563.

Castle BT, Odde DJ (2013). Brownian dynamics of subunit addition-loss kinetics and thermodynamics in linear polymer self-assembly. Biophys J 105, 2528–2540.

Castoldi M, Popov AV (2003). Purification of brain tubulin through two cycles of polymerization–depolymerization in a high-molarity buffer. Protein Expr Purif 32, 8388.

Coombes CE, Yamamoto A, Kenzie MR, Odde DJ, Gardner MK (2013). Evolving tip structures can explain age-dependent microtubule catastrophe. Curr Biol 23, 1342–1348.

Desai A, Mitchison TJ (1997). Microtubule polymerization dynamics. Annu Rev Cell Dev Biol 13, 83–117.

Dhamodharan R, Jordan MA, Thrower D, Wilson L, Wadsworth P (1995). Vinblastine suppresses dynamics of individual microtubules in living interphase cells. Mol Biol Cell 6, 1215–1229.

Dhamodharan R, Wadsworth P (1995). Modulation of microtubule dynamic materials and in vivo by brain microtubule associated proteins. J Cell Sci 108(Pt 4), 1679–1689.

Dillon GM, Tyler WA, Omuro KC, Kambouris J, Tyminski C, Henry S, Haydar TF, Beffert U, Ho A (2017). CLASP2 links reelin to the cytoskeleton during neocortical development. Neuron 93. 1344–1358.

Dogterom M, Leibler S (1993). Physical aspects of the growth and regulation of microtubule structures. Phys Rev Lett 70, 1347–1350.

Doodhi H, Prota AE, Rodríguez-García R, Xiao H, Custar DW, Bragsten K, Katrukha EA, Hilbert M, Hua S, Jiang K, *et al*. (2016). Termination of protofilament elongation by eribulin induces lattice defects that promote microtubule catastrophes. Curr Biol 26, 1713–1721.

Duan AR, Jonasson EM, Alberico EO, Li C, Scripture JP, Miller RA, Alber MS, Goodson HV (2017). Interactions between Tau and different conformations of tubulin: implications for Tau function and mechanism. J Mol Biol 429, 1424–1438.

Duellberg C, Cade NI, Holmes D, Surrey T (2016a). The size of the EB cap determines instantaneous microtubule stability. eLife 5, e13470.

Duellberg C, Cade NI, Surrey T (2016b). Microtubule aging probed by microfluidics-assisted Tubulin washout. Mol Biol Cell 27, 3563–3573.

Fees CP, Estrem C, Moore JK (2017). High-resolution imaging and analysis of individual astral microtubule dynamics in budding yeast. J Vis Exp 2017, 55610.

Fu TC (2011). A review on time series data mining. Engineering Applications of Artificial Intelligence 24, 164–181.

Gardner MK, Charlebois BD, Jánosi IM, Howard J, Hunt AJ, Odde DJ (2011). Rapid microtubule self-assembly kinetics. Cell 146, 582–592.

Gell C, Bormuth V, Brouhard GJ, Cohen DN, Diez S, Friel CT, Helenius J, Nitzsche B, Petzold H, Ribbe J, *et al*. (2010). Microtubule dynamics reconstituted in vitro and imaged by single-molecule fluorescence microscopy. Methods Cell Biol 95, 221–245.

Gierke S, Kumar P, Wittmann T (2010). Analysis of microtubule polymerization dynamics in live cells. Methods Cell Biol 97, 15–33.

Gildersleeve RF, Cross AR, Cullen KE, Fagen AP, Williams RC (1992) Microtubules grow and shorten at intrinsically variable rates. J Biol Chem 267, 7995–8006.

Gillespie DT (1976). A general method for numerically simulating the stochastic time evolution of coupled chemical reactions. J Comput Phys 22, 403–434.
Gillespie DT (1977). Exact stochastic simulation of coupled chemical reactions. J Phys Chem 81, 2340–2361.
Girão H, Okada N, Rodrigues TA, Silva AO, Figueiredo AC, Garcia Z, Moutinho-Santos T, Hayashi I, Azevedo JE, Macedo-Ribeiro S, *et al*. (2020). CLASP2 binding to curved microtubule tips promotes flux and stabilizes kinetochore attachments. J Cell Biol 219, e201905080.
Goodson HV, Jonasson EM (2018). Microtubules and microtubule-associated proteins. Cold Spring Harb Perspect Biol 10, a022608.
Guo Y, Li Di, Zhang S, Yang Y, Liu J-J, Wang X, Liu C, Milkie DE, Moore RP, Tulu US, *et al*. (2018). Visualizing intracellular organelle and cytoskeletal interactions at nanoscale resolution on millisecond timescales. Cell 175, 1430–1442.
Gupta KK, Li C, Duan A, Alberico EO, Kim OV, Alber MS, Goodson HV (2013). Mechanism for the catastrophe-promoting activity of the microtubule destabilizer Op18/Stathmin. Proc Natl Acad Sci USA 110, 20449–20454.
Hastie T, Tibshirani R, Friedman J (2009). Springer Series in Statistics: The Elements of Statistical Learning, 2nd ed., New York: Springer Science+Business Media, LLC.
Howard J, Hyman AA (2009). Growth, fluctuation and switching at microtubule plus ends. Nat Rev Mol Cell Biol 10, 569–574.
Hyman A, Drechsel D, Kellogg D, Salser S, Sawin K, Steffen P, Wordeman L, Mitchison T (1991). Preparation of modified tubulins. Methods Enzymol 196, 478–485.
Hyman AA, Salser S, Drechsel DN, Unwin N, Mitchison TJ (1992). Role of GTP hydrolysis in microtubule dynamics: information from a slowly hydrolyzable analogue, GMPCPP. Mol Biol Cell 3, 1155–1167.
Jánosi IM, Chrétien D, Flyvbjerg H (2002). Structural microtubule cap:s, catastrophe, rescue, and third state. Biophys J 83, 1317–1330.
Janson ME, Dogterom M (2004). Scaling of microtubule force-velocity curves obtained at different tubulin concentrations. Phys Rev Lett 92, 248101.
Jonasson EM, Mauro AJ, Li C, Labuz EC, Mahserejian SM, Scripture JP, Gregoretti IV, Alber M, Goodson HV (2020). Behaviors of individual microtubules and microtubule populations relative to critical concentrations: dynamic instability occurs when critical concentrations are driven apart by nucleotide hydrolysis. Mol Biol Cell 31, 589–618.
Kamath K, Oroudjev E, Jordan MA (2010). Determination of microtubule dynamic instability in living cells. Methods Cell Biol 97, 1–14.
Kapoor V, Hirst WG, Hentschel C, Preibisch S, Reber S (2019). MTrack: automated detection, tracking, and analysis of dynamic microtubules. Sci Rep 9, 3794.
Karaca-Mandic P, Norton EC, Dowd B (2012). Interaction terms in nonlinear models. Health Serv Res 47, 255–274.
Keller PJ, Pampaloni F, Lattanzi G, Stelzer EHK (2008). Three-dimensional microtubule behavior in xenopus egg extracts reveals four dynamic states and state-dependent elastic properties. Biophys J 95, 1474–1486.
Keogh E, Chu S, Hart D, Pazzani M (2001). An online algorithm for segmenting time series. In: Proceedings—IEEE International Conference on Data Mining, ICDM, 289–296.
Kiris E, Ventimiglia D, Feinstein SC (2010). Quantitative analysis of MAP-mediated regulation of microtubule dynamic instability in vitro-focus on tau. Methods Cell Biol 95, 481–503.
Komarova YA, Vorobjev IA, Borisy GG (2002). Life cycle of MTs: persistent growth in the cell interior, asymmetric transition frequencies and effects of the cell boundary. J Cell Sci 115, 3527–3539.
Kruse R, Krantz J, Barker N, Coletta RL, Rafikov R, Luo M, Højlund K, Mandarino LJ, Langlais PR (2017). Characterization of the CLASP2 protein interaction network identifies SOGA1 as a microtubule-associated protein. Mol Cell Proteomics 16, 1718–1735.
Lawrence EJ, Arpag G, Norris SR, Zanic M (2018). Human CLASP2 specifically regulates microtubule catastrophe and rescue. Mol Biol Cell 29, 1168–1177.
Lawrence EJ, Zanic M (2019). Rescuing microtubules from the brink of catastrophe: CLASPs lead the way. Curr Opin Cell Biol 56, 94–101.
Li C, Li J, Goodson HV, Alber MS (2014). Microtubule dynamic instability: the role of cracks between protofilaments. Soft Matter 10, 2069–2080.
Lloyd SP (1982) Least squares quantization in PCM. IEEE Trans Inf Theory 28, 129–136.
Macqueen J (1967). Some methods for classification and analysis of multivariate observations. In: Proceedings of the Fifth Berkeley Symposium on Mathematical Statistics and Probability, Volume 1: Theory of Statistics, 5.1, 281–297. Berkeley and Los Angeles, CA: University of California Press.
Maechler M (2021). R: gap statistic for estimating the number of clusters, 2021. https://stat.ethz.ch/R-manual/R-devel/library/cluster/html/clusGap.html.
Mahrooghy M, Yarahmadian S, Menon V, Rezania V, Tuszynski JA (2015). The use of compressive sensing and peak detection in the reconstruction of microtubules length time series in the process of dynamic instability. Comput Biol Med 65, 25–33.
Majumdar S, Kim T, Chen Z, Munyoki S, Tso S-C, Brautigam CA, Rice LM. (2018) An isolated CLASP TOG domain suppresses microtubule catastrophe and promotes rescue. Mol Biol Cell 29, 1359–1375.
Maly IV (2002). Diffusion approximation of the stochastic process of microtubule assembly. Bull Math Biol 6, 213–238.
Mangeol P, Prevo B, Peterman EJG (2016). KymographClear and KymographDirect: two tools for the automated quantitative analysis of molecular and cellular dynamics using kymographs. Mol Biol Cell 27, 1948–1957.
Margolin G, Goodson HV, Alber MS (2011). Mean-field study of the role of lateral cracks in microtubule dynamics. Phys Rev E 83, 041905.
Margolin G, Gregoretti IV, Cickovski TM, Li C, Shi W, Alber MS, Goodson HV (2012). The mechanisms of microtubule catastrophe and rescue: implications from analysis of a dimer-scale computational model. Mol Biol Cell 23, 642–656.
Matov A, Applegate K, Kumar P, Thoma C, Krek W, Danuser G, Wittmann T (2010). Analysis of microtubule dynamic instability using a plus-end growth marker. Nat Methods 7, 761–768.
Matuschek H, Kliegl R (2018). On the ambiguity of interaction and nonlinear main effects in a regime of dependent covariates. Behav Res Methods 50, 1882–1894.
Maurer SP, Cade NI, Bohner G, Gustafsson N, Boutant E, Surrey T (2014). EB1 accelerates two conformational transitions important for microtubule maturation and dynamics. Curr Biol 24, 372–384.
Mauro AJ, Jonasson EM, Goodson HV (2019). Relationship between dynamic instability of individual microtubules and flux of subunits into and out of polymer. Cytoskeleton 76, 21557.
McIntosh RJ, O'Toole E, Morgan G, Austin J, Ulyanov E, Ataullakhanov F, Gudimchuk N (2018). Microtubules grow by the addition of bent guanosine triphosphate tubulin to the tips of curved protofilaments. J Cell Biol 217, 2691–2708.
Mickolajczyk KJ, Geyer EA, Kim T, Rice LM, Hancock WO (2019). Direct observation of individual tubulin dimers binding to growing microtubules. Proc Natl Acad Sci USA 116, 7314–7322.
Mitchison T, Kirschner M (1984). Dynamic instability of microtubule growth. Nature 312, 237–242.
Moriwaki T, Goshima G (2016). Five factors can reconstitute all three phases of microtubule polymerization dynamics. J Cell Biol 215, 357–368.
Odde DJ, Buettner HM, Cassimeris L (1996). Spectral analysis of microtubule assembly dynamics. AlChE J 42, 1434–1442.
Odde DJ, Cassimeris L, Buettner HM (1995). Kinetics of microtubule catastrophe assessed by probabilistic analysis. Biophys J 69, 796–802.
Panda D, Jordan MA, Chu KC, Wilson L (1996). Differential effects of vinblastine on polymerization and dynamics at opposite microtubule ends. J Biol Chem 271, 29807–29812.
Patel RJ, Murray KS, Martin PO, Sinclair M, Scripture JP, Goodson HV, Mahserejian SM (2020). Using STADIA to quantify dynamic instability in microtubules. Methods Cell Biol 158, 117–143.
Pedigo S, Williams RC (2002). Concentration dependence of variability in growth rates of microtubules. Biophys J 83, 1809–1819.
Pham DT, Dimov SS, Nguyen CD (2005). Selection of K in K-means clustering. Proc Inst Mech Eng Part C J Mech Eng Sci 219, 103–119.
Portran D, Schaedel L, Xu Z, Théry M, Nachury MV (2017). Tubulin acetylation protects long-lived microtubules against mechanical ageing. Nat Cell Biol 19, 391–398.
Prahl LS, Castle BT, Gardner MK, Odde DJ (2014). Quantitative analysis of microtubule self-assembly kinetics and tip structure. Methods Enzymol 540, 35–52.
Rawlings J, Pantula S, Dickey D (eds.) (1998). Applied Regression Analysis. Applied Regression Analysis (Second Edition), New York, NY: Springer-Verlag.
Rickman J, Duellberg C, Cade NI, Griffin LD, Surrey T (2017). Steady-state EB cap size fluctuations are determined by stochastic microtubule growth and maturation. Proc Nat Acad Sci USA 114, 3427–3432.
Rusan NM, Fagerstrom CJ, Yvon AMC, Wadsworth P (2001). Cell cycle-dependent changes in microtubule dynamics in living cells expressing green fluorescent protein-α tubulin. Mol Biol Cell 12, 971–980.
Sammak PJ, Borisy GG (1988). Direct observation of microtubule dynamics in living cells. Nature 332, 724–726.

Schek HT, Gardner MK, Cheng J, Odde DJ, Hunt AJ (2007). Microtubule assembly dynamics at the nanoscale. Curr Biol 17, 1445–1455.
Schulze E, Kirschner M (1988). New features of microtubule behaviour observed in vivo. Nature 334, 356–359.
Smal I, Grigoriev I, Akhmanova A, Niessen WJ, Meijering E (2010). Microtubule dynamics analysis using kymographs and variable-rate particle filters. IEEE Trans Image Process 19, 1861–1876.
Sousa A, Reis R, Sampaio P, Sunkel CE (2007). The *Drosophila* CLASP homologue, mast/orbit regulates the dynamic behaviour of interphase microtubules by promoting the pause state. Cell Motil Cytoskeleton 64, 605–620.
Steinley D (2006). K-means clustering: a half-century synthesis. Br J Math Stat Psychol 59, 1–34.
Tibshirani R, Walther G, Hastie T (2001). Estimating the number of clusters in a data set via the gap statistic. J R Statist Soc Series B Methodol 63, 411423.
Toso RJ, Jordan MA, Farrell KW, Matsumoto B, Wilson L (1993) Kinetic stabilization of microtubule dynamic instability in vitro by vinblastine. Biochemistry 32, 1285–1293.
Tran PT, Walker RA, Salmon ED (1997). A metastable intermediate state of microtubule dynamic instability that differs significantly between plus and minus ends. J Cell Biol 138, 105–117.
VanBuren V, Cassimeris L, Odde DJ (2005). Mechanochemical model of microtubule structure and self-assembly kinetics. Biophys J 89, 2911–2926.
Verde F, Dogterom M, Stelzer E, Karsenti E, Leibler S (1992). Control of microtubule dynamics and length by cyclin a- and cyclin B-dependent kinases in xenopus egg extracts. J Cell Biol 118, 1097–1108.
Walker RA, O'Brien ET, Pryer NK, Soboeiro MF, Voter WA, Erickson HP, Salmon ED (1988). Dynamic instability of individual microtubules analyzed by video light microscopy: rate constants and transition frequencies. J Cell Biol 107, 1437–1448.
Waterman-Storer CM, Salmon ED (1997). Actomyosin-based retrograde flow of microtubules in the lamella of migrating epithelial cells influences microtubule dynamic instability and turnover and is associated with microtubule breakage and treadmilling. J Cell Biol 139, 417–434.
Yenjerla M, Lopus M, Wilson L (2010). Analysis of dynamic instability of steady-state microtubules in vitro by video-enhanced differential interference contrast microscopy with an appendix by emin oroudjev. Methods Cell Biol 95, 189–206.
Zakharov P, Gudimchuk N, Voevodin V, Tikhonravov A, Ataullakhanov FI, Grishchuk EL (2015). Molecular and mechanical causes of microtubule catastrophe and aging. Biophys J 109, 2574–2591.
Zaliapin I, Gabrielov A, Keilis-Borok V (2003). Multiscale trend analysis. Fractals 12, 275–292.
Zaliapin I, Semenova I, Kashina A, Rodionov V (2005). Multiscale trend analysis of microtubule transport in melanophores. Biophys J 88, 4008–4016.
Zanic M (2016). Measuring the effects of microtubule-associated proteins on microtubule dynamics in vitro. In: The Mitotic Spindle, New York: Humana Press, 47–61.
Zanic M, Widlund PO, Hyman AA, Howard J (2013). Synergy between XMAP215 and EB1 increases microtubule growth rates to physiological levels. Nat Cell Biol 15, 688–693.
Zwetsloot AJ, Tut G, Straube A (2018). Measuring microtubule dynamics. Essays Biochem 62, 725–735.

Supplemental Materials

Molecular Biology of the Cell

Mahserejian *et al*.

<u>Primary Supplement</u> to the manuscript "Quantification of Microtubule Stutters: Dynamic Instability Behaviors that are Strongly Associated with Catastrophe"

Primary Supplement Table of Contents

Separate Supplemental files

MOVIES: Separate supplemental files (**Movies 1-4**) contain movies from the *in vitro* control data corresponding to the kymographs in **Figure 6** of the main text. Note that the images were acquired at 2 fps, while the movies are presented at 7 fps, meaning that the movies are presented at 3.5 x the time labeled on the kymographs and length-history plots.

Movie 1: Corresponds to the kymograph in **Figure 6A** – Example of **Abrupt Catastrophe**
Movie 2: Corresponds to the kymograph in **Figure 6B** – Example of **Abrupt Catastrophe**
Movie 3: Corresponds to the kymograph in **Figure 6C** – Example of **Transitional Catastrophe**
Movie 4: Corresponds to the kymograph in **Figure 6D** – Example of **Transitional Catastrophe**

Each kymograph and corresponding movie also contains at least one example of **Interrupted Growth**, as indicated in **Figure 6**.

Secondary Supplement: The Secondary Supplement is intended for readers who are already familiar with the material in the main text Results and Methods as well as the Primary Supplement. The Secondary Supplement contains **Supplemental Section S2** (STADIA parameter sensitivity analysis), **Supplemental Section S3** (Data acquisition rate sensitivity analysis), and **Supplemental Section S4** (Negative control: two-state model).

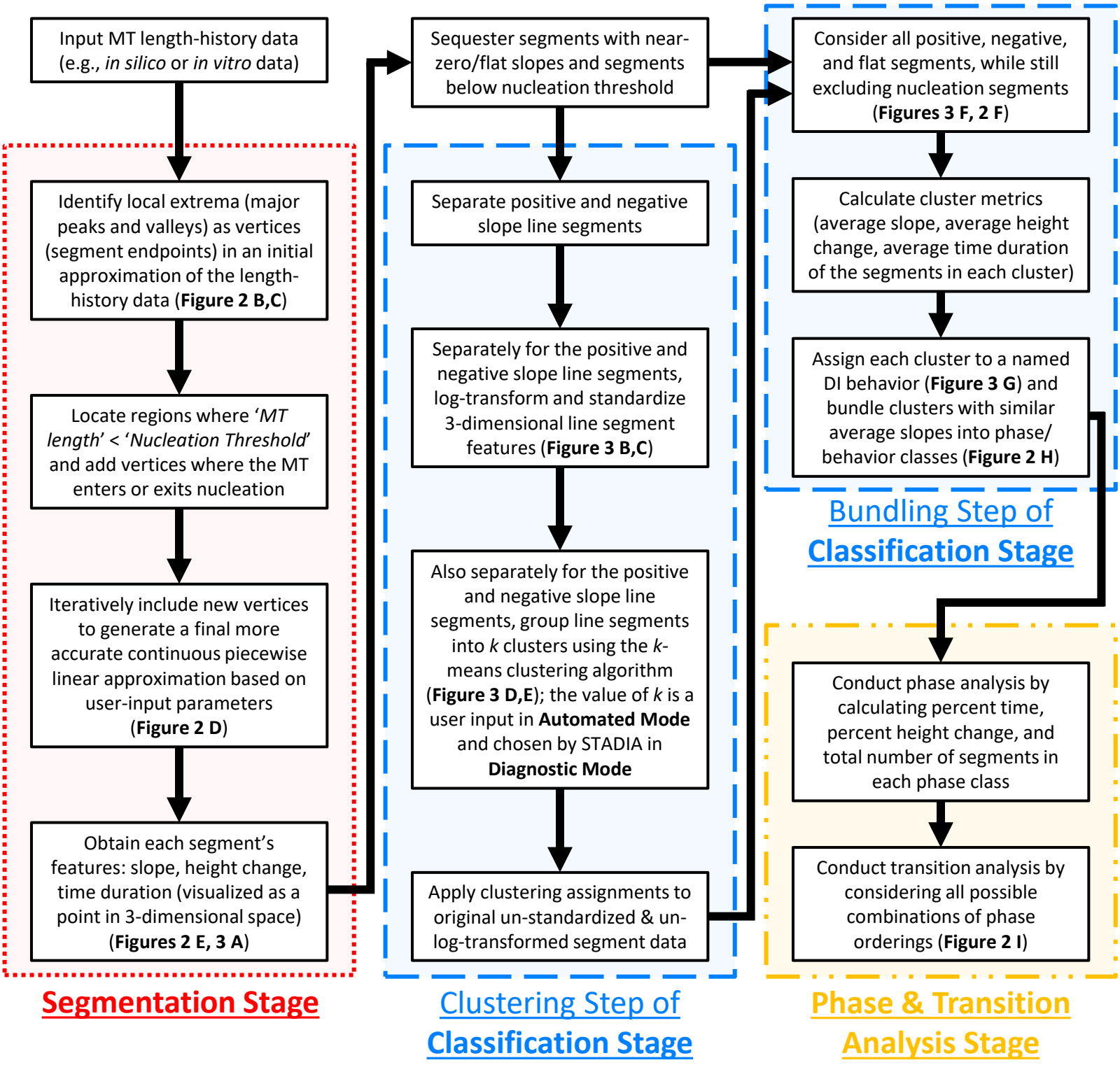

Figure S1.1. Workflow diagram outlining main steps in each stage of STADIA. Note that **Automated Mode** performs all the steps shown in the workflow diagram. **Diagnostic Mode** performs the steps through the end of the clustering step of the classification stage. Running STADIA in **Diagnostic Mode** before **Automated Mode** provides information to aid the user in choosing the optimal number of clusters (*k*-values) to input into **Automated Mode**. Additional information regarding the technical details of STADIA can be found in Methods Sections 4.4 to 4.6 of the main text.

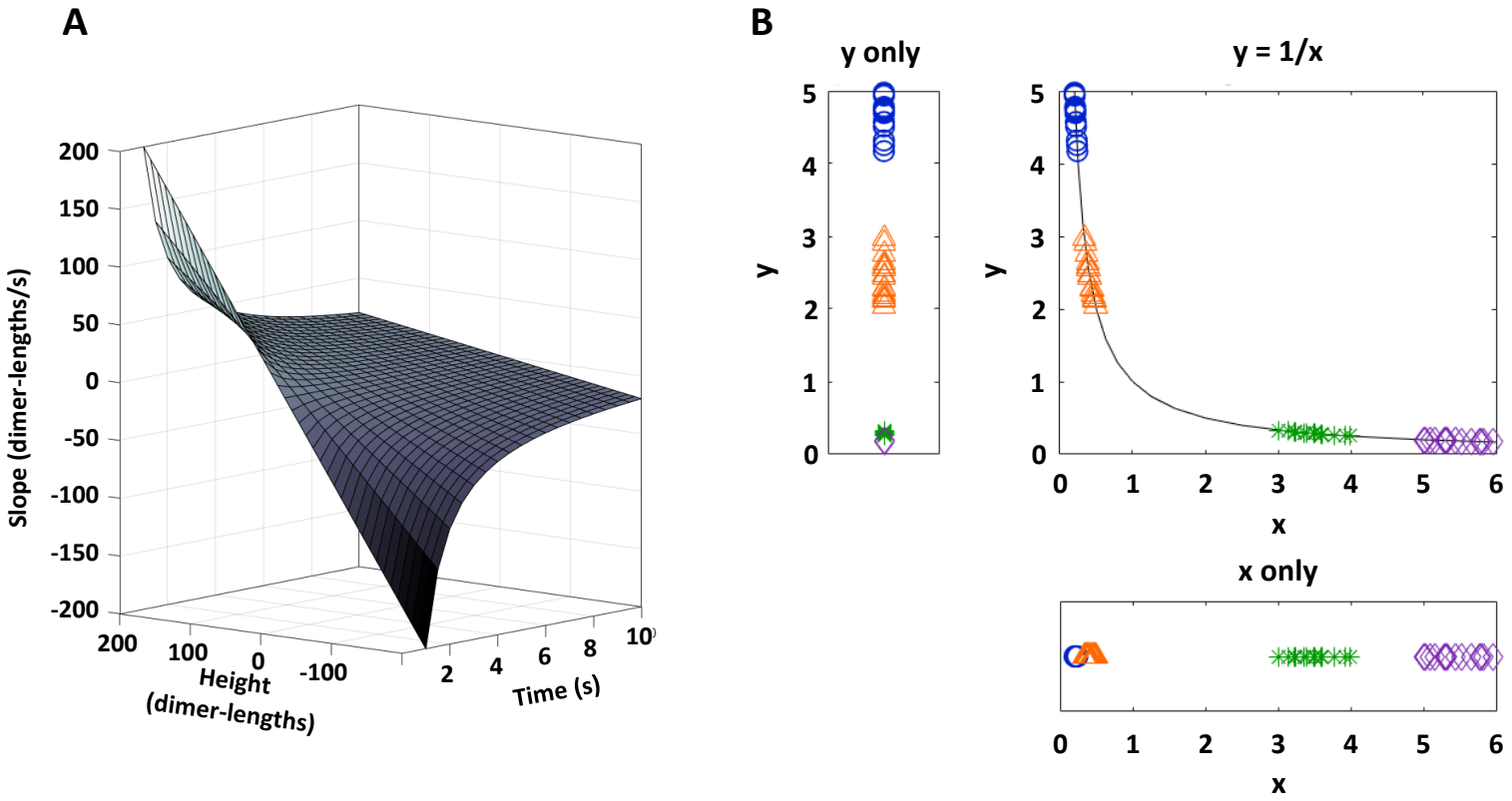

Figure S1.2. Slope=height/time surface in 3-dimensional space, and analogous example in 2 dimensions. (A) Data points representing each line segment from the piecewise linear approximation of length-history data (**Figure 2 D-F**) reside on this Z = Y/X manifold (surface), where Z = slope, X = time, and Y = height. **(B)** A parallel example in two dimensions helps justify using all three segment features (height, time, and slope) in the classification stage. The plotted 2-dimensional dataset contains four clusters (groups) of points that fall on the curve y = 1/x. Plotting using only one dimension (e.g., only y or only x) creates the appearance that this dataset contains only three clusters of points. In contrast, when the data are plotted in two dimensions (y=1/x plot), the data are separated sufficiently to reveal that the dataset actually contains four clusters of points. For similar reasons, we need to consider all three variables in our line segment data to properly identify the clusters in our datasets (see main text Methods Section 4.5.1.5 for additional discussion).

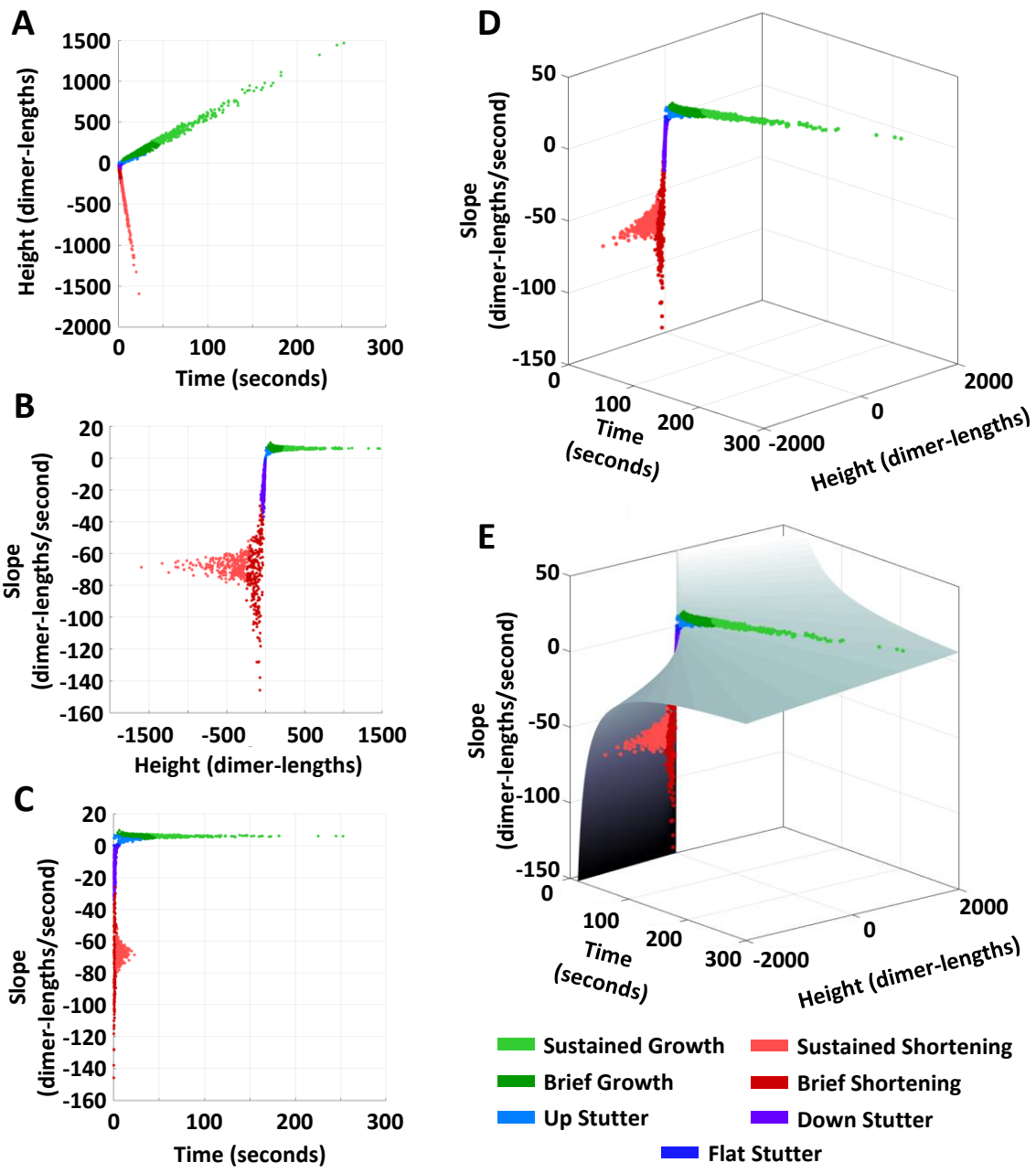

Figure S1.3. The segment features (slope, height change, and time duration) for line segments identified from the piecewise linear approximation of the dimer-scale *in silico* length-history data. Each point corresponds to one line segment from the length-history approximation (**Figure 2 D-F**) and is colored according to the cluster identified by STADIA (**Figure 4**). **(A-C)** Multiple perspectives of the segment feature data represented in two dimensions (Height and Time (A), Slope and Height (B), Slope and Time (C)) demonstrate the lack of separability between points when only two dimensions are considered (similar to the example in **Supplemental Figure S1.2 B**). **(D)** Final clustering profile of all un-standardized and un-log-transformed segment data following the Classification Stage, provided to help visualize the 3-dimensional data. **(E)** An illustration of how the segment points lie on the Z=Y/X manifold described in **Supplemental Figure S1.2 A**.

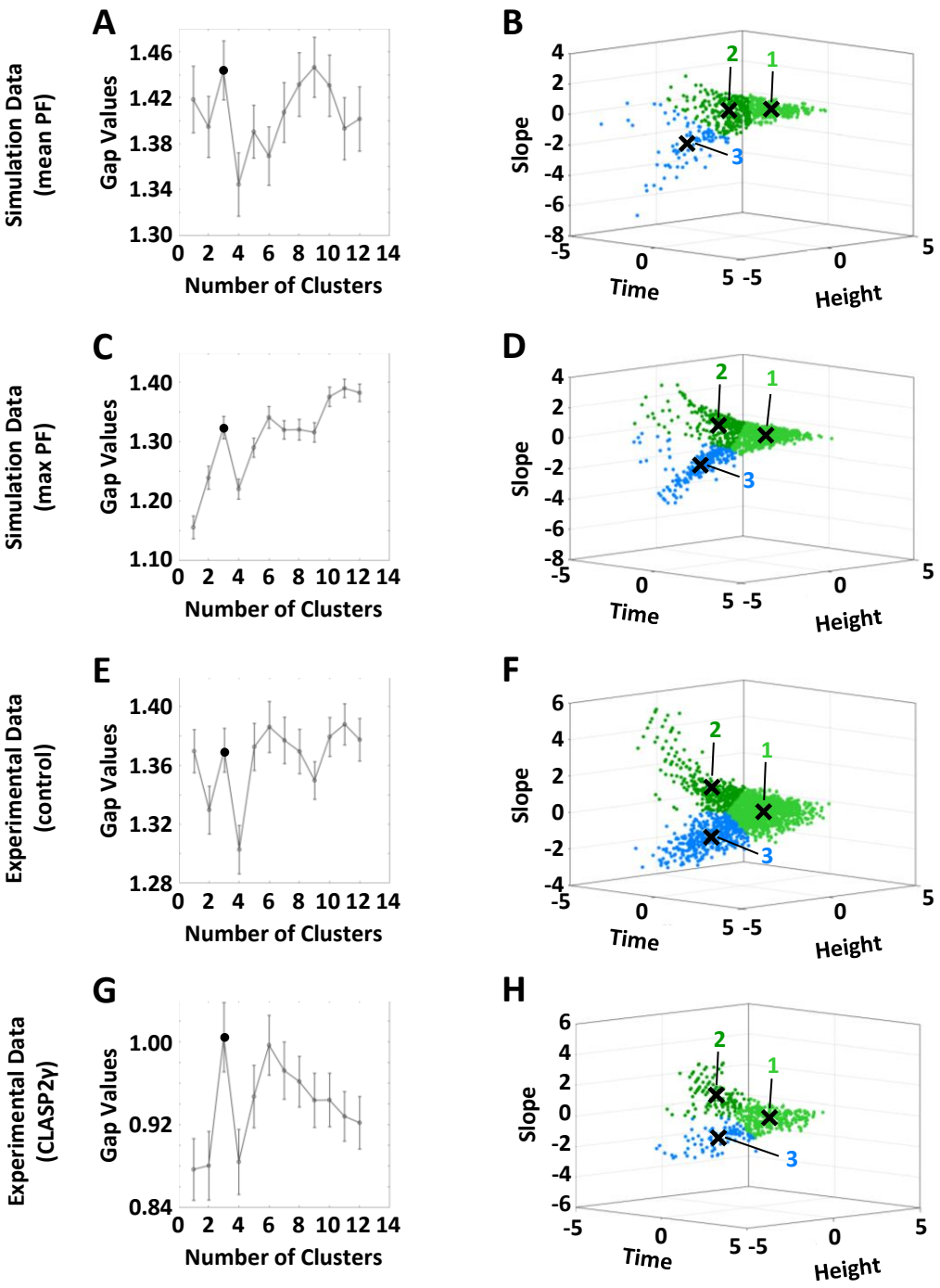

Figure S1.4. Gap statistic plots (left column) and corresponding clustering profiles (right column) for <u>positive</u> slope segments in each dataset. Within each of the cluster profiles (right column), the values of the segment features on each axis are log-transformed and standardized. When using the gap statistic (left column) to suggest the best number of clusters (*k*-value) to use in *k*-means clustering, a common rule of thumb is to use the first *k*-value where the gap statistic plot shows a local maximum. However, the user should also take into consideration visual examination of the cluster profiles and other local maxima in the gap statistic plots. Here, the 3-dimensional data structure (right column) for each of the datasets shows multiple appendages, which indicates that *k* is greater than one (in contrast, a single globular cloud of points would have supported *k*=1). Thus, for all the datasets we selected *k*=3, which is the first local maximum in (C,G) and the second local maximum in (A,E). Consequently, for all positive slope segment data, we performed *k*-means clustering by separating the data into 3 clusters.

These data for the positive slope segments also show that the clustering profile of the simulation data using the max PF length, rather than the mean PF length, more closely resembles the clustering profile of the experimental data (note that for the mean PF data, there are fewer rapid, short duration segments in cluster 2). Therefore, we chose to use the max PF data instead of the mean PF data for presenting the STADIA results in the main text.

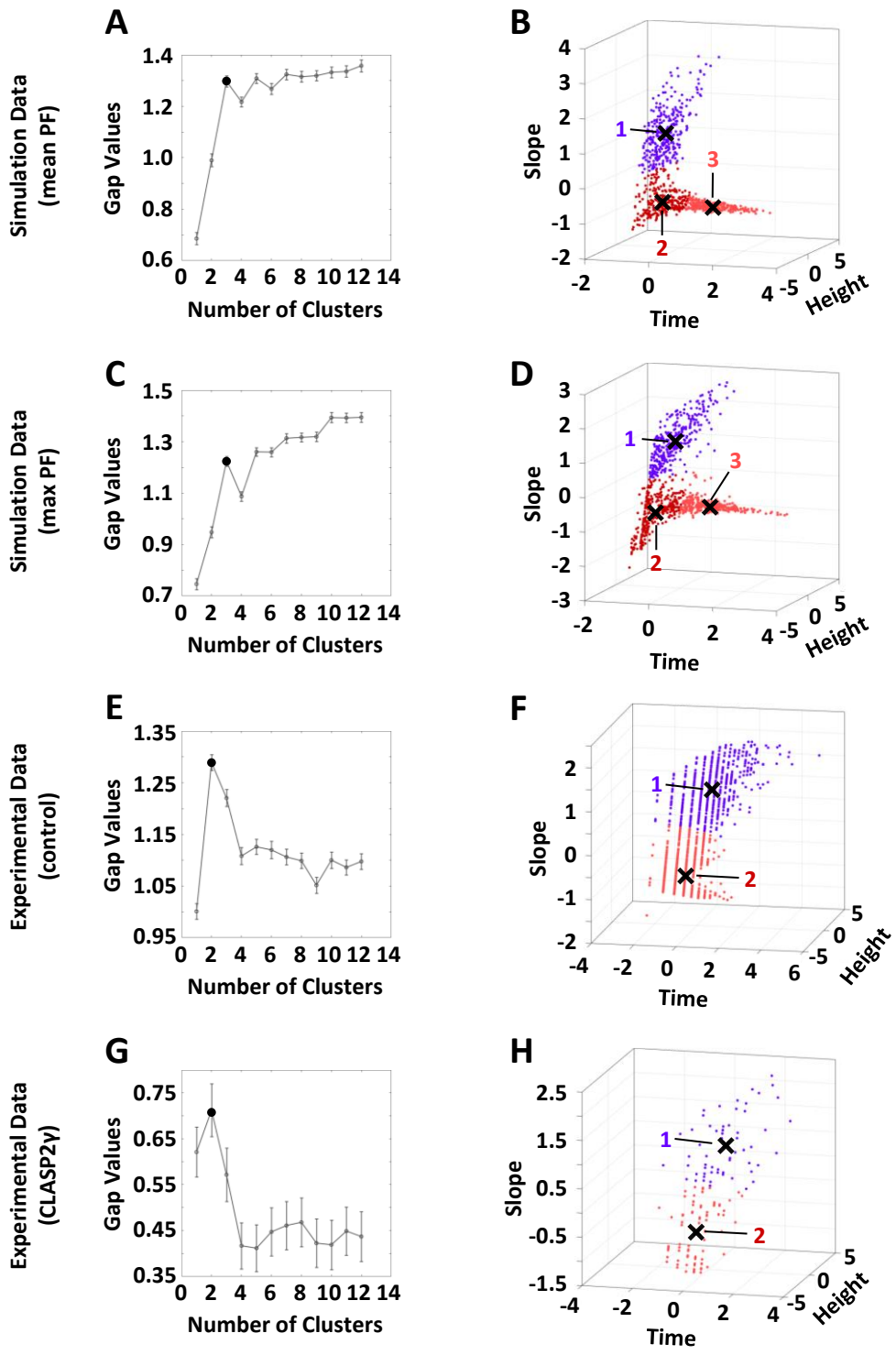

Figure S1.5. Gap statistic plots (left column) and corresponding clustering profiles (right column) for <u>negative</u> slope segments in each dataset. Within each of the cluster profiles (right column), the values of the segment features on each axis are log-transformed and standardized. As noted in **Figure S1.4**, when using the gap statistic (left column) to suggest the best number of clusters to use in *k*-means clustering, a common rule of thumb is to use the first *k*-value where the gap statistic plot shows a local maximum. These data for the negative slope segments show that for the two simulation datasets, the gap statistic attains the first local maximum at *k*=3 (A,C), whereas the experimental datasets indicate *k*=2 for the negative slope segments (E,G). We attribute this difference to the fact that in these experimental datasets, only the beginnings of depolymerization phases were captured, thus omitting long time duration shortening segments from the dataset. Therefore, for negative slope segments, we performed *k*-means clustering separating the dimer-scale simulation data into 3 clusters (B,D) and the experimental data into 2 clusters (F,H).

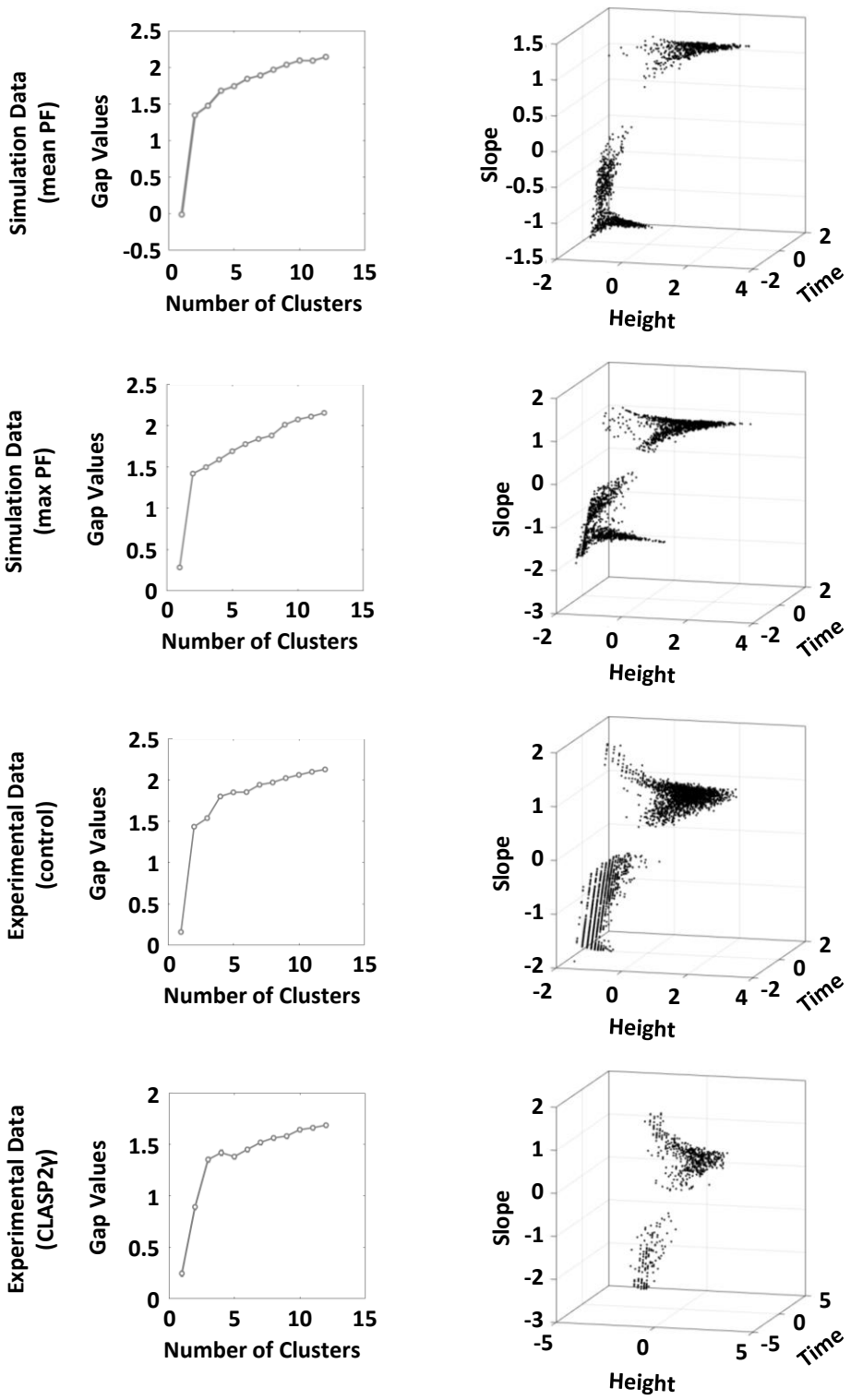

Figure S1.6. Gap statistic plots (left column) and segment feature plots (right column) for an analysis where all slope segments in each dataset were considered together (excluding flat segments), not separated into positive and negative slopes as in Supplemental Figures S1.4 and S1.5. Within each of the cluster profiles (right column), the values of the segment features on each axis are log-transformed and standardized. The gap statistic plots (left column) are generally increasing with no clear local maxima, indicating that the initial dataset was too complex for effective calculation of the gap statistic and that we needed to subdivide it before further analysis. For this reason, the data are not color-coded as in the previous two figures. Note that these plots are simply for demonstrating that consideration of all segments together is not conclusive, thus providing justification for analyzing positive and negative slope segments separately.

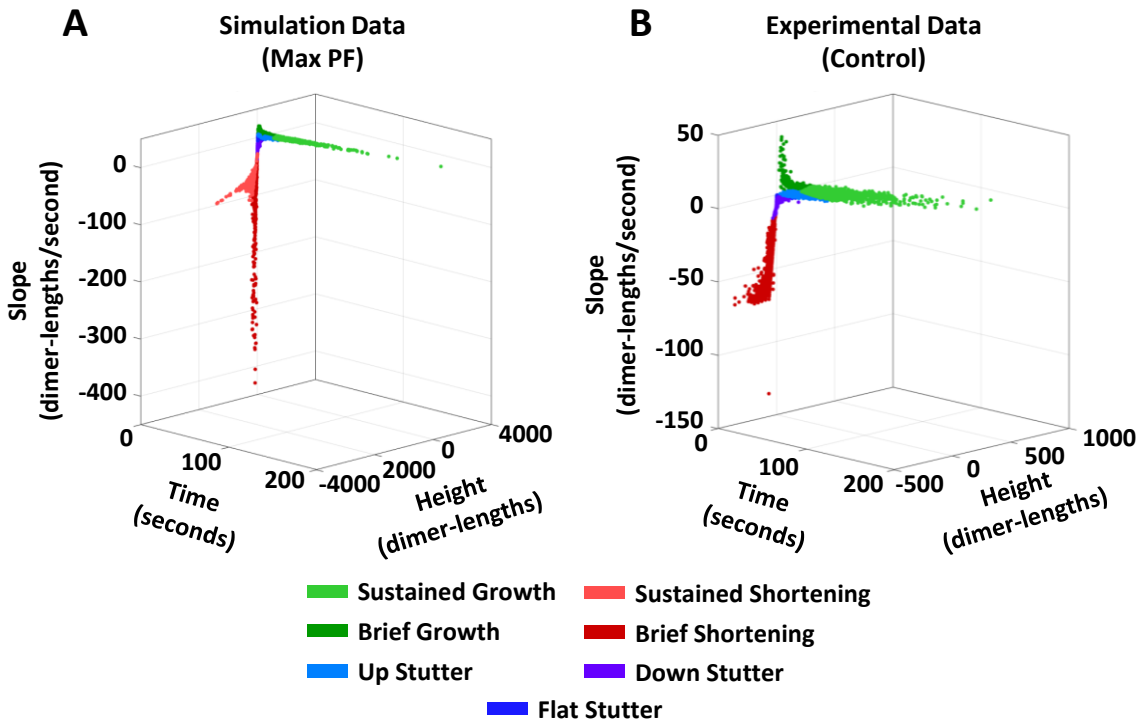

Figure S1.7. Clustering profiles for ALL segments of *in silico* and *in vitro* data (not log-transformed or standardized). Following separate classification of the positive and negative slope segments (**Supplemental Figures S1.4** and **S1.5**), cluster assignments were applied to the original un-log-transformed and un-standardized segment data. Note that the classification step has already taken place, and these figures are simply for visualizing how the clusters exist in relation to each other in the original 3-dimensional space. Recall that each data point in the 3-dimensional space represents the time duration, height change, and slope of one line segment from the piecewise linear approximation of length-history data (**Figure 2 D-F**).

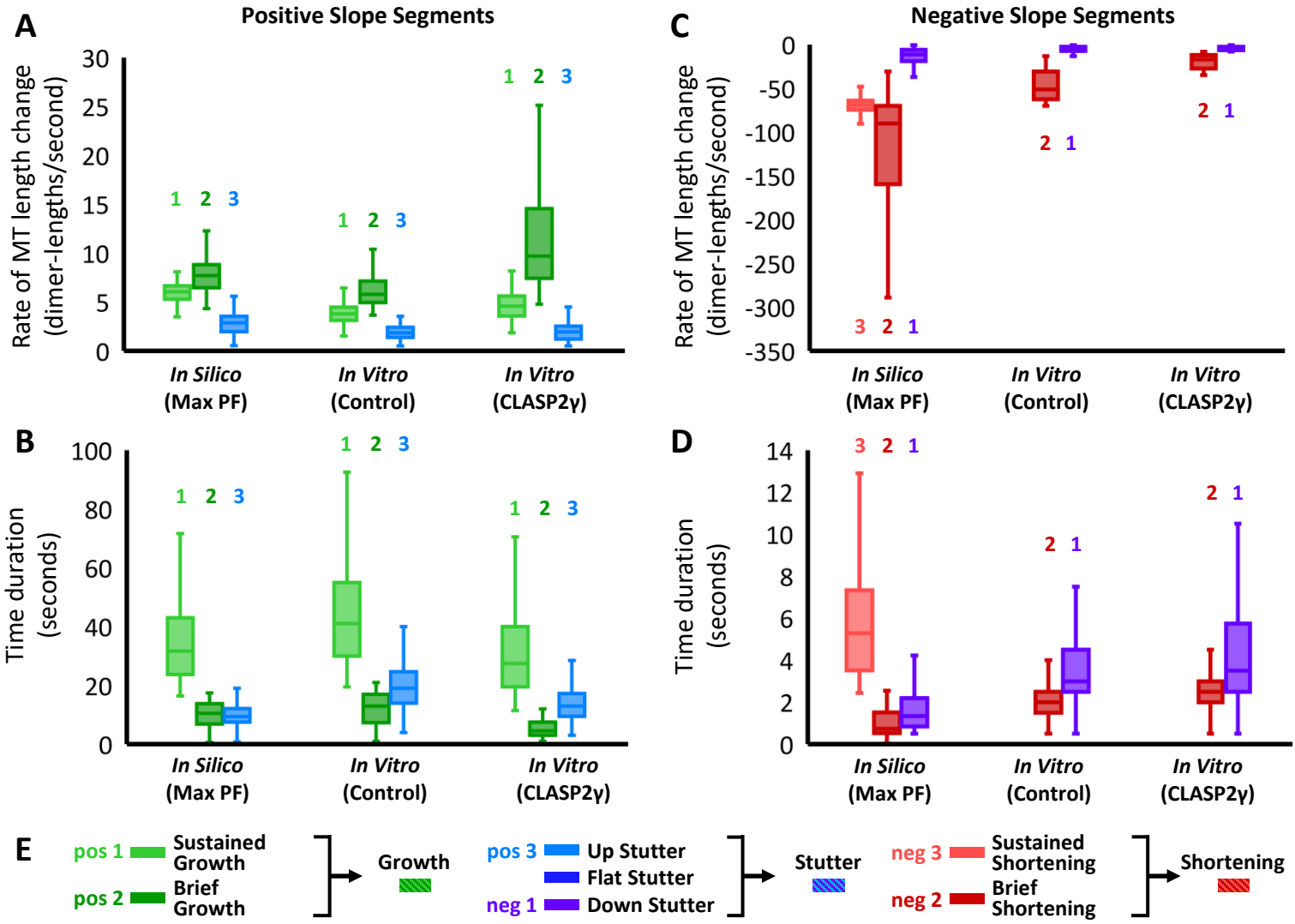

Figure S1.8. Motivation for cluster names and phase/behavior bundling. Left column: positive slope segments. Right column: negative slope segments. The *in silico* and *in vitro* control data in **A** and **C** are the same as the data presented in **Figure 4 C** and **F**, respectively. This figure also provides rate of length change data for the *in vitro* CLASP2γ dataset and time duration data for all three datasets. **(A-D)** Box and whisker plots of the rates of length changes (i.e., slopes; A,C) and time durations (B,D) of the segments in each cluster. Outliers were excluded from these plots using the default definition in MATLAB (i.e., any value that is more than 1.5 times the interquartile range away from the bottom or top of the box is considered an outlier). Note that positive slope cluster 3 and negative slope cluster 1 have slower rates of length change (i.e., shallower slopes) compared to the other positive and negative slope segment clusters, respectively. **(E)** Clusters with similar average slopes are bundled together into larger phase/behavior classes based on the results in the box plots. More specifically, clusters of shallow-slope segments are grouped into 'Stutter'. Clusters of segments with steeper positive and negative slopes are grouped into 'Growth' and 'Shortening', respectively. The descriptors 'Brief' and 'Sustained' are applied to clusters within the Growth and Shortening classes to reflect the differences in their time durations. The descriptors 'Up', 'Flat', and 'Down' are applied to the clusters in the Stutters category based on the segment slopes being positive, near-zero, or negative, respectively.

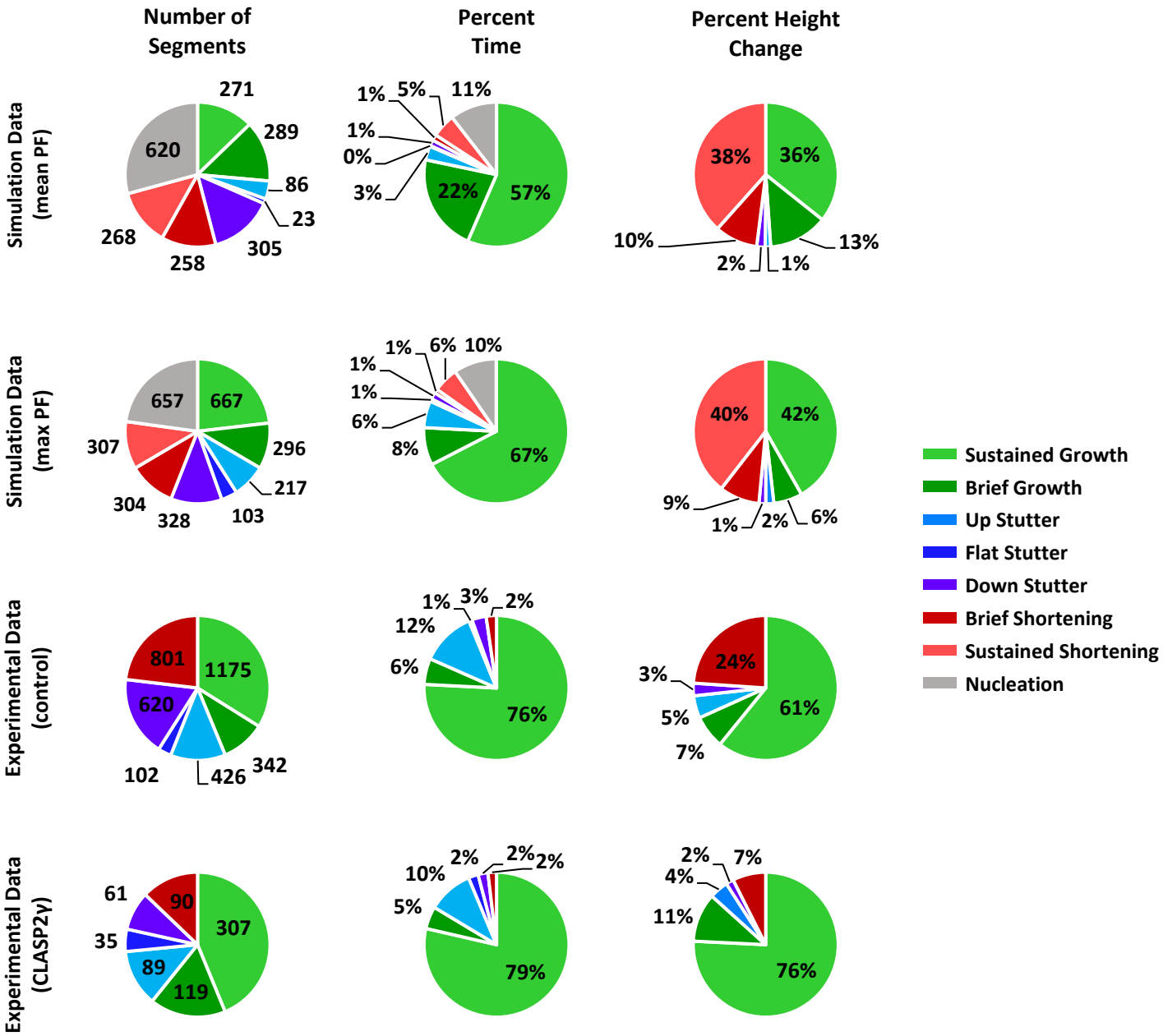

Figure S1.9. Segment statistics for all *in silico* and *in vitro* datasets. Number of segments, percent time, and percent height change for each cluster are recorded for each dataset. As noted throughout the paper, the *in vitro* depolymerizations were not captured in their entirety, so the number of segments, percent time, and percent height change attributed to shortening is largely underrepresented. In contrast, for the *in silico* datasets, the full spectrum of DI behaviors including complete depolymerizations are present, so the measured values are more accurate representations of the share attributable to each type of DI behavior.

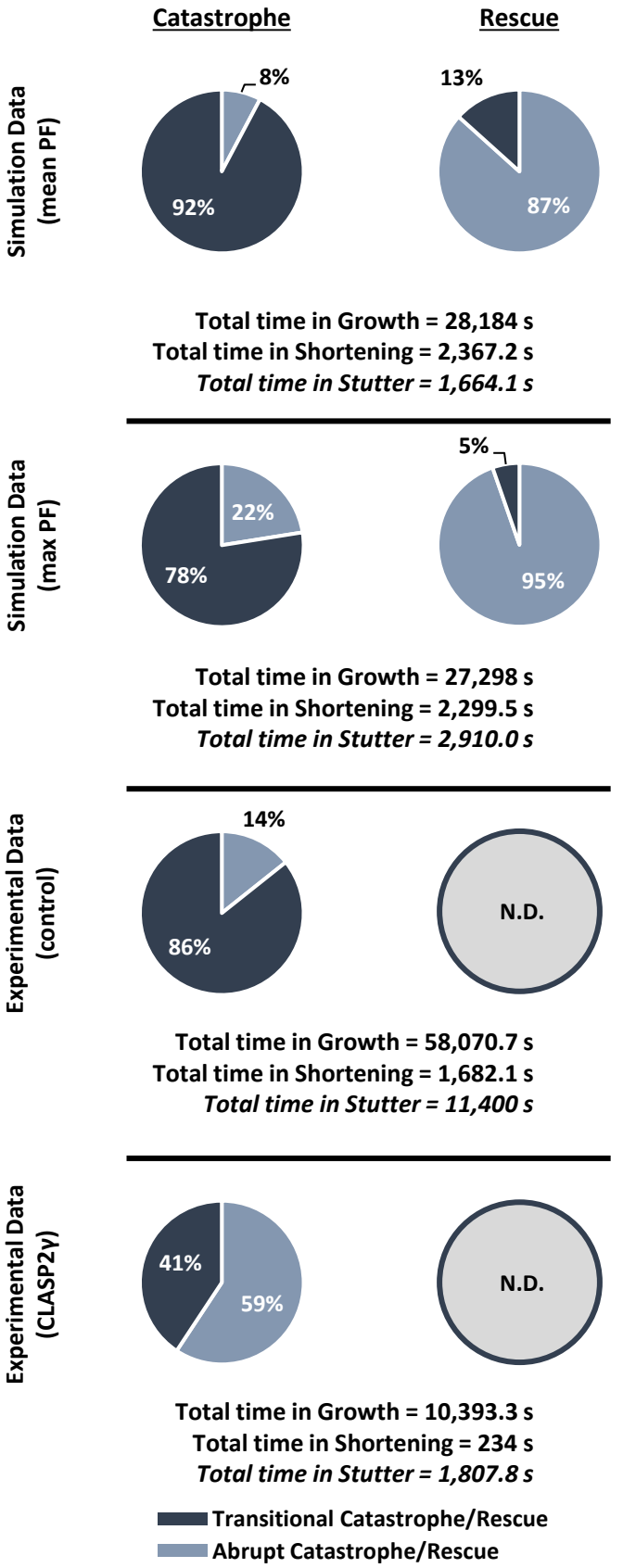

Transition Statistics		
Transition Type	**Count**	**Frequency (s^{-1})**
Simulation Data (mean PF)		
Abrupt Catastrophe	20	0.00071
Transitional Catastrophe	238	0.0084
Total Catastrophe	**258**	**0.00911**
Abrupt Rescue	39	0.0164
Transitional Rescue	6	0.0025
Total Rescue	**45**	**0.0189**
Interrupted Growth	75	0.0027
Interrupted Shortening	32	0.0135
Simulation Data (max PF)		
Abrupt Catastrophe	67	0.0025
Transitional Catastrophe	231	0.0085
Total Catastrophe	**298**	**0.0110**
Abrupt Rescue	71	0.0307
Transitional Rescue	4	0.0017
Total Rescue	**75**	**0.0324**
Interrupted Growth	293	0.0107
Interrupted Shortening	48	0.0207
Experimental Data (control)		
Abrupt Catastrophe	105	0.0018
Transitional Catastrophe	629	0.0108
Total Catastrophe	**734**	**0.0126**
Abrupt Rescue	18	**N.D.**
Transitional Rescue	0	
Total Rescue	**18**	
Interrupted Growth	211	0.0036
Interrupted Shortening	0	**N.D.**
Experimental Data (CLASP2γ)		
Abrupt Catastrophe	51	0.0049
Transitional Catastrophe	35	0.0034
Total Catastrophe	**86**	**0.0083**
Abrupt Rescue	45	**N.D.**
Transitional Rescue	7	
Total Rescue	**52**	
Interrupted Growth	92	0.0088
Interrupted Shortening	1	**N.D.**

Figure S1.10. Detailed transition statistics for each dataset. Both *in silico* datasets as well as the control experimental dataset demonstrate that a significant majority of catastrophes occur via stutter (i.e., transitional catastrophe), while the CLASP2γ dataset shows a shift to MTs exhibiting abrupt catastrophes along with a decrease in total catastrophe frequency. The presence of CLASP2γ markedly reduces the frequency of transitional catastrophe and increases the frequency of interrupted growth (see also **Figure 7** and Results Section 2.5). Rescue data for *in silico* MTs indicate that most rescues occur abruptly. Note that frequencies of rescue and interrupted shortening were not determined (N.D.) for the *in vitro* data because depolymerizations were not captured in their entirety for the *in vitro* MTs.

STADIA: User-defined Parameters	
Nucleation Height Threshold	75 dimer-lengths
Minimum Segment Duration	0.5 seconds
Maximum Error Tolerance	20 dimer-lengths
Maximum Height Change Magnitude for Flat Stutters	3 dimer-lengths
Maximum Slope Magnitude for Flat Stutters	0.5 dimer-lengths/sec
Number of centroids for positive slope segments (all datasets)	$k = 3$
Number of centroids for negative slope segments (*in silico* data)	$k = 3$
Number of centroids for negative slope segments (*in vitro* data)	$k = 2$

Classical Analysis: User-defined Parameters	
Minimum peak height	95 dimer-lengths
Minimum rescue length	95 dimer-lengths
Minimum prominence for major peaks	20 dimer-lengths
Minimum prominence for minor peaks	0.1 dimer-lengths
Minimum regression R^2	0.95

Table S1.1. User-defined parameters for STADIA and classical analysis. See **Supplemental Sections S2 & S3** for STADIA parameter sensitivity analysis.

Stochastic Dimer-Scale 13-PF MT Model Parameters	
Number of protofilaments	13
Tubulin concentration	10 μM
Simulation time	10 hours
Seam shift	1.5 dimer-lengths
Compete for tubulin	No
Hydrolysis rate	0.7 dimers/sec
HalfMax	200
kgrowT	250
kgrowD	250
kshortT	0.02
kshortD	20
kbondTT	100
kbondTD	100
kbondDT	100
kbondDD	100
kbreakTT	70
kbreakTD	90
kbreakDT	90
kbreakDD	400
Seam kbondTT	200
Seam kbondTD	200
Seam kbondDT	200
Seam kbondDD	200
Seam kbreakTT	140
Seam kbreakTD	180
Seam kbreakDT	180
Seam kbreakDD	800

Table S1.2. Computational model parameters used to generate the dimer-scale simulation data. Parameter values used are from Margolin et al. 2012. Please see Methods Section 4.2 for more information about the model.

<u>Secondary Supplement</u> to the manuscript "Quantification of Microtubule Stutters: Dynamic Instability Behaviors that are Strongly Associated with Catastrophe"

Note: The Secondary Supplement is intended for readers who are already familiar with the material in the main text Results and Methods as well as the Primary Supplement.

Secondary Supplement Table of Contents

The simulation data used in the main text and in **Supplemental Sections S1, S2, and S3** were generated from the stochastic dimer-scale 13-PF model described in the main text Methods. In contrast, **Supplemental Section S4** presents and analyzes simulation data from a different model, which was designed to only have two states (growth and shortening) and uses user-input values of V_{growth}, V_{short}, F_{cat}, and F_{res}.

Supplemental Section S2: STADIA Parameter Sensitivity Analysis

Overview: The analyses presented here serve two related purposes: one, to provide guidance to users of STADIA regarding how changes to the STADIA input parameters affect the outputs of STADIA; two, to test the robustness of the main conclusions of our manuscript to changes in the STADIA input parameters. To perform these analyses, we varied the values of the user-input STADIA segmentation parameters Minimum Segment Duration and Maximum Error Tolerance while keeping the inputted length-history data fixed. The values of these two parameters directly affect the output of the segmentation stage of STADIA, and consequently have downstream effects on the results of the classification stage and the phase & transition analysis stage. We performed these analyses using the dimer-scale *in silico* and TIRF-imaged *in vitro* datasets from the main text.

In brief, the conclusions being considered are as follows: **(1)** MTs exhibit more behaviors than just growth and shortening, with stutters being distinguishable behaviors that are prevalent throughout length-history data, **(2)** transitional catastrophes are more frequent than abrupt catastrophes, and **(3)** the anti-catastrophe factor CLASP2γ reduces catastrophe frequency by promoting stuttering MTs to return to growth. The table of contents below directs readers to the figures related to each of the above conclusions.

Section S2 Table of Contents

Information on procedure for varying STADIA segmentation parameters

STADIA has two parameters that directly affect segmentation of MT length-history data and are determined entirely by the user:

1) Minimum Segment Duration: the shortest time duration allowed for any line segment in the approximation of MT length-history data;
2) Maximum Error Tolerance: the largest difference allowed between each data point and the corresponding line segment in the approximation.

For the *in silico* dataset†, the parameter space considered is as follows:

- Minimum Segment Duration = 0.3, 0.5, 1.0, 1.5, 2.0, 3.0 seconds, and
- Maximum Error Tolerance = 5, 10, 15, 20, 25, 30, 35, 40, 63 tubulin dimer-lengths (i.e., 40-500 nm).

The parameter space considered for the *in vitro* datasets is identical except that because the Data Acquisition Time Step was 0.5 seconds (i.e., 2 fps) for the *in vitro* data, these datasets were not analyzed using a Minimum Segment Duration of 0.3 seconds (Minimum Segment Duration must be ≥ Data Acquisition Time Step). For comparison, the specific segmentation parameter values used in the main text and **Supplemental Section S1** were Minimum Segment Duration = 0.5 seconds and Maximum Error Tolerance = 20 dimer-lengths.

Throughout the range of values considered for each parameter, analysis was conducted for every possible combination (i.e., every Minimum Segment Duration is used with every Maximum Error Tolerance). Therefore, the layout of each figure is a grid where the columns correspond to fixed values of the Minimum Segment Duration and the rows correspond to fixed values of the Maximum Error Tolerance.

A note for users of the STADIA code: it is not always possible for the segmentation to satisfy both the Minimum Segment Duration and the Maximum Error Tolerance input parameters. More specifically, during the iterative process of adding new vertices to improve the accuracy of the continuous piecewise linear approximation of length-history data, it is not always possible to select new vertices such that new segments satisfy both input parameters. Such 'irreconcilable errors' are especially likely in cases where the user has chosen a long Minimum Segment Duration with a small Maximum Error Tolerance. For additional information about irreconcilable errors and how to interpret them, please see the main text Methods Section 4.6.

† All *in silico* data in this section use the max PF length from the **full resolution** data, which has dimer-scale spatial resolution, and temporal resolution of one output per dimer-scale biochemical event (see the main text Methods Section 4.2 for more information). In contrast, **Supplemental Section S3** tests the effects of varying the temporal resolution of the *in silico* data.

Subsection S2.1: Gap Statistic Figures

The gap statistic plots aid in determining the *k*-values (number of clusters) to use in the clustering step of STADIA (for more information, see main text Box 1 and Sections 4.4.3 and 4.5.2.2).

Figure S2.1: Positive slope segments, *in silico* max PF dataset
Figure S2.2: Positive slope segments, *in vitro* control dataset
Figure S2.3: Negative slope segments, *in silico* max PF dataset
Figure S2.4: Negative slope segments, *in vitro* control dataset

Description: Panel **A** of each figure: The gap statistic plots are outputs from running STADIA in Diagnostic Mode with the values of Minimum Segment Duration and Maximum Error Tolerance as indicated by the column and row headings, respectively.

Each gap statistic plot is labeled with the *k*-value that we selected based on examination of that gap statistic plot and corresponding cluster profile. Our selected *k*-value usually corresponds to either the first or second local maximum of the gap statistic plot. The *k*-value of the second local maximum was chosen if the *k*-value at the second local maximum showed better agreement with the cluster profile AND the gap value at the second local maximum was greater than at the first local maximum. Italics indicate cases where the selected *k*-value differs from the *k*-value outputted by Diagnostic Mode, which uses the criteria from Tibshirani et al. (2001) as described in the main text Methods. **Green** in **Figures S2.1-S2.2** (positive slope segments) and **red** in **Figures S2.3-S2.4** (negative slope segments) are used to indicate agreement with the *k*-values selected in the main text results (**Figure 4, Supplemental Figures S1.4, S1.5**); **gray** indicates parameter combinations resulting in *k*-values different from the main text results; plots with ***** are monotonically increasing, and therefore lack a clear local maximum and are inconclusive for suggesting an optimal *k*-value.

The **dark blue** box indicates the parameter space for which cluster profiles (**Figures S2.5-S2.6**) and labeled length-history plots (**Figures S2.7-S2.8**) are provided. These parameters combinations were chosen for further analysis due to their physical relevance (i.e., they correspond to experimentally feasible spatial and temporal scales, while also resulting in segmentations that do not underfit or overfit the data relative to filament-scale DI behaviors). The gap statistic plots outside the dark blue box are included for completeness in the exploration of the parameter space.

Panel **B** of each figure (bottom right): A representative gap statistic plot shows the axes for each plot in (A). The x-axis (*k*-value) range is the same for all plots. The y-axis (gap value) has differing ranges (not shown) for each plot, but the specific numerical values of the gap statistic are not relevant to interpreting the plots because identification of the optimal *k*-value is based on local maxima within each gap statistic plot. In other words, the pertinent information is the relationship between the values of the gap statistic at different *k*-values within each plot, not the gap statistic values themselves.

Observations: In each of the four figures (**S2.1-S2.4**), there exists a range of values of Minimum Segment Duration and Maximum Error Tolerance that yield the same *k*-values as the results in the main text (*k*=3 in **Figures S2.1-S2.3**, and *k*=2 in **Figure S2.4** where full depolymerizations were not available in the data).

The positive slope segment data, both *in silico* (**Figure S2.1**) and *in vitro* (**Figure S2.2**), show a clear trend toward lower *k*-values at higher values of the Maximum Error Tolerance, while exhibiting very little sensitivity to changing Minimum Segment Duration. It is worth noting that in many of the cases where *k*=1 was selected for the *in vitro* data (**Figure S2.2**), a second local maximum does occur at *k*=3.

For the negative slope segment data (**Figures S2.3-S2.4**), the *k*-values tend to vary at low values of the Maximum Error Tolerance and high values of the Minimum Segment Duration, but the vast majority of cases show agreement with the *k*-values selected in the main text results.

Interpretations: The gap statistic plots (**Figures S1.1-S1.4**) support the robustness of the *k*-values selected in the main text results and therefore support the conclusion that multiple types of behavior exist within both the positive and negative slope segment data from our datasets. Furthermore, the gap statistic plots in combination with the cluster profiles in **Figures S2.5-S2.6** and the length-history plots in **Figures S2.7-S2.8** support the robustness of the conclusion that stutters in particular exist as a distinct behavior within both the positive and negative slope segments. Additionally, the complexity of behaviors, as observed in the cluster profiles and length-history plots, may justify rejecting a first local maximum at k=1 in more cases than we have done here, which further supports the robustness of the classification results.

However, analysis must be conducted using segmentation parameters that are reasonable for capturing behaviors at the scale that stutters exist. Recall that the Minimum Segment Duration places a lower limit on the timescale of behaviors being analyzed, while the Maximum Error Tolerance places an upper limit on the difference between the continuous piecewise linear approximation and the inputted length-history data. Small values of Minimum Segment Duration and intermediate values of Maximum Error Tolerance (e.g., parameter combinations in or near the dark blue boxes in **Figure S1.1-S1.4**) work well for both the positive and negative slope segments.

Additional discussion: With regard to the gap statistic plots at long Minimum Segment Durations in **Figure S2.3**, consider that shortening or depolymerization behaviors exhibited by MTs often do not last 3 seconds (**Figure S1.8**), so it is conceivable that thresholds are interfering even with the appropriate detection of shortening phases when analysis is conducted at this timescale. Thus, by the very nature of shortening phases of MTs, it follows that the gap statistic plots at long Minimum Segment Durations should be treated with caution.

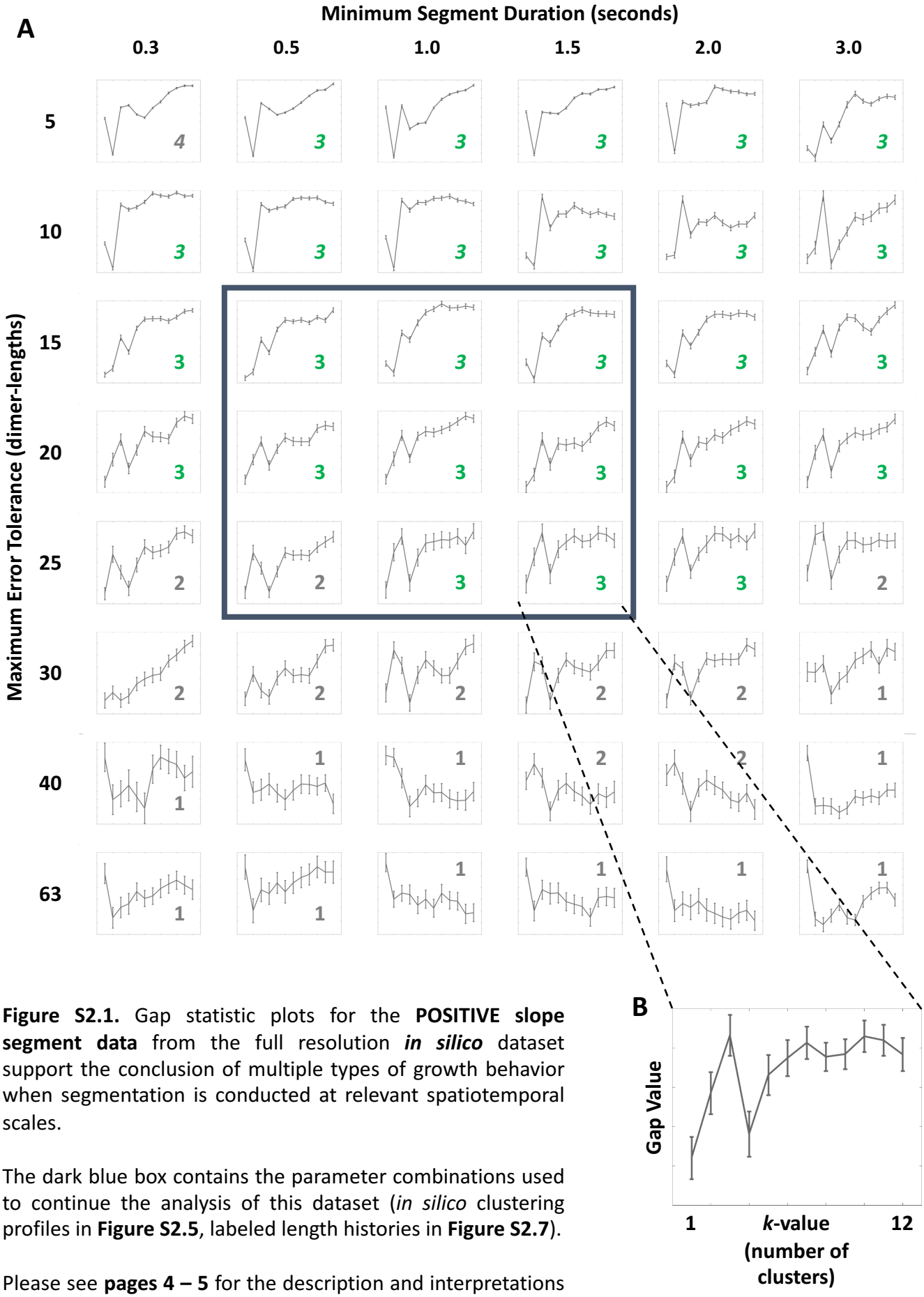

Figure S2.1. Gap statistic plots for the **POSITIVE slope segment data** from the full resolution ***in silico*** dataset support the conclusion of multiple types of growth behavior when segmentation is conducted at relevant spatiotemporal scales.

The dark blue box contains the parameter combinations used to continue the analysis of this dataset (*in silico* clustering profiles in **Figure S2.5**, labeled length histories in **Figure S2.7**).

Please see **pages 4 – 5** for the description and interpretations of the gap statistic figures (**Figures S2.1 – S2.4**).

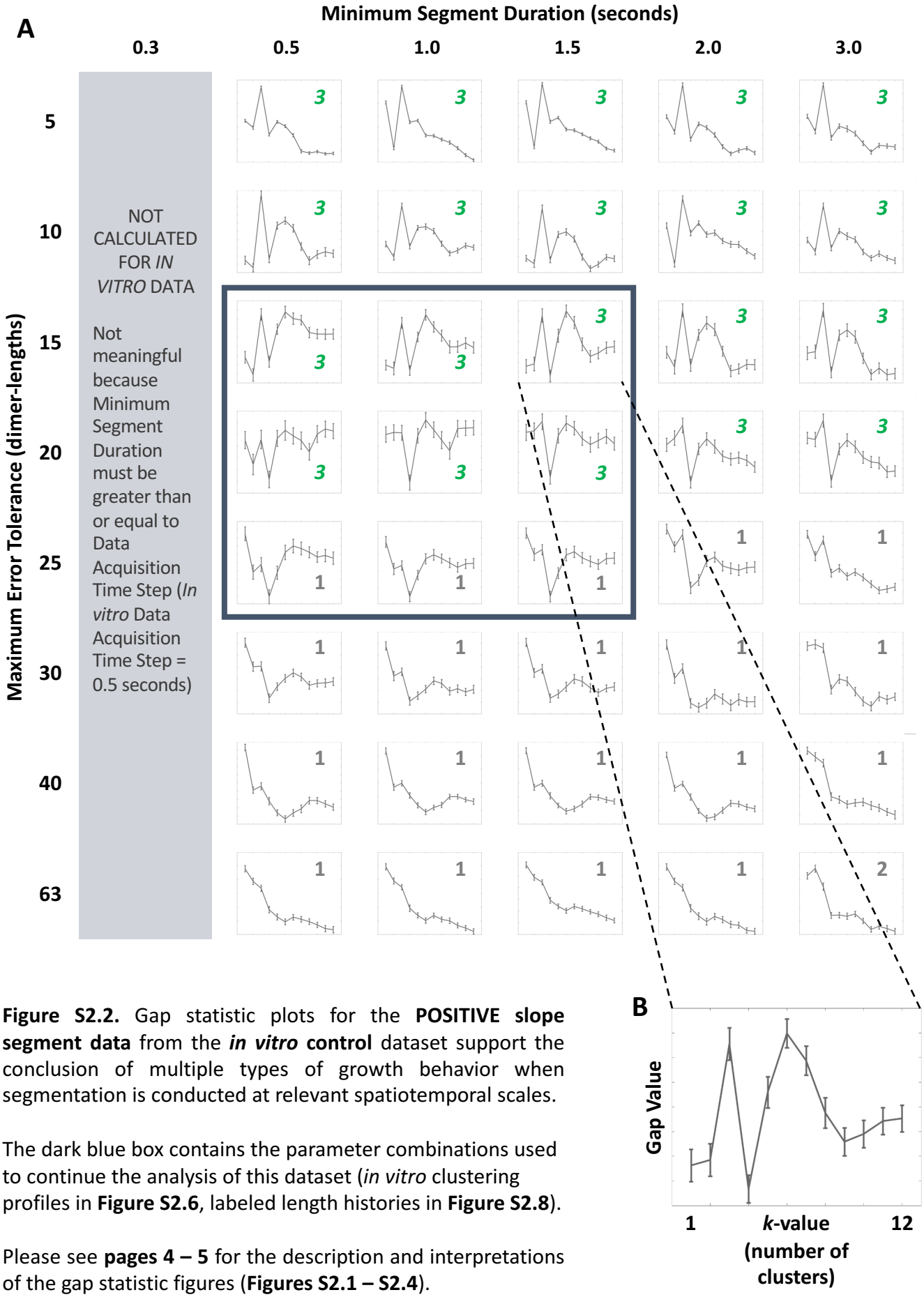

Figure S2.2. Gap statistic plots for the **POSITIVE slope segment data** from the ***in vitro* control** dataset support the conclusion of multiple types of growth behavior when segmentation is conducted at relevant spatiotemporal scales.

The dark blue box contains the parameter combinations used to continue the analysis of this dataset (*in vitro* clustering profiles in **Figure S2.6**, labeled length histories in **Figure S2.8**).

Please see **pages 4 – 5** for the description and interpretations of the gap statistic figures (**Figures S2.1 – S2.4**).

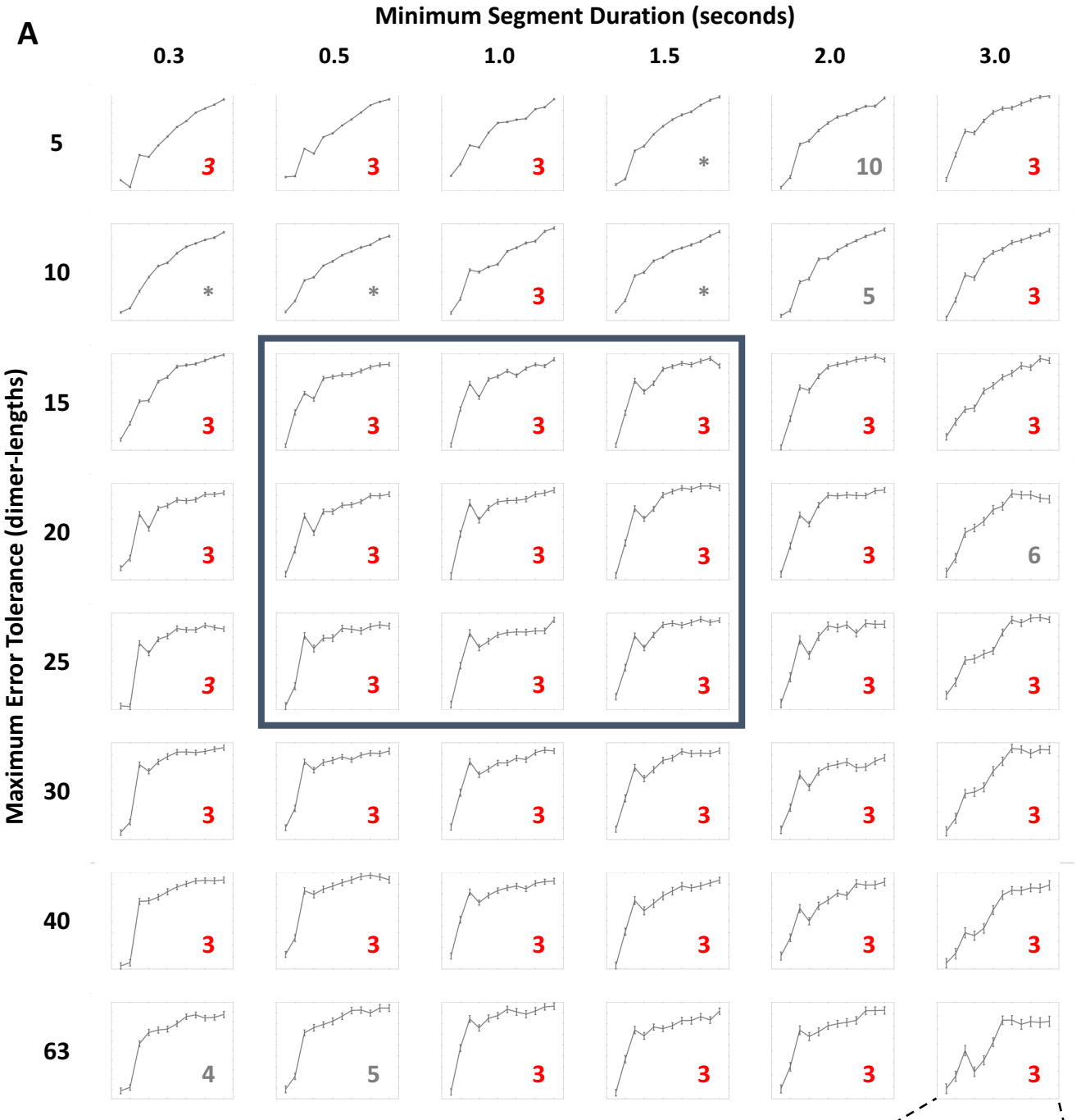

Figure S2.3. Gap statistic plots for the **NEGATIVE slope segment data** from the full resolution ***in silico*** dataset support the conclusion of multiple types of shortening behavior when segmentation is conducted at relevant spatiotemporal scales.

The dark blue box contains the parameter combinations used to continue the analysis of this dataset (*in silico* clustering profiles in **Figure S2.5**, labeled length histories in **Figure S2.7**).

Please see **pages 4 – 5** for the description and interpretations of the gap statistic figures (**Figures S2.1 – S2.4**).

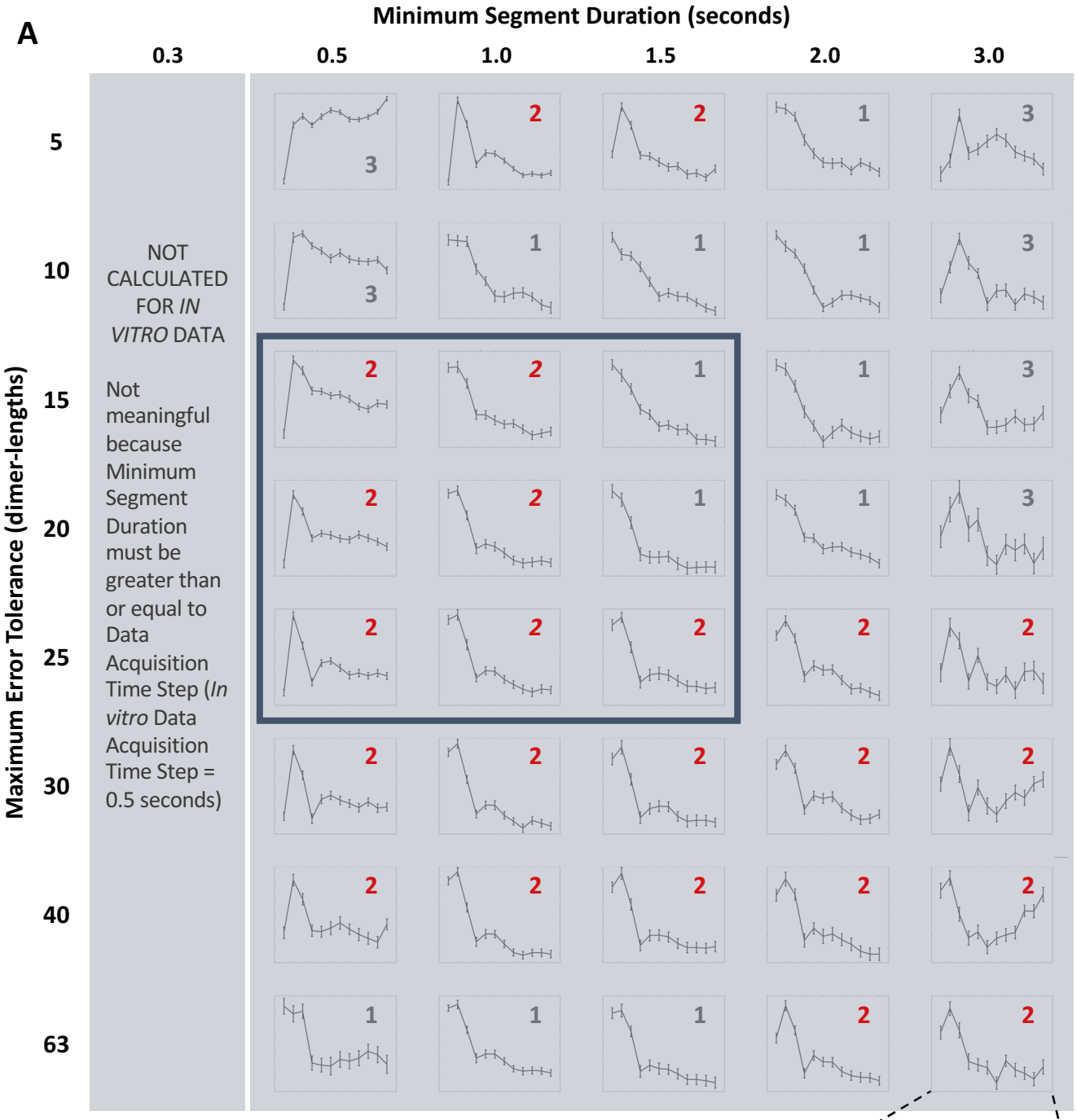

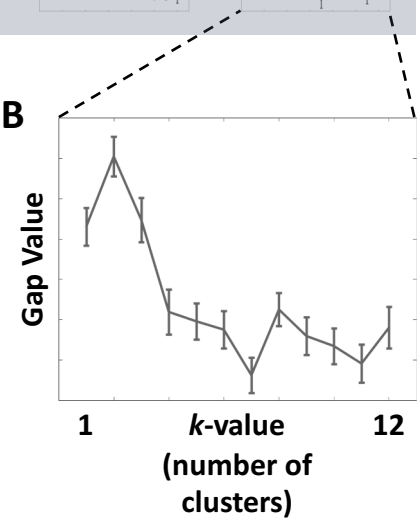

Figure S2.4. Gap statistic plots for the **NEGATIVE slope segment data** from the ***in vitro* control** dataset. The gray shading over the plots is used to indicate the incompleteness of these results (recall that depolymerizations were not tracked in their entirety for the *in vitro* data).

The dark blue box contains the parameter combinations used to continue the analysis of this dataset (*in vitro* clustering profiles in **Figure S2.6**, labeled length histories in **Figure S2.8**).

Please see **pages 4 – 5** for the description and interpretations of the gap statistic figures (**Figures S2.1 – S2.4**).

Subsection S2.2: Cluster Profile Figures

The cluster profiles show how segments are grouped together in the classification stage of STADIA.
Figure S2.5: *in silico* max PF dataset
Figure S2.6: *in vitro* control dataset

Description: The cluster profiles represent the clustering results from using STADIA in Automated Mode, where *k*-means clustering was performed using the *k*-values indicated by the corresponding gap statistic plots in **Figures S2.1-S2.4**. Each data point in the cluster profiles corresponds to a line segment from the segmentation stage of STADIA. Recall that the segment feature data are log-transformed and standardized prior to running through *k*-means clustering (see main text Methods Section 4.5.2.2), as display in these plots. ***Flat stutters** (segments with near-zero slope) are not included in the cluster profiles because flat stutter segments are identified by user-defined thresholds, not by *k*-means clustering (see main text Methods Section 4.5.2.1).

Observations: The cluster profiles maintain the same general shape over the range of Maximum Error Tolerances and Minimum Segment Durations in **Figures S2.5-S2.6**. In particular, the cluster profiles still have 3 'appendages' for the *in silico* positive and negative slope segment data and the *in vitro* positive slope segment data. For the *in vitro* negative slope segment data, the appendage corresponding to segments with longer time durations is missing because the experimentally obtained dataset contained only the beginnings of depolymerization phases, but the overall shape of the cluster profile is fairly consistent across the parameter space.

Significantly, the appendage corresponding to stutters (i.e., lower left appendage in the positive slope plots, upper left appendage in the negative slope plots) is present in all cases, even when $k<3$ was suggested by the gap statistic plots.

A difference across the varying parameter values is that the overall density of data points decreases as the Maximum Error Tolerance and/or the Minimum Segment Duration is increased (i.e., highest density occurs in the upper left of the 3x3 grid, and lowest density in the bottom right of the grid). Overall, there appears to be less change in density for the *in vitro* dataset than the *in silico* dataset. However, for both the *in silico* and *in vitro* datasets, when loss of density does occur, much of the loss appears to be among the more rapid short-duration segments of the brief growth cluster.

Interpretations: The consistent presence of multiple appendages in the cluster profiles in **Figures S2.5-S2.6** supports the conclusion that multiple behaviors exist within both the positive and negative slope segments. In particular, the presence in all cases of the appendage corresponding to shallow-slope segments gives strong support to the conclusion that stutters exist.

Relatedly, the cluster profiles bolster the *k*-values selected from the gap statistic plots (**Figures S2.1-S2.4**) in most cases. The notable exception is the selection of $k=1$ for the *in vitro* positive slope segments when using Maximum Error Tolerance = 25 dimer-lengths. The cluster profiles in this case still display multiple appendages and a similar overall shape to the other positive slope segment cluster profiles, which indicates that the first local maximum of the corresponding gap statistic plots at $k=1$ does not capture the presence of the subgroups in the data. Thus, the second local maximum at $k=3$ may be a more viable option.

Additional Discussion: With regards to the decrease in the density of the data points as the input parameters increase, recall that the Minimum Segment Duration and the Maximum Error Tolerance directly affect the accuracy of the piecewise linear approximation to the length-history data, and therefore also affect the temporal scale of the dynamics being identified. Higher values of Minimum Segment Duration and Maximum Error Tolerance result in a less accurate approximation and thus fewer line segments. Because the segments in the piecewise linear approximation are represented as data points in the cluster profiles, fewer segments in the approximation lead to cluster profiles with lower density. Thus, the consequences of any overfitting or underfitting at the segmentation stage propagate into the classification stage and can affect the clustering results. Note that such changes in density are only seen in a limited capacity in the subset of the parameter space explored in **Figures S2.5-S2.6**.

Density can impact clustering results because *k*-means clustering, like most clustering algorithms, seeks to exploit low density areas as the natural separations to identify boundaries between potential clusters detectable by their higher density. Therefore, for clustering analysis to succeed in distinguishing MT behaviors, a large enough amount of data is needed to cover the landscape of possible MT behaviors.

More specifically, users should be cautioned that using an insufficient amount of data can have at least two potential outcomes. First, a low-density region may be artificially identified as a space between clusters, which can result in identifying more cluster boundaries than actually exist. This situation is unlikely in the data explored here since most cases yielded no more than k=3 as the ideal number of clusters (the exception being some edge cases, or cases where no ideal *k*-value was found). A second potential outcome of sparse data is when a region that should be associated with a particular behavior has relatively little density and is therefore missed as a distinguishable cluster. This situation is more likely, especially when considering parameter sets that deliver less accurate approximations incapable of capturing some nuanced behaviors in MT dynamics (such as stutters). Indeed, this situation played out in cases using higher Maximum Error Tolerance values in **Figures S2.1-S2.2**, which yielded lower *k*-values. This further justifies using segmentation parameters in or close to the range of parameters values used in **Figures S2.5-S2.6**.

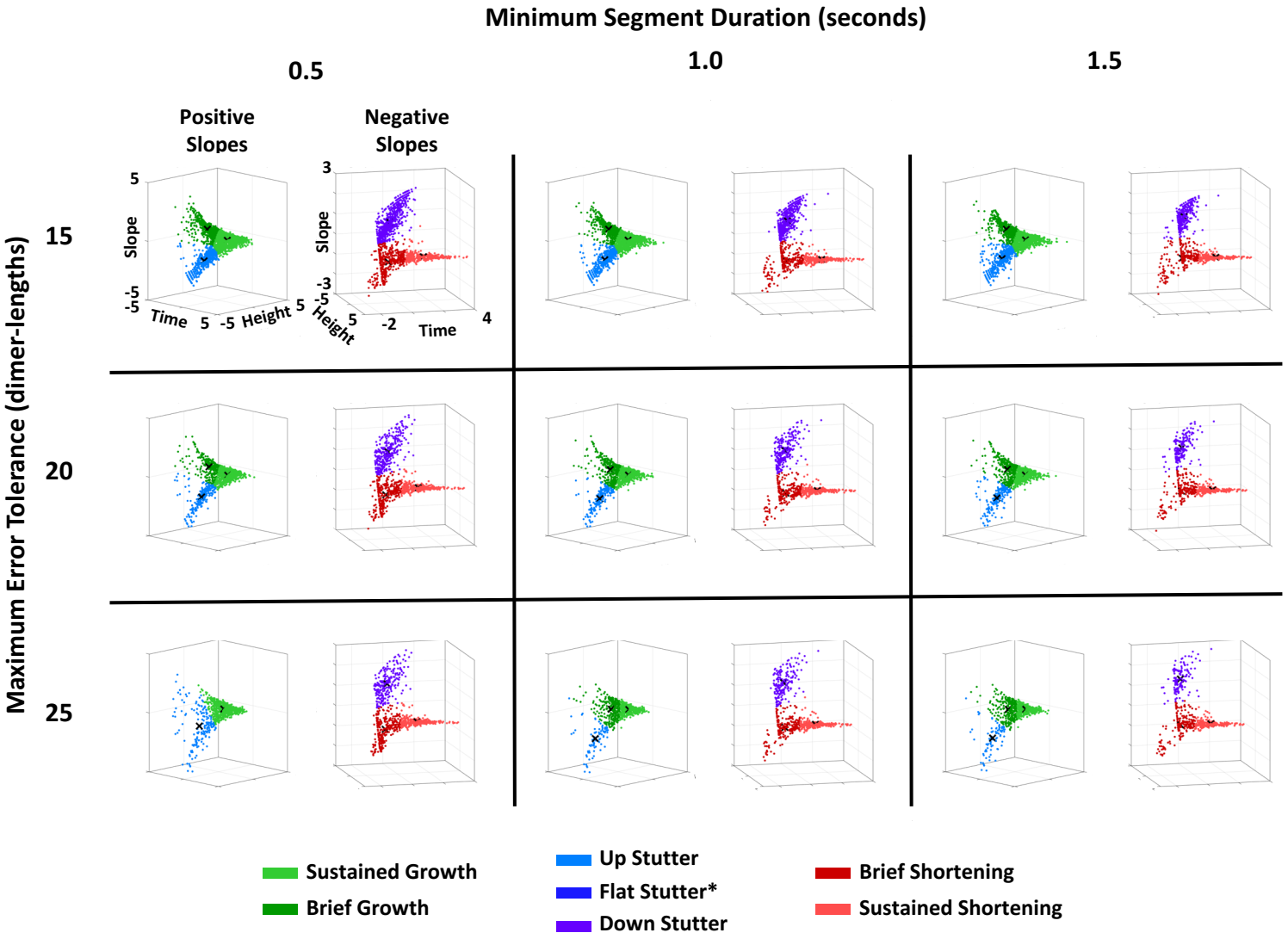

Figure S2.5. The cluster profiles of the positive and negative slope segment data from the full resolution ***in silico*** dataset support the existence of stutters. The cluster profiles result from performing *k*-means clustering using the *k*-value displayed in the corresponding gap statistic plot in **Figures S2.1** and **S2.3** for the positive and negative slope segments, respectively.

Please see **pages 10 – 11** for the description and interpretations of the cluster profile figures (**Figures S2.5 – S2.6**).

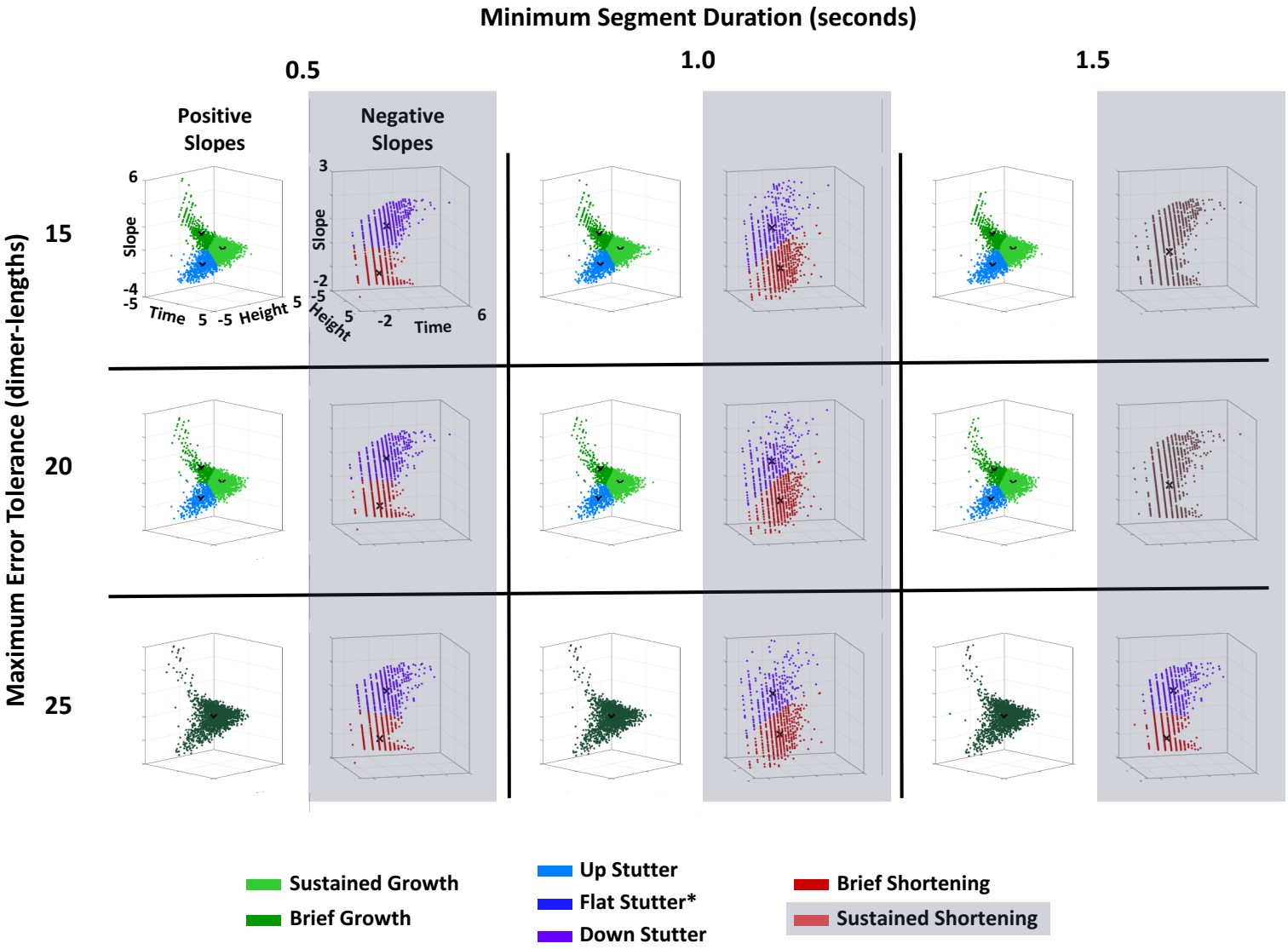

Figure S2.6. The cluster profiles of positive and negative slope segment data from the ***in vitro*** **control** dataset support the existence of stutters. The cluster profiles result from performing *k*-means clustering using the *k*-value displayed in the corresponding gap statistic plot in **Figures S2.2** and **S2.4** for the positive and negative slope segments, respectively.

The gray shading over the cluster profiles for the negative slope segment data is used to indicate the incompleteness of these results. More specifically, the sustained shortening cluster is missing because depolymerizations were not tracked in their entirety for the *in vitro* data (e.g., **Figure 1 D**), as explained in the main text Section 4.1.

Please see **pages 10 – 11** for the description and interpretations of the cluster profile figures (**Figures S2.5 – S2.6**).

Subsection S2.3: Length-History Figures

The segments in the length-history plots are color-coded according to the classification results.
Figure S2.7: *in silico* max PF dataset
Figure S2.8: *in vitro* control dataset

Description: The same portion of the inputted length-history data (white lines) is plotted in each panel. The data were analyzed using STADIA in Automated Mode with each combination of input parameters (row and column headings). Consequently, each panel shows a different continuous piecewise linear approximation (black lines) resulting from the segmentation stage, which leads to different clustering results (colored backgrounds) in the classification stage.

As indicated in the key at the bottom of the figures, the color of the background behind each segment represents the cluster to which the segment was assigned. The cluster assignments (**Figures S2.5-S2.6**) resulted from using *k*-means clustering with the *k*-values selected from the corresponding gap statistic plots (**Figures S2.1-S2.4**) for each set of parameters.

The zoomed-in portraits in each panel show the catastrophe indicated by the black box in the top left panel.

Observations: The labeled length-history plots illustrate that detection of stutters is reduced when segmentation is performed using higher values for Minimum Segment Duration or Maximum Error Tolerance.

For increasing values of Maximum Error Tolerance, fewer stutters are detected throughout the plotted region of length-history data.

To provide an example of the effect of the Minimum Segment Duration in each of **Figures S2.7** and **S2.8**, the zoomed-in portraits in the upper corner of each panel show a catastrophe that is clearly transitional in the inputted length-history data (white line) but is miscategorized as abrupt when using Minimum Segment Durations > 0.5 seconds. The miscategorization occurs because the piecewise linear approximation (black line segments) does not segment the data with enough accuracy to detect the stutter when using Minimum Segment Durations > 0.5 seconds.

In general, less diverse behavior is captured when using high values for both parameters, and the associated underfitting is more obvious in the zoomed-in plots in cases where the segmented approximation (black lines) does not closely follow the inputted data (white lines).

Interpretations: Labeled length-history plots provide a qualitative check on the classification and transition analyses and provide further insight into appropriate parameter choices. While the gap statistic plots and cluster profiles inform the *k*-value (i.e., the number of behaviors) and the robustness with which those behaviors are detected (i.e., the consistency of the clustering results across an appropriate parameter range), the labeled length-history data allow for visual inspection of the transitions between behaviors. For example, the labeled length-history plots shown here indicate that the parameters chosen for the STADIA analysis in the main text and **Supplemental Section S1** (i.e., Minimum Segment Duration = 0.5 seconds, Maximum Error Tolerance = 20 dimer-lengths) are appropriate for accurately detecting the stutter before catastrophe shown here. The effect of the user-input parameters on the detection of transitional catastrophes more generally is examined in **Figures S2.9-S2.11**.

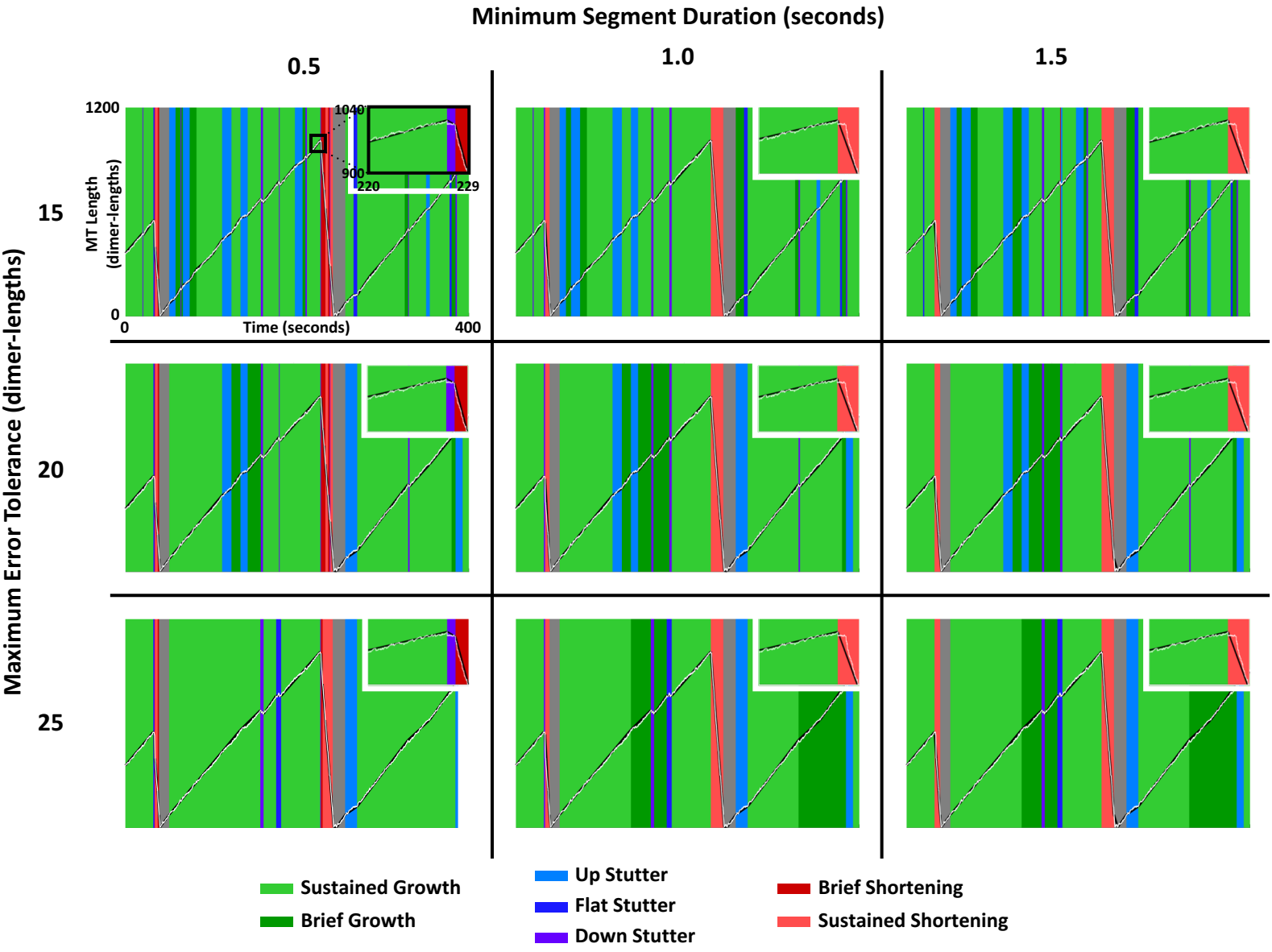

Figure S2.7. Labeled length-history plots for the full resolution ***in silico*** dataset demonstrate that fewer stutters are detected when segmentation is performed using higher values for Minimum Segment Duration or Maximum Error Tolerance. The colored background behind each segment represents the cluster to which the segment was assigned in the *k*-means clustering results in **Figure S2.5**.

Please see **page 14** for the description and interpretations of the length-history figures (**Figures S2.7 – S2.8**).

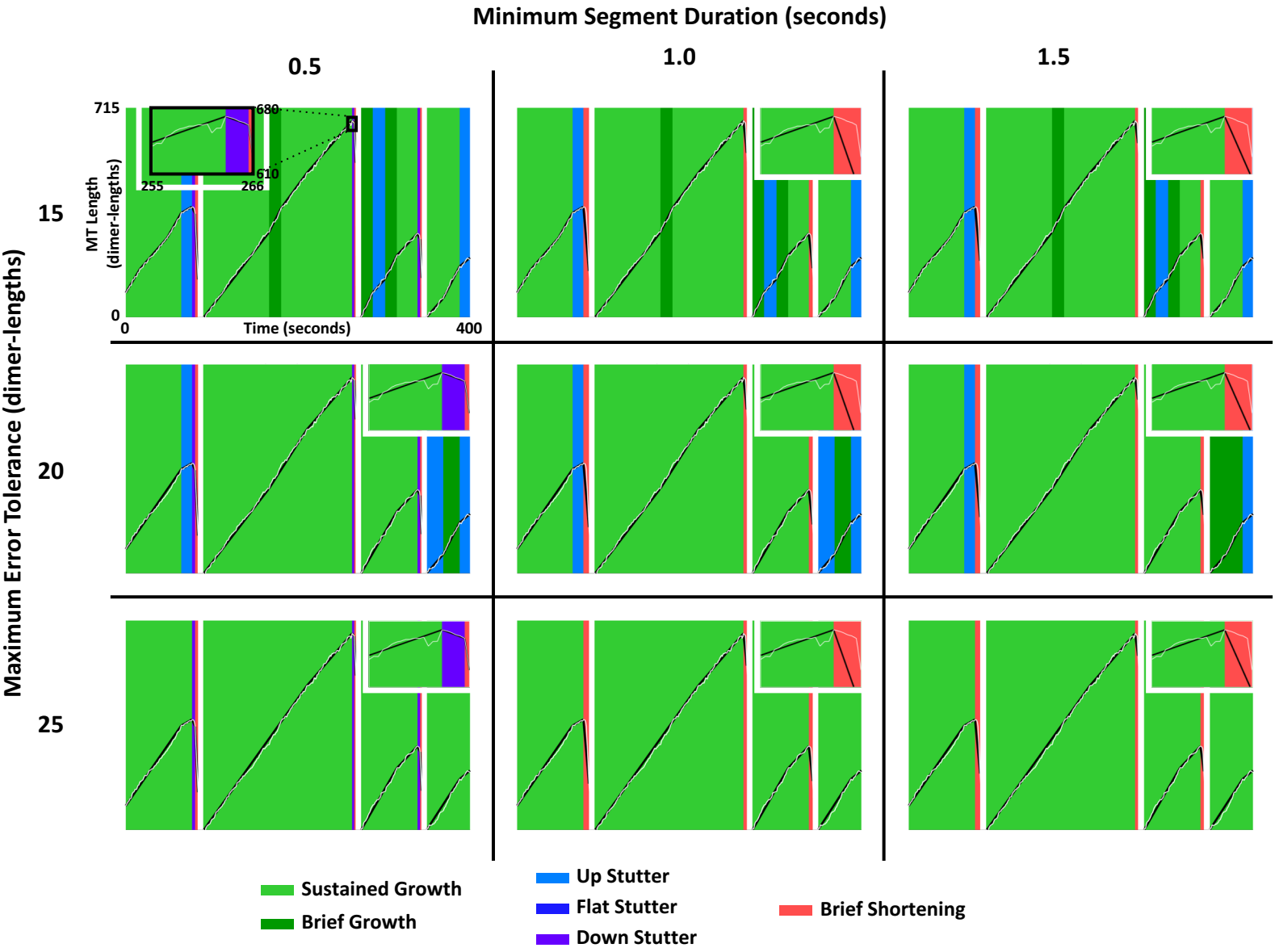

Figure S2.8. Labeled length-history plots for the ***in vitro* control** dataset demonstrate that fewer stutters are detected when segmentation is performed using higher values for Minimum Segment Duration or Maximum Error Tolerance. The colored background behind each segment represents the cluster to which the segment was assigned in the *k*-means clustering results in **Figure S2.6**.

Please see **page 14** for the description and interpretations of the length-history figures (**Figures S2.7 – S2.8**).

Subsection S2.4: Transition Frequency Figures

These figures compare the frequencies of the different types of transitions that begin from growth: abrupt catastrophe (growth->shortening), transitional catastrophe (growth->stutter->shortening), and interrupted growth (growth->stutter->growth). These results support the robustness of the conclusions that most catastrophes are transitional in the *in silico* and *in vitro* control datasets, and that CLASP2γ reduces catastrophe frequency by promoting growth of stuttering MTs.

Figure S2.9: *in silico* max PF dataset
Figure S2.10: *in vitro* control dataset
Figure S2.11: *in vitro* CLASP2γ dataset

Description: For all combinations of Minimum Segment Duration and Maximum Error Tolerance shown, these measured transition frequencies are the results from using STADIA in Automated Mode with the *k*-values identified in the main text Results: *k*=3 for both positive and negative slope segments in the *in silico* dataset (**Figure S2.9**); *k*=3 for positive and *k*=2 for negative slope segments in the *in vitro* control dataset (**Figure S2.10**) and the *in vitro* CLASP2γ dataset (**Figure S2.11**).

Panels **A-C** of each figure: Transition frequencies across the full parameter space considered in **Supplemental Section S2**. The frequency of abrupt catastrophe ($F_{AbruptCat}$, A), frequency of transitional catastrophe ($F_{TransCat}$, B), and frequency of interrupted growth ($F_{IntGrowth}$, C) are reported in table form. The highlighted column (Minimum Segment Duration = 0.5 seconds) and row (Maximum Error Tolerance = 20 dimer-lengths) of each table correspond to the data plotted in (D-G).

Panels **D,E** of each figure: These plots compare the frequencies of the two types of catastrophes: abrupt and transitional. $F_{AbruptCat}$ and $F_{TransCat}$ are plotted for varying Minimum Segment Durations while holding the Maximum Error Tolerance constant at 20 dimer-lengths (D) and for varying Maximum Error Tolerances while holding the Minimum Segment Duration constant at 0.5 seconds (E). The measured frequencies and their total ($F_{cat} = F_{AbruptCat} + F_{TransCat}$) are plotted corresponding to the left-hand y-axes; the ratio of $F_{AbruptCat}$ to $F_{TransCat}$ is plotted corresponding to the right-hand y-axes. Note that $F_{AbruptCat}/F_{TransCat} < 1$ indicates $F_{TransCat} > F_{AbruptCat}$.

Panels **F,G** of each figure: These plots compare the fates of the two types of transitions that begin with growth-to-stutter: transitional catastrophes and interrupted growth. $F_{TransCat}$ and $F_{IntGrowth}$ are plotted for varying Minimum Segment Durations while holding the Maximum Error Tolerance constant at 20 dimer-lengths (F) and for varying Maximum Error Tolerances while holding the Minimum Segment Duration constant at 0.5 seconds (G). The measured frequencies and their total ($F_{IntGrowth} + F_{TransCat}$) are plotted corresponding to the left-hand y-axes; the ratio of $F_{IntGrowth}$ to $F_{TransCat}$ is plotted corresponding to the right-hand y-axes. For small Maximum Error Tolerances, please see the tables in (A-C) for the frequencies that are too high to be visible in **Figures S2.9**(E,G), **S2.10**(G), and **S2.11**(E,G).

Observations regarding catastrophes (abrupt and transitional):
In all three datasets (**Figures S2.9-S2.11**), the total F_{cat} (which equals $F_{AbruptCat} + F_{TransCat}$) is relatively steady over the range of Minimum Segment Durations (D, Maximum Error Tolerance = 20 dimer-lengths), albeit nosier in the *in vitro* datasets than the *in silico* dataset. With increasing Maximum Error Tolerance (F, Minimum Segment Duration = 0.5 seconds), the total F_{cat} decreases in all three datasets, but levels off to fairly steady values in the *in silico* and *in vitro* control datasets at high Maximum Error Tolerances.

More importantly, consistent with the results in the main text, in the *in silico* and *in vitro* control datasets (**Figure S2.9-S2.10**), $F_{TransCat}$ is greater than $F_{AbruptCat}$ (i.e., $F_{AbruptCat}/F_{TransCat} < 1$) for sufficiently small Minimum Segment Durations in (D) and for a range of Maximum Error Tolerances in (F). In particular, $F_{TransCat} > F_{AbruptCat}$ holds for the *in silico* dataset with Minimum Segment Duration < 1.5 seconds (D) and Maximum Error Tolerance between 10 and 40 dimer-lengths (E), and for the *in vitro* control data with Minimum Segment Duration = 0.5 seconds (D) and Maximum Error Tolerance less than or equal to 40 dimer-lengths (E).

Also consistent with the results in the main text and in contrast to the *in vitro* control data, in the *in vitro* CLASP2γ dataset (**Figure S2.11**), $F_{TransCat}$ is less than $F_{AbruptCat}$ (i.e., $F_{AbruptCat}/F_{TransCat} > 1$) for all Minimum Segments Durations in (D) and all Maximum Error Tolerances in (E).

Observations regarding growth-to-stutter transitions (interrupted growth and transitional catastrophes):
In each of the three datasets (**Figures S2.9-S2.11**), the frequency of growth-to-stutter transitions $F_{IntGrowth} + F_{TransCat}$ (F,G) appears to change more significantly than the total $F_{cat} = F_{AbruptCat} + F_{TransCat}$ (D,E) when varying either the Minimum Segment Duration (D versus F; Maximum Error Tolerance = 20 dimer-lengths) or Maximum Error Tolerance (E versus G; Minimum Segment Duration = 0.5 seconds).

Also in each of the datasets, $F_{IntGrowth}$ and $F_{TransCat}$ both decrease with increasing Maximum Error Tolerance (G); further, $F_{IntGrowth}$ decreases more rapidly than $F_{TransCat}$, resulting in a decrease in their ratio $F_{IntGrowth}/F_{TransCat}$ (except in the CLASP2γ dataset at high Maximum Error Tolerances). Additionally, $F_{IntGrowth}$ and $F_{TransCat}$ each individually change more with varying Maximum Error Tolerance (G) than with varying Minimum Segment Duration (F)

In the *in vitro* CLASP2γ dataset (**Figure S2.11**), $F_{IntGrowth}$ is consistently greater than $F_{TransCat}$ (i.e., $F_{IntGrowth}/F_{TransCat} > 1$) for all data in (F, G). In contrast, the ratio $F_{IntGrowth}/F_{TransCat}$ in the *in vitro* control dataset (**Figure S2.10**) is much less than 1 for Minimum Segment Duration = 0.5 seconds in (F) and for Maximum Error Tolerance > 15 dimer-lengths in (G).

Interpretations:
The above observations support the conclusion that catastrophes are more often transitional than abrupt in both the *in silico* dataset and the *in vitro* control dataset. This conclusion is robust over a range of intermediate Maximum Error Tolerances, provided that the Minimum Segment Duration is short enough (**Figures S2.9-S2.10**).

The above observations also support the conclusions that catastrophes in the presence of CLASP2γ are abrupt more often than transitional, and that growth-to-stutter occurrences with CLASP2γ result in interrupted growth more often than they result in transitional catastrophes (i.e., CLASP2γ promotes growth of stuttering MTs). These conclusions are robust across the segmentation parameters in (D-G) of **Figure S2.11**.

The general decreases in each of $F_{TransCat}$ and $F_{IntGrowth}$ with increasing Minimum Segment Duration or increasing Maximum Error Tolerance are indicative of a decrease in stutter detection. This effect of the parameters on STADIA's ability to detect individual stutter segments is also evidenced by the decreasing density of the cluster profiles in **Figures S2.5-S2.6** and by the loss of detection of particular stutters in the labeled length-history plots in **Figures S2.7-S2.8**.

Additionally, the total frequency of transitions tends to decrease with increasing Minimum Segment Duration or increasing Maximum Error Tolerance, consistent with a smaller total number of segments being identified in the piecewise linear approximations as these segmentation parameters are increased. This change is particularly dramatic when going from low to intermediate values of Maximum Error Tolerance (e.g., 5 to 25 dimer-lengths; E,G).

Additional Discussion:
While $F_{IntGrowth}$ and $F_{TransCat}$ each decrease with increasing Maximum Error Tolerances, the decreases in both the total frequency ($F_{IntGrowth} + F_{TransCat}$) and the ratio ($F_{IntGrowth}/F_{TransCat}$) can be attributed primarily to the large decrease in the frequency of interrupted growth. This larger decrease in $F_{IntGrowth}$ than in $F_{TransCat}$ suggests that detection of stutters interrupting growth is more sensitive to the Maximum Error Tolerance than is detection of stutters preceding catastrophes.

A

Frequency of ABRUPT CATASTROPHE						
Max Error Tolerance (dimer-lengths)	Minimum Segment Duration (s)					
	0.3	0.5	1.0	1.5	2.0	3.0
5	0.0883	0.1107	0.1002	0.0642	0.0439	0.0186
10	0.0050	0.0067	0.0105	0.0149	0.0158	0.0151
15	0.0046	0.0029	0.0045	0.0061	0.0071	0.0075
20	0.0024	0.0025	0.0041	0.0059	0.0068	0.0070
25	0.0023	0.0031	0.0042	0.0057	0.0067	0.0068
30	0.0025	0.0027	0.0042	0.0059	0.0068	0.0068
40	0.0029	0.0031	0.0043	0.0059	0.0068	0.0066
63	0.0047	0.0048	0.0046	0.0060	0.0070	0.0057

B

Frequency of TRANSITIONAL CATASTROPHE						
Max Error Tolerance (dimer-lengths)	Minimum Segment Duration (s)					
	0.3	0.5	1.0	1.5	2.0	3.0
5	0.0607	0.0648	0.0402	0.0217	0.0127	0.0052
10	0.0131	0.0122	0.0094	0.0076	0.0068	0.0045
15	0.0101	0.0095	0.0071	0.0053	0.0042	0.0030
20	0.0090	0.0085	0.0060	0.0042	0.0030	0.0021
25	0.0083	0.0074	0.0055	0.0038	0.0026	0.0019
30	0.0075	0.0072	0.0052	0.0035	0.0024	0.0017
40	0.0067	0.0064	0.0049	0.0033	0.0023	0.0018
63	0.0045	0.0043	0.0040	0.0029	0.0019	0.0009

C

Frequency of INTERRUPTED GROWTH						
Max Error Tolerance (dimer-lengths)	Minimum Segment Duration (s)					
	0.3	0.5	1.0	1.5	2.0	3.0
5	0.5378	0.3763	0.1998	0.1404	0.1000	0.0574
10	0.1321	0.1155	0.0758	0.0537	0.0431	0.0338
15	0.0332	0.0343	0.0290	0.0228	0.0198	0.0152
20	0.0104	0.0107	0.0092	0.0084	0.0079	0.0061
25	0.0033	0.0013	0.0035	0.0033	0.0032	0.0028
30	0.0015	0.0015	0.0015	0.0014	0.0014	0.0016
40	0.0003	0.0003	0.0004	0.0004	0.0004	0.0007
63	0.0000	0.0000	0.0000	0.0000	0.0001	0.0001

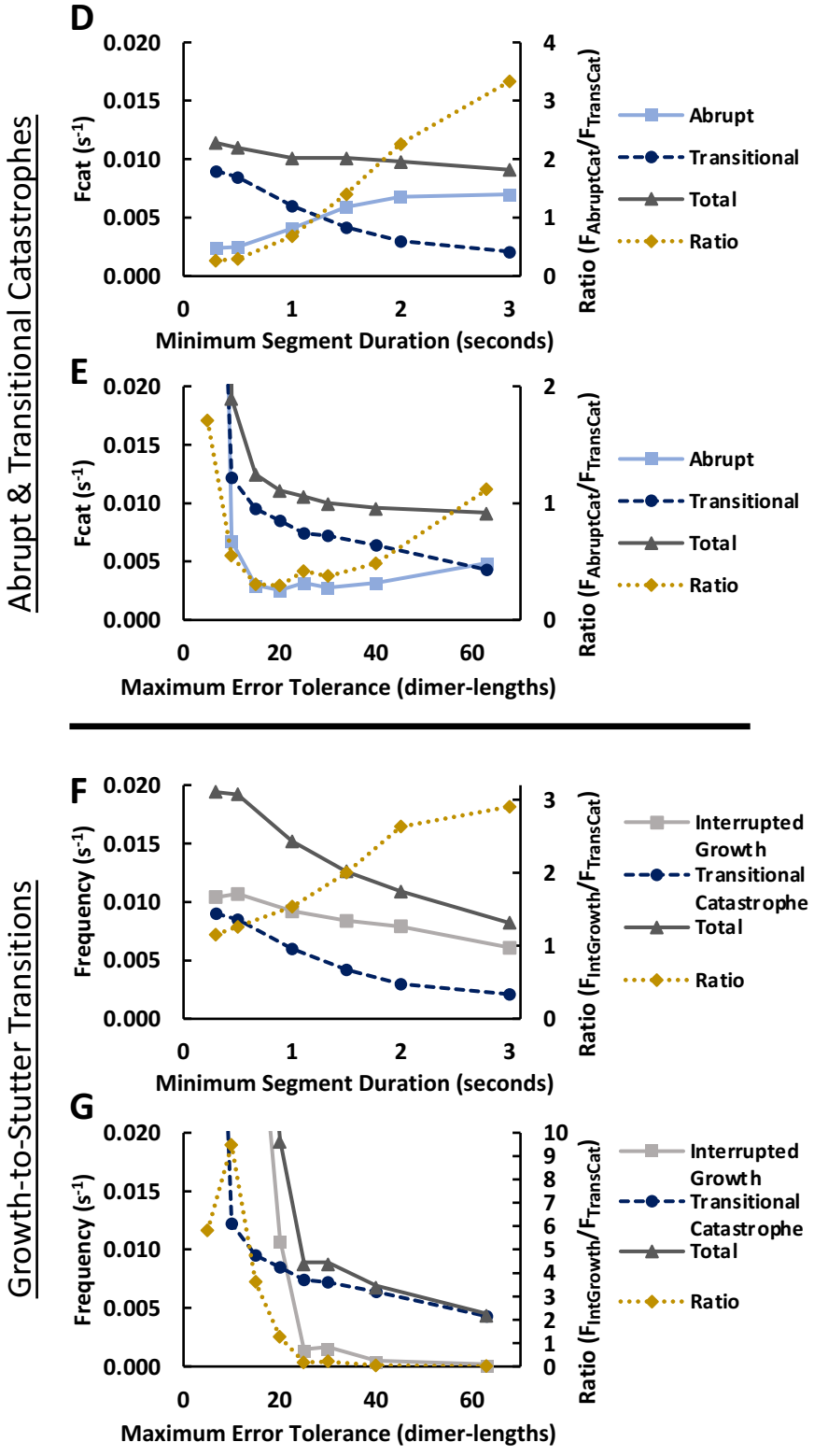

Figure S2.9. Transition analysis across Minimum Segment Durations and Maximum Error Tolerances provides robust support for prevalence of transitional catastrophes in the full resolution ***in silico*** dataset.

Please see **pages 17 – 18** for the description and interpretations of the transition frequency figures for each dataset (**Figures S2.9 – S2.11**).

A

Frequency of ABRUPT CATASTROPHE						
Max Error Tolerance (dimer-lengths)	Minimum Segment Duration (s)					
	0.3	0.5	1.0	1.5	2.0	3.0
5	Not Calculated for *In Vitro* data	0.0012	0.0072	0.0062	0.0047	0.0037
10		0.0013	0.0069	0.0059	0.0045	0.0038
15		0.0015	0.0065	0.0105	0.0047	0.0040
20		0.0018	0.0062	0.0098	0.0050	0.0041
25		0.0030	0.0072	0.0035	0.0051	0.0046
30		0.0028	0.0063	0.0059	0.0055	0.0050
40		0.0032	0.0067	0.0062	0.0057	0.0053
63		0.0061	0.0072	0.0068	0.0064	0.0063

B

Frequency of TRANSITIONAL CATASTROPHE						
Max Error Tolerance (dimer-lengths)	Minimum Segment Duration (s)					
	0.3	0.5	1.0	1.5	2.0	3.0
5	Not Calculated for *In Vitro* data	0.0166	0.0069	0.0061	0.0058	0.0059
10		0.0137	0.0049	0.0043	0.0045	0.0052
15		0.0121	0.0032	0.0051	0.0033	0.0043
20		0.0108	0.0025	0.0042	0.0026	0.0037
25		0.0077	0.0002	0.0072	0.0019	0.0030
30		0.0085	0.0020	0.0017	0.0018	0.0026
40		0.0067	0.0015	0.0014	0.0013	0.0019
63		0.0031	0.0006	0.0005	0.0005	0.0007

C

Frequency of INTERRUPTED GROWTH						
Max Error Tolerance (dimer-lengths)	Minimum Segment Duration (s)					
	0.3	0.5	1.0	1.5	2.0	3.0
5	Not Calculated for *In Vitro* data	0.0846	0.0822	0.0739	0.0495	0.0325
10		0.0205	0.0202	0.0197	0.0178	0.0156
15		0.0077	0.0078	0.0058	0.0072	0.0064
20		0.0036	0.0038	0.0029	0.0035	0.0034
25		0.0006	0.0007	0.0006	0.0020	0.0019
30		0.0010	0.0010	0.0010	0.0009	0.0009
40		0.0003	0.0003	0.0002	0.0003	0.0002
63		0.0001	0.0001	0.0001	0.0001	0.0000

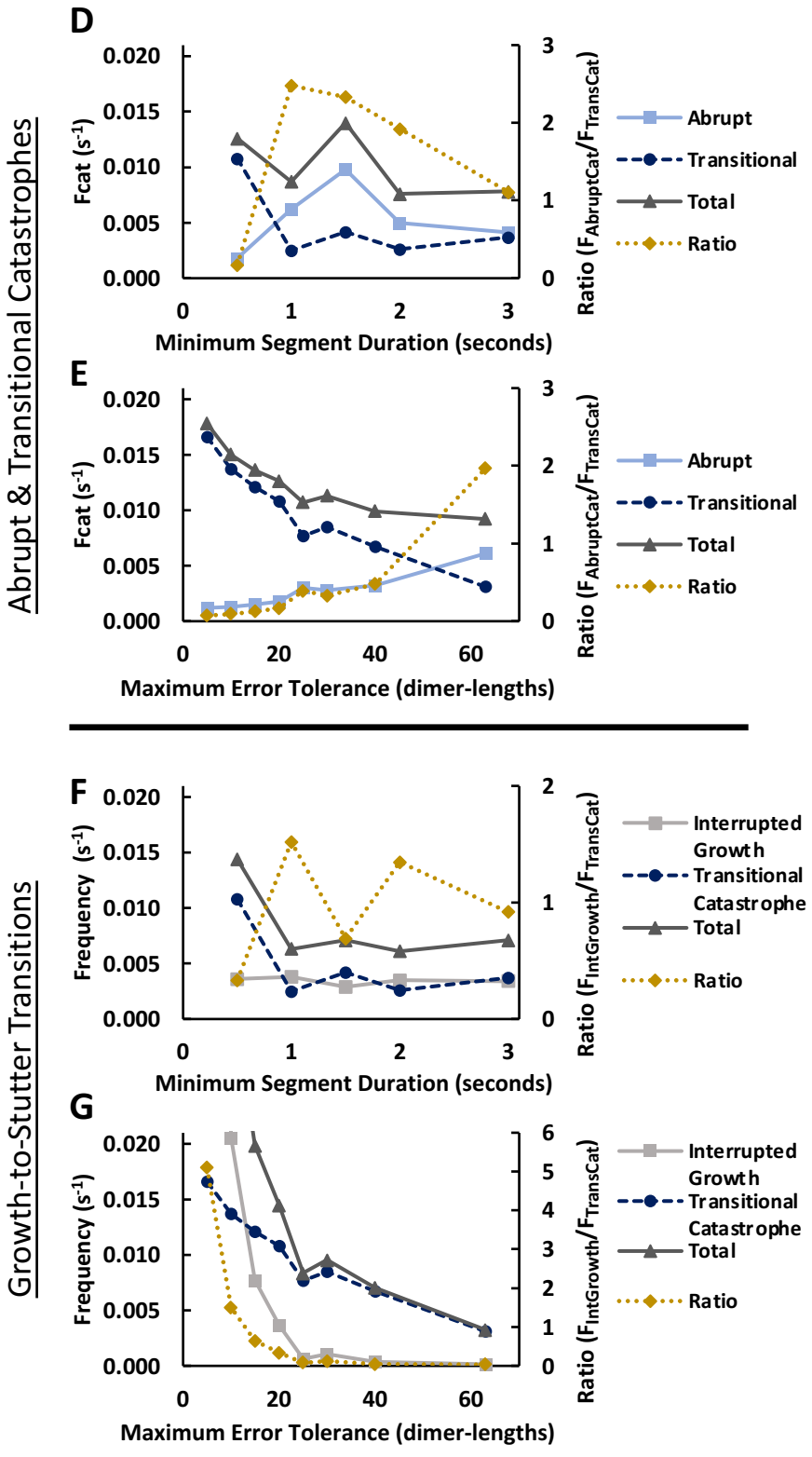

Figure S2.10. Transition analysis across Minimum Segment Durations and Maximum Error Tolerances provides robust support for prevalence of transitional catastrophes in the ***in vitro* control** dataset.

Please see **pages 17 – 18** for the description and interpretations of the transition frequency figures for each dataset (**Figures S2.9 – S2.11**). Please see **page 23** for **Figure S2.12**, which compares the transition frequencies from the *in vitro* control and CLASP2γ datasets.

A

Frequency of ABRUPT CATASTROPHE						
Max Error Tolerance (dimer-lengths)	Minimum Segment Duration (s)					
	0.3	0.5	1.0	1.5	2.0	3.0
5	Not Calculated for *In Vitro* data	0.0379	0.0412	0.0160	0.0078	0.0112
10		0.0176	0.0178	0.0165	0.0109	0.0059
15		0.0087	0.0082	0.0089	0.0083	0.0050
20		0.0049	0.0057	0.0055	0.0074	0.0050
25		0.0037	0.0041	0.0042	0.0048	0.0024
30		0.0042	0.0046	0.0049	0.0042	0.0025
40		0.0034	0.0033	0.0035	0.0059	0.0055
63		0.0023	0.0021	0.0054	0.0050	0.0054

B

Frequency of TRANSITIONAL CATASTROPHE						
Max Error Tolerance (dimer-lengths)	Minimum Segment Duration (s)					
	0.3	0.5	1.0	1.5	2.0	3.0
5	Not Calculated for *In Vitro* data	0.0148	0.0144	0.0124	0.0088	0.0053
10		0.0074	0.0063	0.0033	0.0032	0.0029
15		0.0046	0.0040	0.0029	0.0024	0.0017
20		0.0034	0.0024	0.0018	0.0022	0.0015
25		0.0032	0.0023	0.0026	0.0044	0.0030
30		0.0017	0.0019	0.0019	0.0028	0.0025
40		0.0011	0.0009	0.0010	0.0008	0.0008
63		0.0003	0.0003	0.0000	0.0000	0.0000

C

Frequency of INTERRUPTED GROWTH						
Max Error Tolerance (dimer-lengths)	Minimum Segment Duration (s)					
	0.3	0.5	1.0	1.5	2.0	3.0
5	Not Calculated for *In Vitro* data	0.1129	0.0720	0.0760	0.0460	0.0279
10		0.0321	0.0291	0.0204	0.0162	0.0102
15		0.0137	0.0124	0.0100	0.0089	0.0061
20		0.0088	0.0075	0.0039	0.0071	0.0056
25		0.0050	0.0030	0.0022	0.0044	0.0013
30		0.0030	0.0018	0.0016	0.0042	0.0011
40		0.0020	0.0014	0.0010	0.0020	0.0008
63		0.0008	0.0008	0.0007	0.0020	0.0011

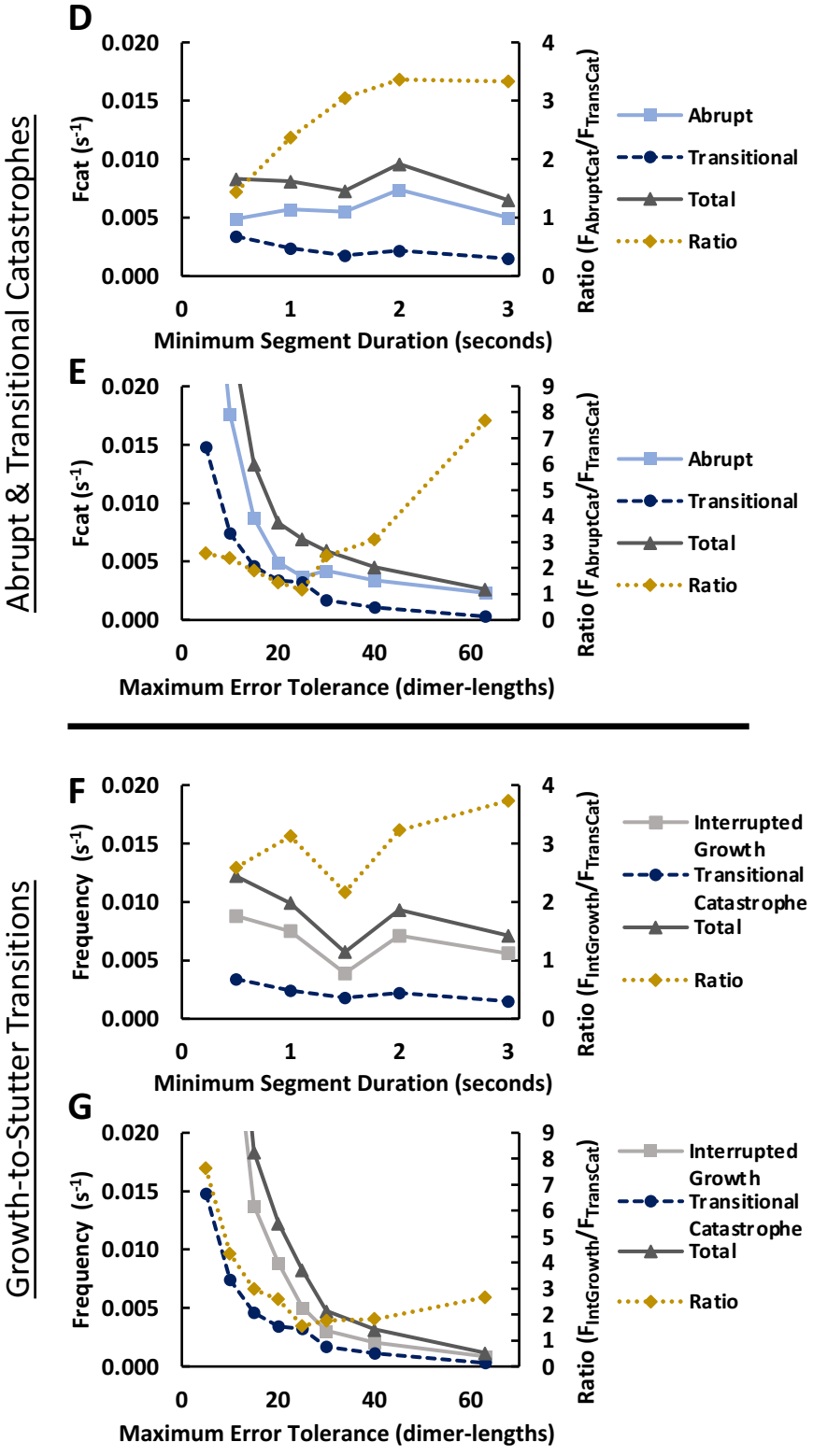

Figure S2.11. Transition analysis across Minimum Segment Durations and Maximum Error Tolerances provides robust support for reduced transitional catastrophe frequency and increased interrupted growth frequency in the ***in vitro*** **CLASP2γ** dataset.

Please see **pages 17 – 18** for the description and interpretations of the transition frequency figures for each dataset (**Figures S2.9 – S2.11**). Please see **page 23** for **Figure S2.12**, which compares the transition frequencies from the *in vitro* control and CLASP2γ datasets.

Transition Frequency Comparison Figure

Figure S2.12: *in vitro* control and *in vitro* CLASP2γ datasets

Description: Each panel compares transition frequencies from the *in vitro* control dataset (orange dashed lines, square markers) and *in vitro* CLASP2γ dataset (yellow solid lines, circle markers). These control and CLASP2γ data are replotted from **Figures S2.10** and **S2.11**, respectively, for the purpose of comparing the frequencies from the two different datasets on the same graph.

The measured frequencies F_{Cat} (A,B), $F_{TransCat}$ (C,D), $F_{IntGrowth}$ (E,F) and the ratio $F_{IntGrowth}/F_{TransCat}$ (G,H) are plotted for varying Minimum Segment Durations while holding the Maximum Error Tolerance constant at 20 dimer-lengths (A,C,E,G) and varying Maximum Error Tolerances while holding the Minimum Segment Duration constant at 0.5 seconds (B,D,F,H).

For the values of the frequencies that are too high to be visible in (B,F) at small Maximum Error Tolerances, please see the tables in **Figures S2.10 C** and **S2.11 A,B,C**.

Observations: For most of the values of Minimum Segment Duration and Maximum Error Tolerance in (A,B), the total F_{cat} is smaller in the *in vitro* CLASP2γ dataset than in the *in vitro* control dataset (the few exceptions are at Minimum Segment Duration = 2 seconds in (A), and Maximum Error Tolerance < 15 dimers-lengths in (B)).

For *all* combinations of Minimum Segment Duration and Maximum Error Tolerance in (G,H), the ratio $F_{IntGrowth}/F_{TransCat}$ is greater in the CLASP2γ dataset than in the control dataset. In particular, the presence of CLASP2γ reduces $F_{TransCat}$ (C,D) and increases $F_{IntGrowth}$ (E,F) compared to the control data in almost all cases (the only exceptions are two data points in (C) where the values of $F_{TransCat}$ are very similar in the two datasets).

Interpretations: The observations above demonstrate that the conclusion that CLASP2γ suppresses catastrophe by promoting growth of stuttering MTs is robust to changes in the STADIA segmentation parameters.

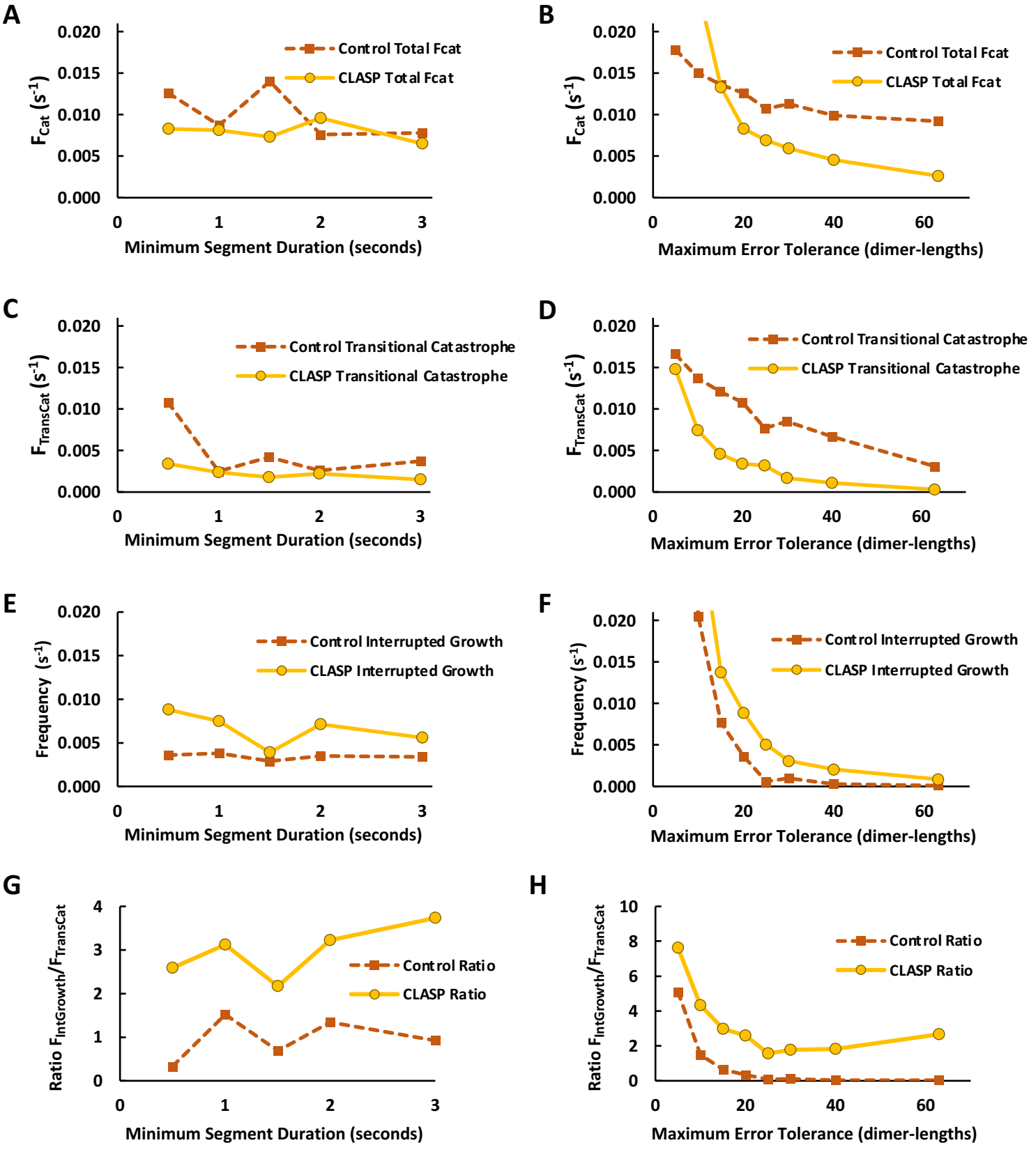

Figure S2.12. Comparison of transition analysis results from the *in vitro* datasets for varying Minimum Segment Durations and Maximum Error Tolerances supports the conclusion that CLASP2γ suppresses transitional catastrophes and promotes interrupted growths.

Please see **page 22** for the description and interpretations of this figure.

Supplemental Section S3: Data Acquisition Rate Sensitivity Analysis

Overview: The analyses presented in the previous section (**Supplemental Section S2**) tested the effects of varying the values of the user-input STADIA segmentation parameters Minimum Segment Duration and Maximum Error Tolerance. Here in **Supplemental Section S3**, we examine sensitivity to the temporal resolution of the inputted length-history data itself, in addition to varying the STADIA parameters Minimum Segment Duration and Maximum Error Tolerance. This analysis uses the dimer-scale *in silico* dataset. The analyses presented here serve two related purposes: one, to provide guidance to users of STADIA regarding how changes to the temporal resolution of the inputted length-history data affect the outputs of STADIA; two, to test the robustness of the main conclusions of our manuscript to changes in the temporal resolution.

In this section, the conclusions being considered are as follows: **(1)** MTs exhibit more behaviors than just growth and shortening, with stutters being distinguishable behaviors that are prevalent throughout length-history data, and **(2)** transitional catastrophes are more frequent than abrupt catastrophes. The table of contents below directs readers to the figures related to each of the above conclusions.

Section S3 Table of Contents

Information on procedure for varying temporal resolution of input length-history data

In **Supplemental Section S2**, we explored the impact of changing STADIA parameters on all three datasets used in the main text. Here in **Supplemental Section S3**, we examine the effect of changing the data acquisition rate ("frame" rate), which is a property of the input length-history data itself. This analysis uses the ***in silico*** data to allow for varying the data acquisition rate across a wide range of values, including rates faster than the *in vitro* frame rate. We achieve this variation by imposing various fixed data acquisition rates on the original full resolution *in silico* dataset ("full resolution" defined in the next paragraph). We then compare the results from STADIA analysis of these reduced resolution datasets to those obtained from the full resolution dataset.

In the following figures, "Full Resolution Data" refers to the raw simulation output, which includes a data point for every dimer-scale biochemical event. For the input simulation parameters used to generate the *in silico* data in this manuscript, approximately 1650 events occurred per second. See main text Methods Section 4.2 for more information. The *in silico* dataset used in the main text and in **Supplemental Sections S1 & S2** was also the full resolution dataset.

The setup of the following analyses is similar to the parameter sensitivity analyses presented in **Supplemental Section S2**. However, here we vary the Data Acquisition Time Step, in addition to varying the two STADIA parameters examined in **Supplemental Section S2**. Note that 'data acquisition rate in frames per second' = 1/'Data Acquisition Time Step in seconds' (e.g., 2 fps corresponds to a Data Acquisition Time Step of 0.5 seconds). As a result of the need to examine three variables, the layout of figures in **Supplemental Section S3** differs from **Supplemental Section S2**. Specifically, here in **Supplemental Section S3**, there are three sets of three figures: gap statistic plots for positive slope segments (**Figures S3.1-S3.3**), gap statistic plots for negative slope segments (**Figures S3.4-S3.6**), and cluster profiles for the positive and negative slope segments along with labeled length-history plots (**Figures S3.7-S3.9**). Within each set, each figure corresponds to a particular Minimum Segment Duration (0.5, 1.0, or 3.0 seconds). Within the gap statistic figures, the columns correspond to varying values of the Data Acquisition Time Step and the rows correspond to varying values of the Maximum Error Tolerance. Within the cluster profile and length-history figures, the Maximum Error Tolerance is fixed at 20 dimer-lengths and the rows now correspond to varying Data Acquisition Time Steps. For reference, the analysis in the main text and **Supplemental Section S1** used Minimum Segment Duration = 0.5 seconds and Maximum Error Tolerance = 20 dimer-lengths.

Subsection S3.1: Gap Statistic Figures - *in silico* data with varying Data Acquisition Time Steps

The gap statistic plots aid in determining the *k*-values (number of clusters) to use in the clustering step of STADIA.

Positive slope segments:

Figure S3.1: Minimum Segment Duration = 0.5 seconds
Figure S3.2: Minimum Segment Duration = 1.0 seconds
Figure S3.3: Minimum Segment Duration = 3.0 seconds

Negative slope segments:

Figure S3.4: Minimum Segment Duration = 0.5 seconds
Figure S3.5: Minimum Segment Duration = 1.0 seconds
Figure S3.6: Minimum Segment Duration = 3.0 seconds

Description: Panel **A** of each figure: The gap statistic plots are the result of analyzing the *in silico* data with varying Data Acquisition Time Steps (column headings) using the Diagnostic Mode of STADIA with the Minimum Segment Duration indicated in each figure legend and varying Maximum Error Tolerances (row headings).

Each gap statistic plot is labeled with the *k*-value that we selected based on examination of that gap statistic plot and corresponding cluster profile. Our selected *k*-value usually corresponds to either the first or second local maximum of the gap statistic plot. The *k*-value of the second local maximum was chosen if the *k*-value at the second local maximum showed better agreement with the cluster profile AND the gap value at the second local maximum was greater than at the first local maximum. Italics indicate cases where the selected *k*-value differs from the *k*-value outputted by Diagnostic Mode, which uses the criteria from Tibshirani et al. (2001) as described in the main text Methods. **Green** in **Figures S3.1-S3.3** (positive slope segments) and **red** in **Figures S3.4-S3.6** (negative slope segments) are used to indicate agreement with the *k*-values selected in the main text results (**Figure 4, Supplemental Figures S1.4, S1.5**); **gray** indicates parameter combinations resulting in *k*-values different from the main text results; plots with ***** are monotonically increasing, and therefore lack a clear local maximum and are inconclusive for suggesting an optimal *k*-value.

The **dark blue** box indicates the parameter space for which cluster profiles and labeled length-history plots are provided in **Figures S3.7-S3.9**. These parameter combinations were chosen for further analysis due to their physical relevance (i.e., Maximum Error Tolerance of 20 dimer-lengths corresponds to spatial resolution that is both experimentally feasible and sufficient to capture stutters, provided that the Data Acquisition Time Step and Minimum Segment Duration are sufficiently small). The gap statistic plots outside the dark blue box are included for completeness in the exploration of the parameter space.

Panel **B** of each figure (bottom right): A representative gap statistic plot shows the axes for each plot in (A). The x-axis (*k*-value) range is the same for all plots. The y-axis (gap value) has differing ranges (not shown) for each plot, but the specific numerical values of the gap statistic are not relevant to interpreting the plots because identification of the optimal *k*-value is based on local maxima within each gap statistic plot. In other words, the pertinent information is the relationship between the values of the gap statistic at different *k*-values within each plot, not the gap statistic values themselves.

†The **full resolution** *in silico* data (first column) have temporal resolution of one output per dimer-scale biochemical event (see main text Methods Section 4.2 for more information).

Observations: The gap statistic plots resulting from the analysis of the *in silico* data with varying Data Acquisition Time Steps are generally similar to the results from the full resolution data. The identification of k=3 as the optimal k-value is upheld in most cases. The most notable exception is for the negative slope segment data with Data Acquisition Time Steps of 1.5 or 3.0 seconds analyzed with Minimum Segment Duration = 3.0 seconds; for these data, the gap statistic suggests k=1 across most of the Maximum Error Tolerances tested (**Figure S3.6**).

Additional Observations: For the positive slope segment data (**Figures S3.1-S3.3**), the same general pattern (i.e., k=3 for sufficiently small Maximum Error Tolerances and a diminishing number of clusters with increasing Maximum Error Tolerance) is upheld across the Data Acquisition Time Steps and Minimum Segment Durations considered. For the negative slope segment data (**Figures S3.4-S3.6**), the identification of k=3 is generally less sensitive to the Maximum Error Tolerance than for the positive slope segment data, but the prominence of the local maximum at k=3 for the negative slope segment data does vary across the different Data Acquisition Time Steps and STADIA parameter combinations.

Interpretations: The stability of the k-value suggested by the gap statistic plots across most of the Data Acquisition Time Steps (i.e., 0.1, 0.5, and 1.0 seconds) supports the robustness of the conclusion that stutters exist and are not simply a result of analyzing data at fine resolution. The loss of detection of multiple clusters in the negative slope segment data at the slow Data Acquisition Time Steps (i.e., 1.5 and 3.0 seconds) is not surprising. As was noted in the STADIA parameter sensitivity analysis with the full resolution data (**Supplemental Section S2**), MT depolymerizations occur at relatively short time scales (often less than 3 seconds). Therefore, when data are acquired with time steps this long, approximating depolymerizations closely enough to detect multiple behaviors within the negative slope segments can become challenging.

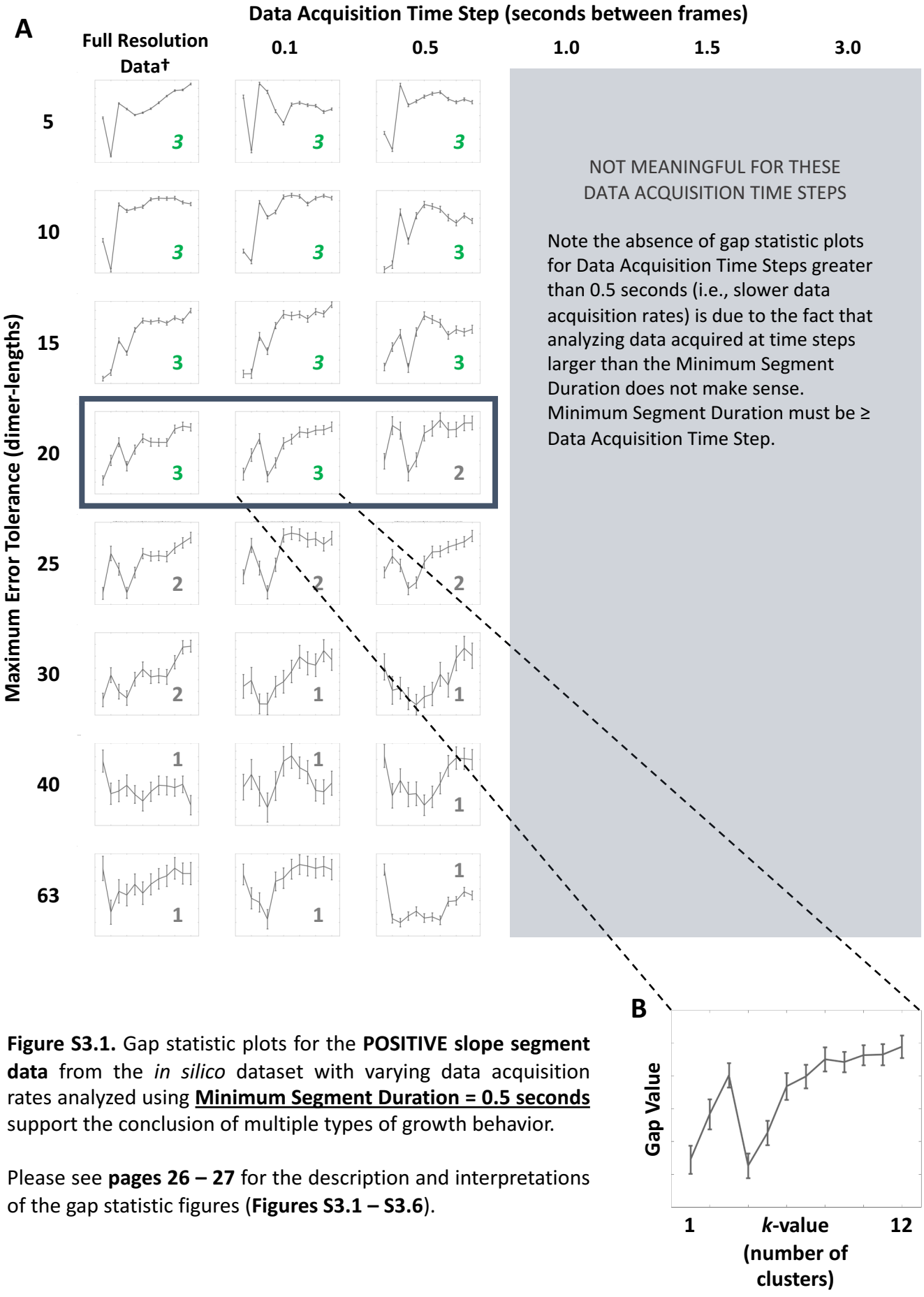

Figure S3.1. Gap statistic plots for the **POSITIVE slope segment data** from the *in silico* dataset with varying data acquisition rates analyzed using **Minimum Segment Duration = 0.5 seconds** support the conclusion of multiple types of growth behavior.

Please see **pages 26 – 27** for the description and interpretations of the gap statistic figures (**Figures S3.1 – S3.6**).

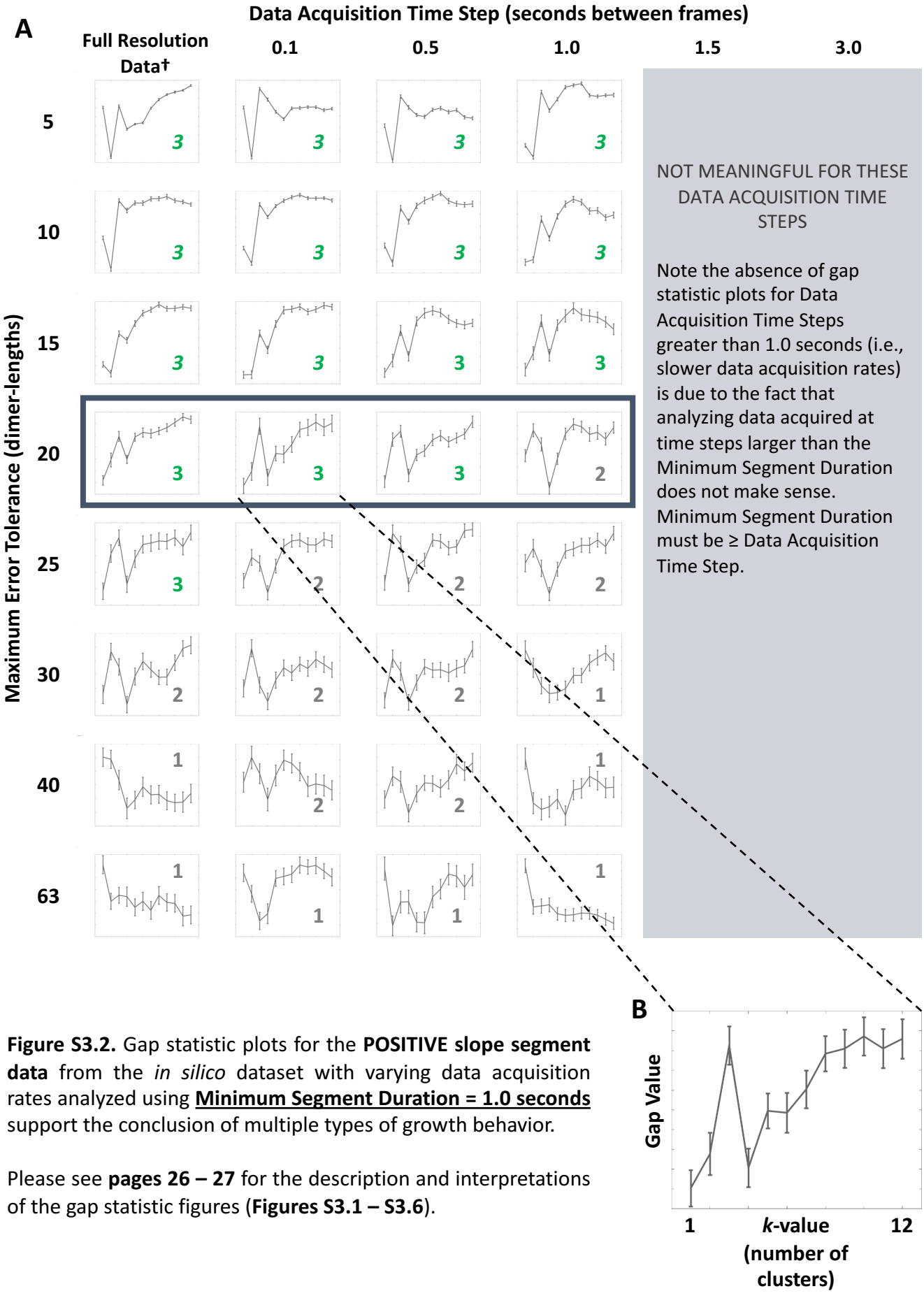

Figure S3.2. Gap statistic plots for the **POSITIVE slope segment data** from the *in silico* dataset with varying data acquisition rates analyzed using **Minimum Segment Duration = 1.0 seconds** support the conclusion of multiple types of growth behavior.

Please see **pages 26 – 27** for the description and interpretations of the gap statistic figures (**Figures S3.1 – S3.6**).

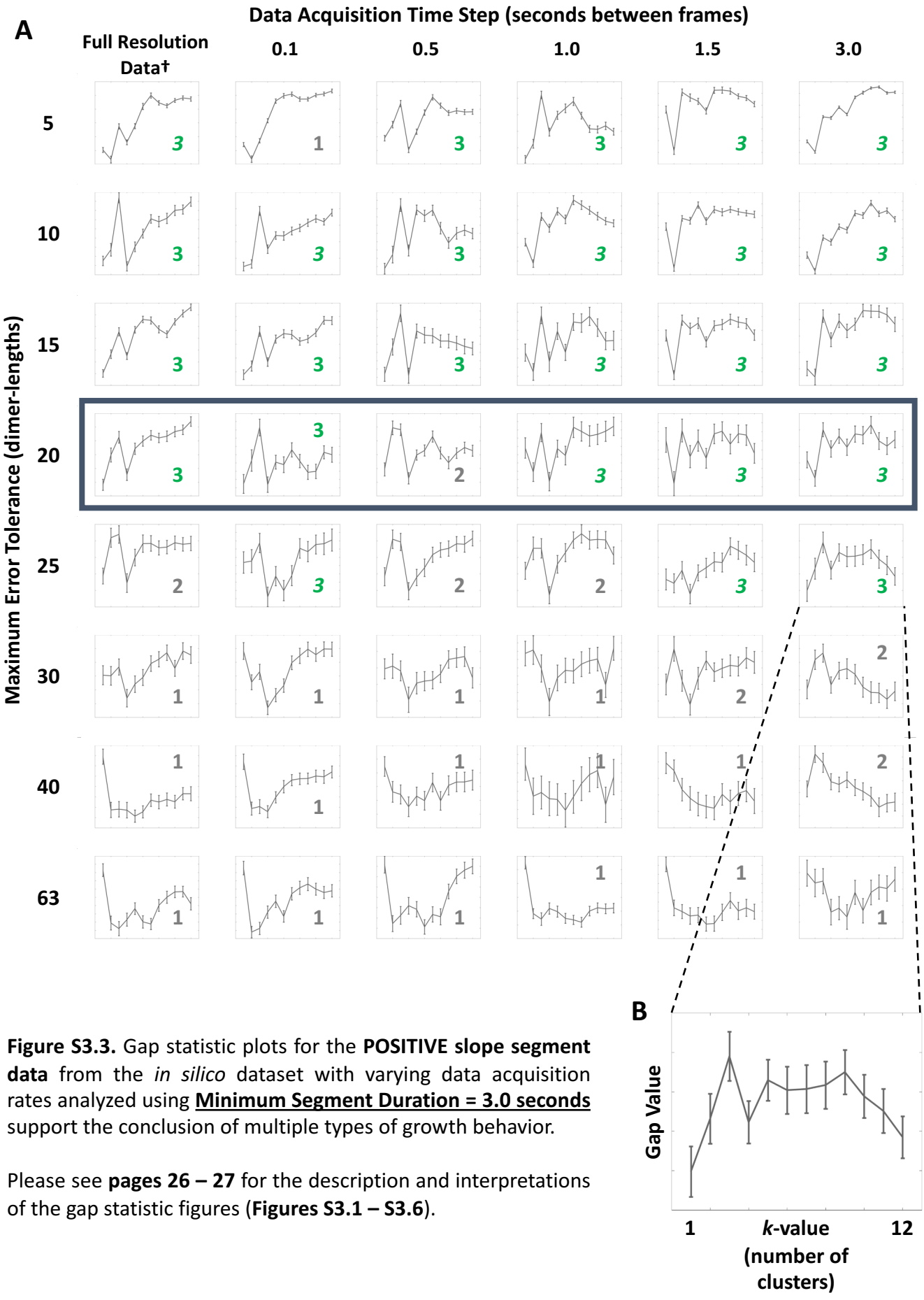

Figure S3.3. Gap statistic plots for the **POSITIVE slope segment data** from the *in silico* dataset with varying data acquisition rates analyzed using **Minimum Segment Duration = 3.0 seconds** support the conclusion of multiple types of growth behavior.

Please see **pages 26 – 27** for the description and interpretations of the gap statistic figures (**Figures S3.1 – S3.6**).

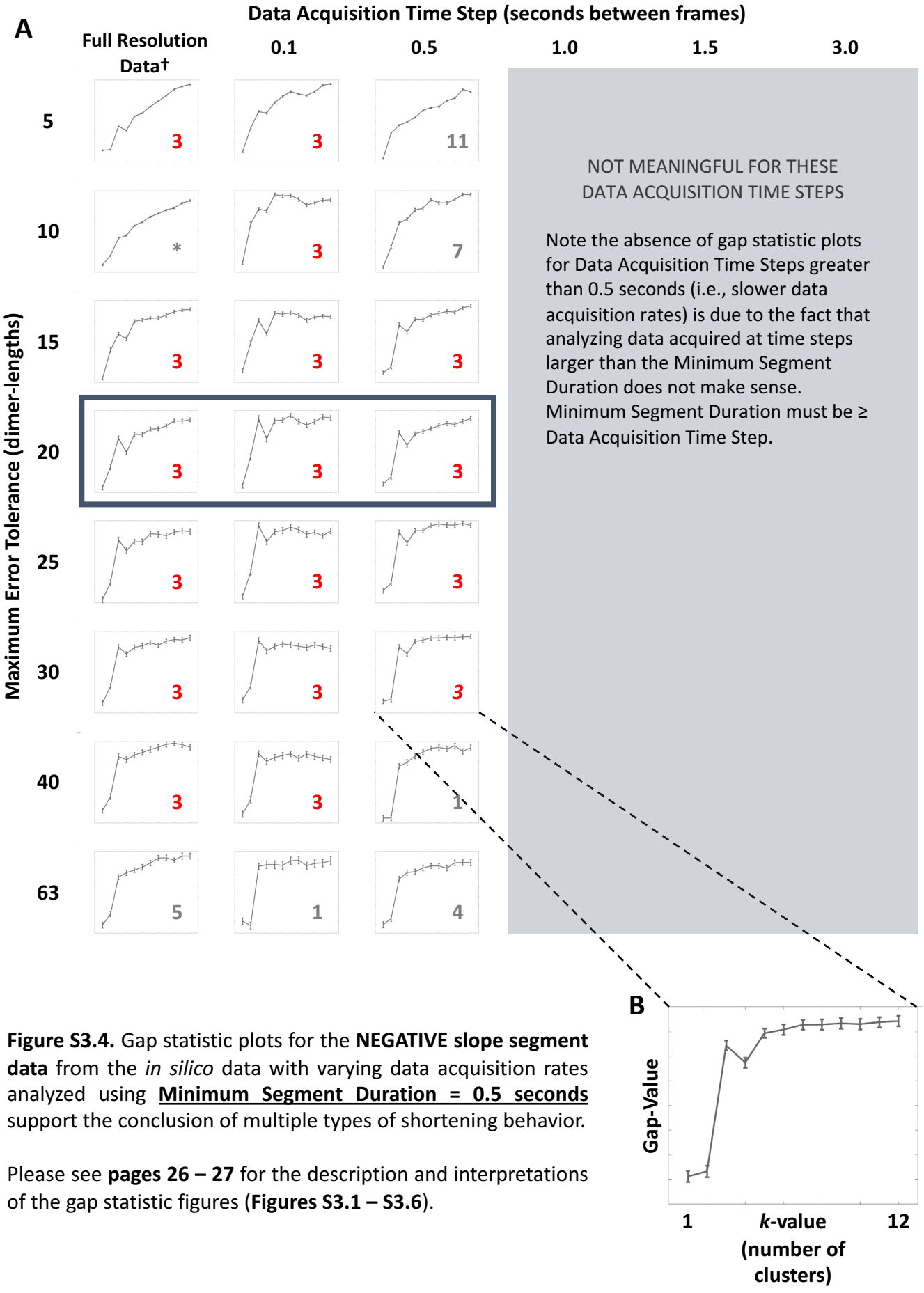

Figure S3.4. Gap statistic plots for the **NEGATIVE slope segment data** from the *in silico* data with varying data acquisition rates analyzed using **Minimum Segment Duration = 0.5 seconds** support the conclusion of multiple types of shortening behavior.

Please see **pages 26 – 27** for the description and interpretations of the gap statistic figures (**Figures S3.1 – S3.6**).

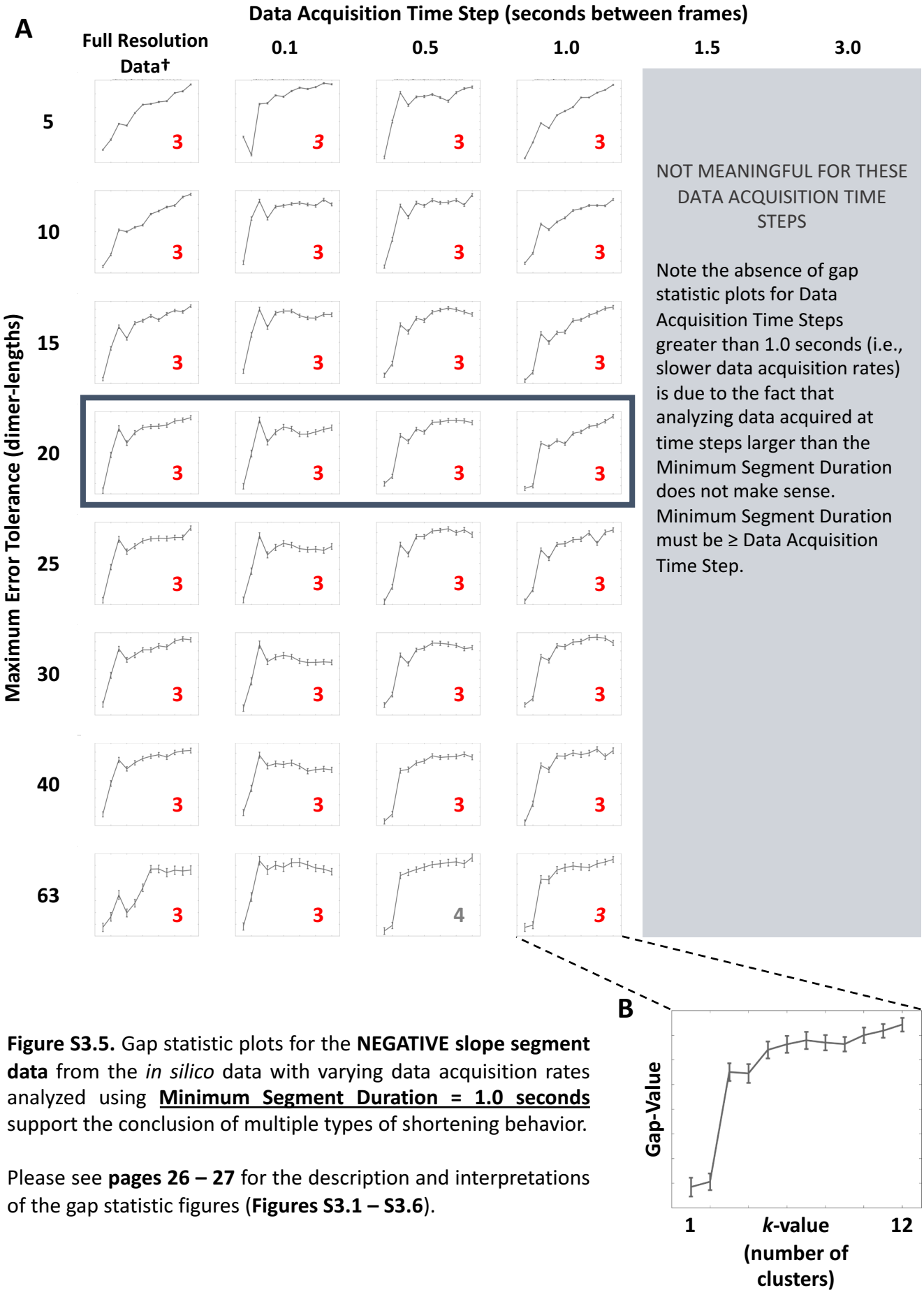

Figure S3.5. Gap statistic plots for the **NEGATIVE slope segment data** from the *in silico* data with varying data acquisition rates analyzed using **Minimum Segment Duration = 1.0 seconds** support the conclusion of multiple types of shortening behavior.

Please see **pages 26 – 27** for the description and interpretations of the gap statistic figures (**Figures S3.1 – S3.6**).

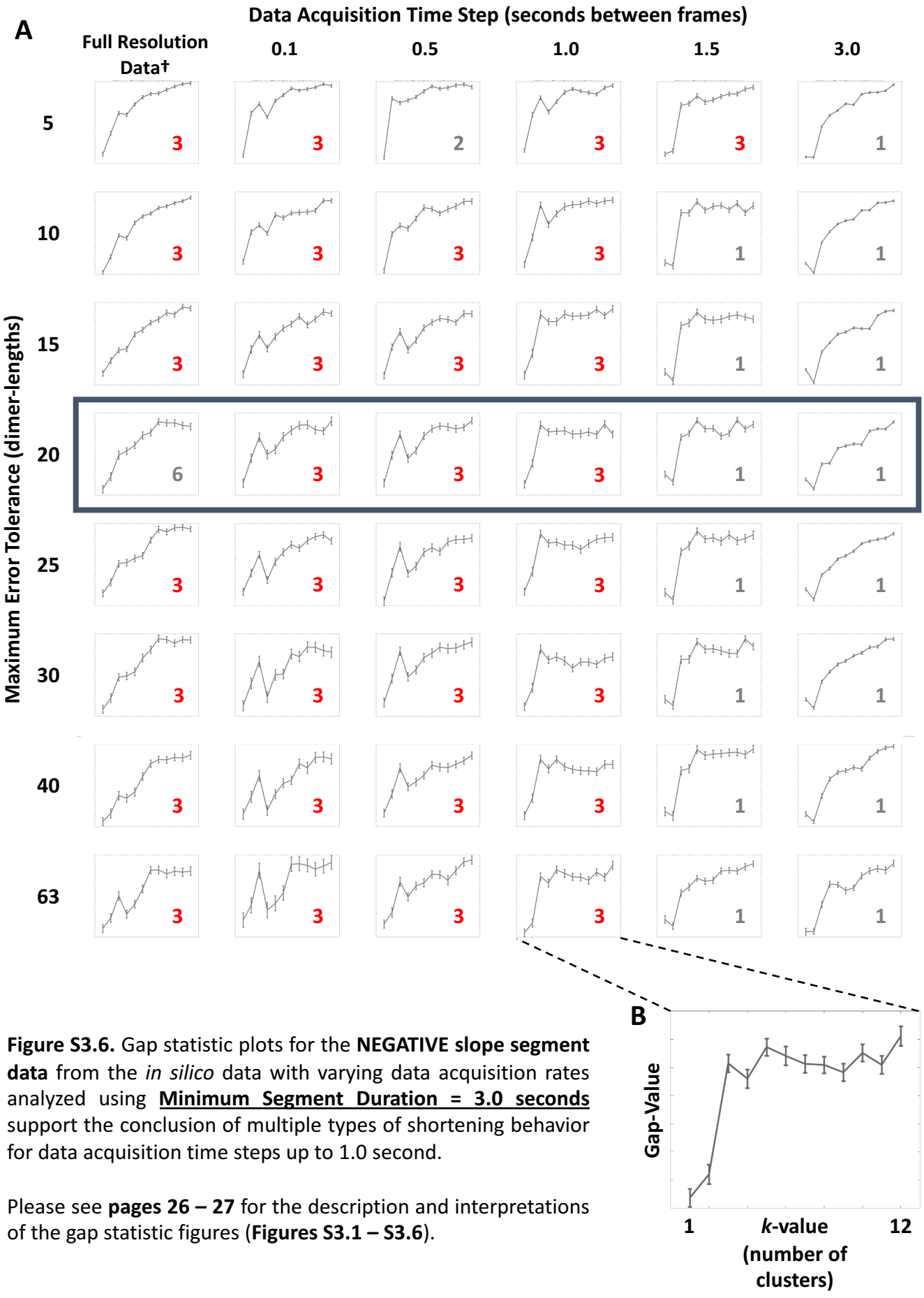

Figure S3.6. Gap statistic plots for the **NEGATIVE slope segment data** from the *in silico* data with varying data acquisition rates analyzed using **Minimum Segment Duration = 3.0 seconds** support the conclusion of multiple types of shortening behavior for data acquisition time steps up to 1.0 second.

Please see **pages 26 – 27** for the description and interpretations of the gap statistic figures (**Figures S3.1 – S3.6**).

Subsection S3.2: Cluster Profile and Length-History Figures - *in silico* data with varying Data Acquisition Time Steps

Each data point in the cluster profiles corresponds to a line segment from the segmentation stage of STADIA. The cluster profiles show how segments are grouped together in the classification stage of STADIA. The segments in the length-history plots are color-coded according to the classification results.

Figure S3.7: Minimum Segment Duration = 0.5 seconds
Figure S3.8: Minimum Segment Duration = 1.0 seconds
Figure S3.9: Minimum Segment Duration = 3.0 seconds

Description: The cluster profiles and labeled length-history plots represent results of analyzing the *in silico* data with varying Data Acquisition Time Steps (row headings) using the Automated Mode of STADIA with the Minimum Segment Duration indicated in each figure legend and Maximum Error Tolerance = 20 dimer-lengths. The analysis was performed using the *k*-values suggested by the corresponding gap statistic plots in **Figures S3.1-S3.6** (except for the full resolution negative slope segment data in **Figure S3.9**, where *k*=3 was used instead of the *k*=6 suggested by the gap statistic).

†The **full resolution** *in silico* data (first row) have temporal resolution of one output per dimer-scale biochemical event (see Methods Section 4.2 in the main text for more information).

Observations regarding the cluster profiles: The cluster profiles maintain the same general shape with varying Data Acquisition Time Steps, but some changes do occur. A notable difference is that the overall density of data points decreases with increasing Data Acquisition Time Steps (i.e., moving down the rows). Particularly for the longer Data Acquisition Time Steps in **Figure S3.9**, the density of (distinguishable) data points is so minimal that drawing any conclusion about the shape of the data structure would be difficult without the profiles from the smaller Data Acquisition Time Steps for comparison. Additionally, the data points become arranged along lines corresponding to fixed values on the time duration axis, with the gaps between these lines widening as the Data Acquisition Time Step increases.

Interpretations regarding the cluster profiles: The relative stability of the shape of the cluster profiles with varying Data Acquisition Time Steps bolsters the conclusions about the number of clusters drawn from the gap statistic plots in **Figures S3.1-S3.6** (recall that the gap statistic drives the decision for the optimal *k*-value, but cluster profiles are also used to inform the *k*-value).

The appearance of a loss of density (particularly in the shortening segments) is due, in part, to the data points collapsing onto lines that correspond to multiples of the Data Acquisition Time Step. Furthermore, with the longer Data Acquisition Time Steps, more loss of density occurs among the short-duration segments (i.e., stutters and brief growth/shortening) than among the long-duration segments (i.e., sustained growth/shortening). Particularly for the negative slope segment data, it is evident that the datasets at long Data Acquisition Time Steps (i.e., 1.5 and 3.0 seconds in **Figure S3.9**) are too sparsely filled to draw conclusion about the number of behaviors; datasets that are this sparse would generally not be considered good candidates for *k*-means clustering.

Additional discussion regarding the cluster profiles: Similar to the analysis of the full resolution data with varying Minimum Segment Durations (**Figure S2.5**), changing the data acquisition rate can affect the shapes and centroid locations of the clusters even if the number of clusters remains the same (e.g., compare the positive slope segment clusters in the first and last rows of **Figure S3.9**). Interestingly, the shapes of the positive slope segment clusters for the longer Data Acquisition Time Steps appear more similar to the results from the full resolution mean PF data than the full resolution max PF data (**Figure S1.4**). This observation leads us to speculate that the most rapid brief growth segments may correspond to tip extensions.

Observations regarding the length-history plots: For increasing values of the Data Acquisition Time Step or the Minimum Segment Duration, fewer stutters are detected throughout the plotted region of length-history data.

Interpretations regarding the length-history plots: The labeled length-history data illustrate that detection of stutters is reliant on both the Minimum Segment Duration and the Data Acquisition Time Step (however, choices of the Minimum Segment Duration are limited by the Data Acquisition Time Step because Minimum Segment Duration must be greater than or equal to the Data Acquisition Time Step considered).

Although stutter clusters are identified at data acquisition rates slower than 2 fps, the clusters contain fewer segments, and the corresponding length-history plots demonstrate that individual stutter segments are missed. Thus, we conclude that data acquired at rates slower than 2 fps are not ideal for thorough detection and analysis of stutter segments.

Additional observations regarding the length-history plots: The zoomed-in portraits in each panel provide an example of how the Data Acquisition Time Step and Minimum Segment Duration affect detection of transitional catastrophes, as follows: With Minimum Segment Duration = 0.5 seconds (**Figure S3.7),** STADIA correctly identifies this catastrophe as transitional regardless of the Data Acquisition Time Step, but the time duration of the stutter appears to decrease as the Data Acquisition Time Step increases. With Minimum Segment Duration = 1.0 or 3.0 seconds (**Figures S3.8-S3.9**), the catastrophe is no longer identified as transitional. In both **Figures S3.8** and **S3.9**, the catastrophe as seen in the inputted length-history data itself (white line) appears to become less transitional as the Data Acquisition Time Step increases, until the catastrophe appears to be undeniably abrupt at Data Acquisition Time Step = 1.0 seconds. In **Figure S3.9**, when the Data Acquisition Time Step is 1.5 seconds, the location of the catastrophe changes and, by chance, the captured data points result in what appears to be a transitional catastrophe again but is not detected as transitional using a Minimum Segment Duration of 3.0 seconds. When the data acquisition rate is increased to 3.0 seconds, the catastrophe is completely abrupt in appearance.

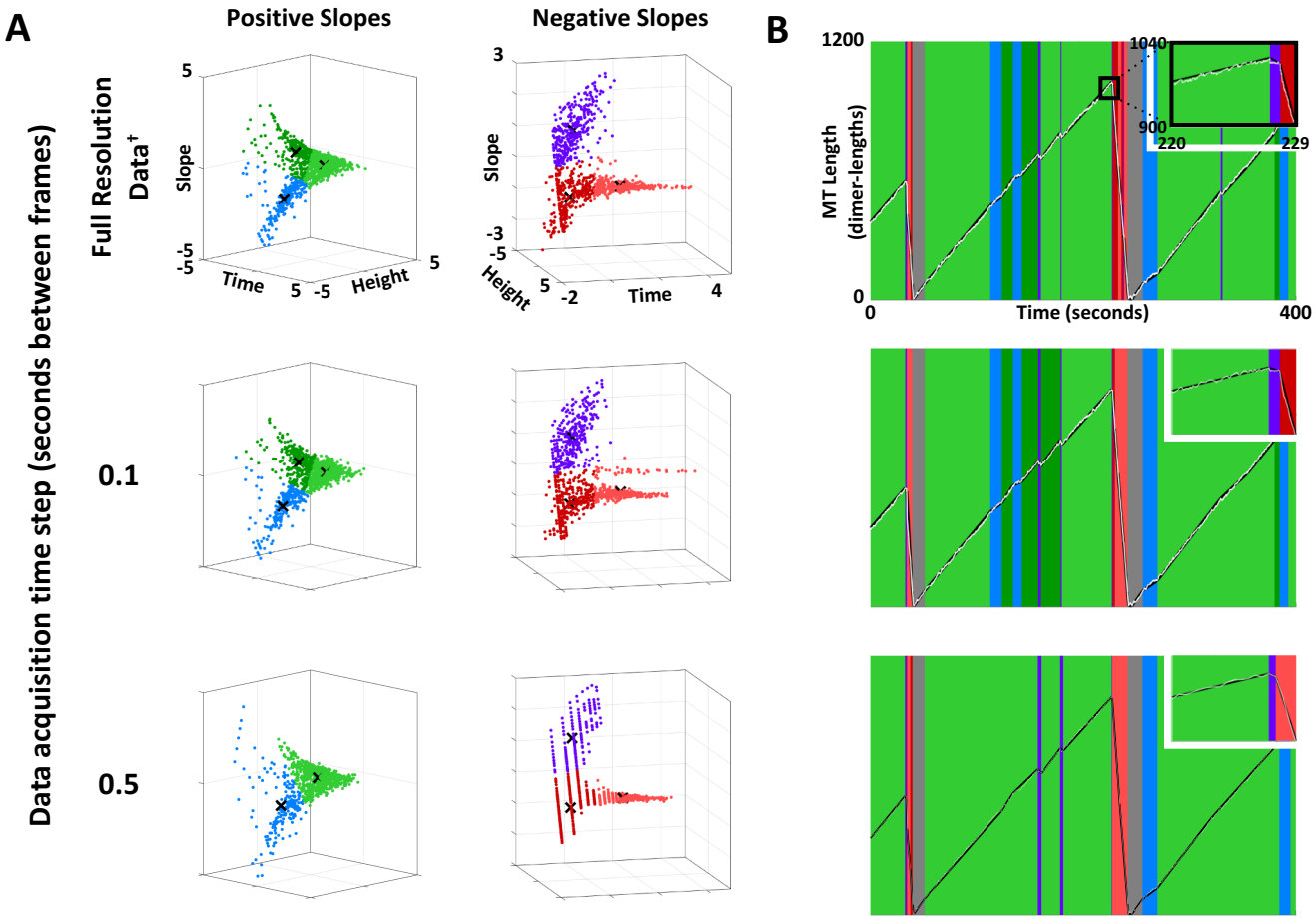

Figure S3.7. Classification results for the *in silico* data with varying data acquisition rates analyzed using **Minimum Segment Duration = 0.5 seconds** and Maximum Error Tolerance = 20 dimer-lengths. **(A)** Cluster profiles of positive and negative slope segment data. **(B)** Representative labeled length-history plots.

Please see **pages 34 – 35** for the description and interpretations of the cluster profiles and length-history figures (**Figures S3.7 – S3.9**).

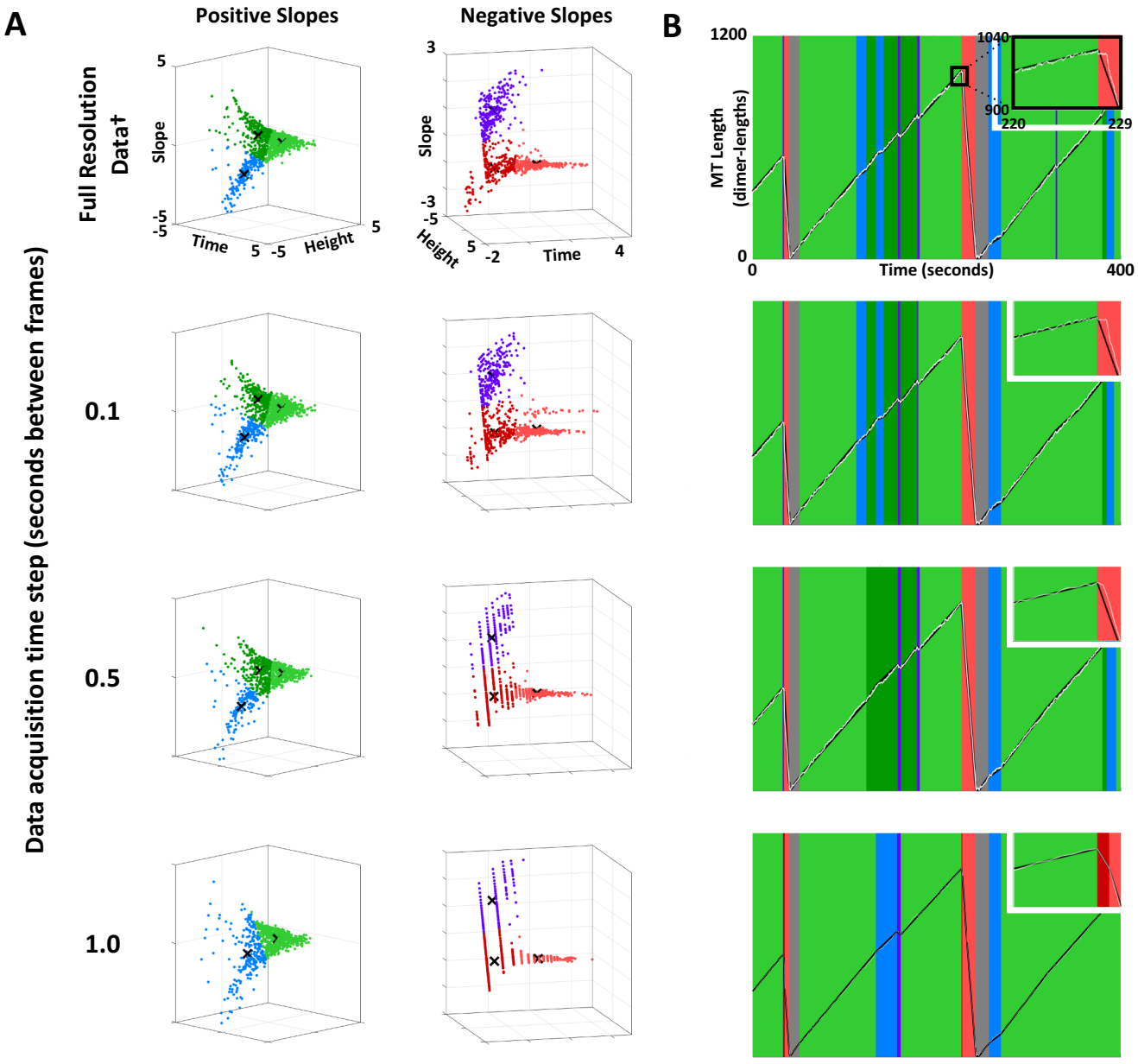

Figure S3.8. Classification results for the *in silico* data with varying data acquisition rates analyzed using **Minimum Segment Duration = 1.0 seconds** and Maximum Error Tolerance = 20 dimer-lengths. **(A)** Cluster profiles of positive and negative slope segment data. **(B)** Representative labeled length-history plots.

Please see **pages 34 – 35** for the description and interpretations of the cluster profiles and length-history figures (**Figures S3.7 – S3.9**).

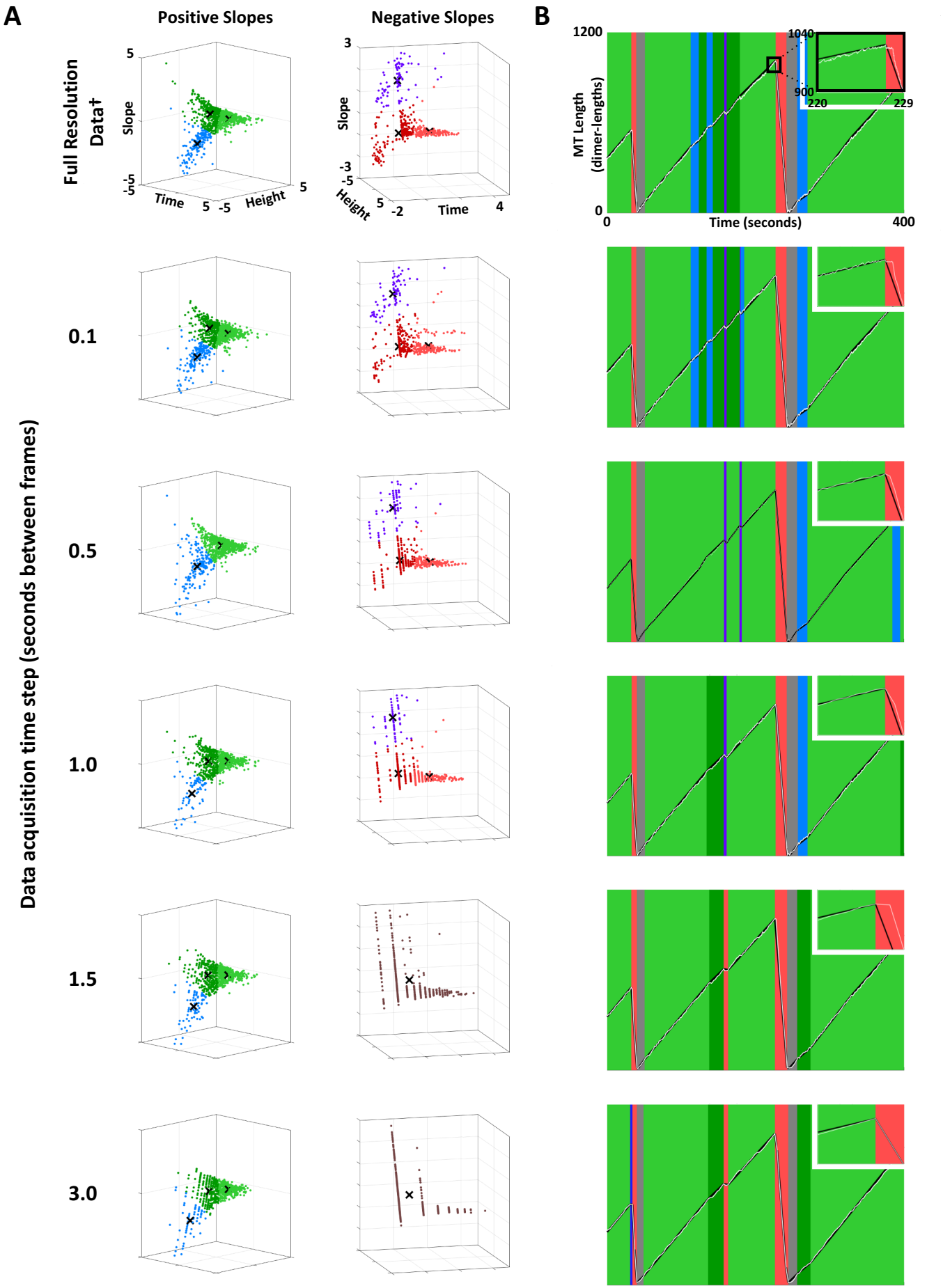

Figure S3.9. Classification results for the *in silico* data with varying data acquisition rates analyzed using **Minimum Segment Duration = 3.0 seconds** and Maximum Error Tolerance = 20 dimer-lengths. **(A)** Cluster profiles of positive and negative slope segment data. **(B)** Representative labeled length-history plots.

Please see **pages 34 – 35** for the description and interpretations of the cluster profiles and length-history figures (**Figures S3.7 – S3.9**).

Summary of Conclusions: Section S3, Data Acquisition Rate Sensitivity Analysis

The analyses in this section aid in answering the following question: do the main conclusions of this manuscript change when the temporal resolution of inputted length-history data is varied?

The results of these analyses indicate that the main conclusions of this manuscript are sound regardless of temporal resolution so long as the Data Acquisition Time Step and Minimum Segment Duration are sufficiently small. Based on the loss of density in the cluster profiles at slower data acquisition rates, we recommend using Data Acquisition Time Steps less than or equal to 0.5 seconds. This recommendation is also consistent with the Minimum Segment Duration results in **Supplemental Section S2**.

More specifically, the results of these analyses demonstrate that the detection of three clusters is upheld in the positive slope segment data for Data Acquisition Time Steps up to 3 seconds, and in the negative slope segment data for Data Acquisition Time Steps up to 1 second, assuming reasonable choices for Maximum Error Tolerance and Minimum Segment Duration. However, even when three clusters are detected, fewer of the shortest duration segments in the clusters of up/down stutters and brief growth/shortening are detected as the Data Acquisition Time Step and/or the Minimum Segment Duration increase. For example, detection of the particular stutter shown in the zoomed-in length-history plots is lost at Minimum Segment Durations of 1 second or greater (**Supplemental Figures S2.7-S2.9**).

Ultimately, though the configuration of clusters and the abundance of stutters are impacted by changing the acquisition rate of the input data, the analysis persists in identifying behaviors during which the MT length changes more slowly than during classically recognized growth and shortening phases. Thus, the detection of stutters is robust over a range of data acquisition rates.

Supplemental Section S4:

Negative Control: Simulations of a Two-State (Growth-Shortening) Model

Table of Contents

Summary

As a negative control, we ran STADIA on length-history simulation data from a model designed to have only two states: growth and shortening. In this two-state model, the traditional DI parameters (V_{growth}, V_{short}, F_{cat}, and F_{res}) are inputs into the model. This model simulates MT behavior at the scale of entire periods of growth and shortening, in contrast to our dimer-scale 13-protofilament model, which simulates individual dimer-scale biochemical reaction events and produces DI as an emergent behavior.

In the STADIA analysis of the two-state simulation data, we varied the values of the Minimum Segment Duration and the Maximum Error Tolerance, as well as the time between data points in the length-history data inputted into STADIA (see **Supplemental Sections S2 & S3** for results of varying these parameter values in the STADIA analysis of the datasets used in the main text). As discussed in the main text, the values of the Minimum Segment Duration and the Maximum Error Tolerance determine how closely the piecewise linear approximation produced by the segmentation stage of STADIA matches the length-history data inputted into STADIA.

The results show that STADIA does ***not*** identify clusters of up stutters or down stutters when analyzing the positive slope segments or the negative slope segments, respectively (**Figures S4.1, S4.2**). For data with relatively large time steps between data points (0.5 seconds or more), STADIA did identify a small number of flat stutters in rare cases where a time step between two consecutive data points happened to straddle a catastrophe or rescue in such a way as to produce a near-flat segment (one example in **Figure S4.3**, row D, right panel, orange bracket). However, the locations where such flat stutters were identified were *not* robust across different data acquisition time steps. Furthermore, these artifactual flat stutters were very short in duration and totaled to less than 0.09% of the total simulation time; this percentage is approximately two orders of magnitude smaller than the percent time spent in stutters in the dimer-scale 13-PF simulation data (see **Figures S1.9, S1.10**).

Below we provide more details about the two-state simulation method and the STADIA analysis of the two-state simulation data.

Two-state simulation method

In the two-state simulations, each microtubule grows from a stable seed and is assumed to be in either a growth state or a shortening state at each point in time. The traditional DI parameters are input parameters in the two-state model; this is in contrast to the dimer-scale 13-PF model, where the DI parameters are emergent properties resulting from dimer-scale biochemical reaction events and are measured from the length-history data outputted by the simulation.

To generate the two-state length-history data, the DI parameter values measured from the "classical" analysis of the dimer-scale 13-PF simulation data (first row of **Table 1**) were used as the values of the inputted DI parameters in the two-state simulations. The time duration of each growth segment (i.e., the time from the start of a growth segment until a catastrophe) was sampled from an exponential distribution with rate parameter of F_{cat} = 0.659 min^{-1}. The slope or growth velocity (V_{growth}) of each growth segment was sampled from a normal distribution with mean of 46.1 nm/s and standard deviation of 5.1 nm/s. The height change of each growth segment was calculated as the sampled time duration multiplied by the sampled slope.

Similarly, the time from the beginning of a shortening segment until a potential rescue was sampled from an exponential distribution with rate parameter of F_{res} = 2.483 min^{-1}. The slope or shortening velocity (V_{short}) of each shortening segment was sampled from a normal distribution with mean of 540.0 nm/s and standard deviation of 47.9 nm/s. The height change of each shortening segment was calculated as the sampled time duration multiplied by the sampled slope. If this calculated height change would result in the MT length becoming negative, then the sampled segment was truncated so that the depolymerization would terminate when the MT length reached zero. In this case, the actual time duration of the segment was less than, not equal to, the sampled time until a potential rescue; then, the actual time duration was calculated from the sampled slope and the height change from the start of the shortening segment until the MT length reached zero.

One MT was simulated for 10 hours of simulation time, chosen to produce a comparable amount of data as the dimer-scale 13-PF simulation. To generate the length-history data to input into STADIA, the raw length-history data from the two-state simulation were interpolated to have a fixed data acquisition rate ("frame" rate) of 20 fps, 2 fps, or 1/3 fps. As in **Supplemental Section S3**, 'data acquisition rate in frames per second' = 1/'Data Acquisition Time Step in seconds'.

Main results and conclusions of STADIA analysis of the two-state simulation data

The results of the STADIA analysis of the two-state simulation data are shown in **Figures S4.1-S4.3**. In these figures, the values of the Data Acquisition Time Step of the inputted length-history data, as well as the Minimum Segment Duration and Maximum Error Tolerance used in the STADIA analysis, are indicated above each row. The clustering results for the positive and negative slope segments are shown in **Figures S4.1** and **S4.2**, respectively. Specifically, **Figures S4.1** and **S4.2** provide the gap statistic plots (used to inform the optimal *k*-value, i.e., number of clusters), cluster profiles plotted in the log-transformed and standardized feature space, and box plots of the segment features (time duration, height change, and slope) for each cluster. The clusters identified in **Figures S4.1** and **S4.2** are applied to label the length-history plots in **Figure S4.3.**

Depending on the values of the indicated parameters (Data Acquisition Time Step, Minimum Segment Duration, and Maximum Error Tolerance), the gap statistic plots suggest k=1 or k=2 in almost all cases (**Figures S4.1, S4.2**; the one exception is in **Figure S4.2 D** where the gap statistic plot is monotonically increasing and therefore has no clear local maximum to suggest a *k*-value). These results differ from the k=3 result that was observed for the dimer-scale 13-PF simulation data (positive and negative slope segments) and the *in vitro* data (positive slope segments) (**Figures S1.4, S1.5**).

Furthermore, the 3-dimensional segment feature plots for the two-state simulation data (second column of **Figures S4.1, S4.2**) show a cloud of points with no distinct appendages, thus supporting the k=1 selection; however, the cloud is oblong, which could support k=2. In contrast, the 3 appendages visible in the segment feature plots from the dimer-scale 13-PF simulation data and the positive slope segments of the *in vitro* data support the selection of k=3 for those datasets (**Figures 4 A,B,D, S1.4, S1.5**).

Significantly, in the two-state simulation data, no clusters of shallow-slope segments that would correspond to stutters were detected in any cases (see slope box plots in the fifth column of **Figures S4.1, S4.2**). In contrast, for the dimer-scale 13-PF simulation data and the *in vitro* data, stutter clusters were detected in all cases, and their slopes distinguished them from the other clusters (this held even for the incomplete *in vitro* negative slope data with k=2) (**Figures 4 A-F, S1.8**).

The labeled length-history plots also aid in illustrating the conclusion that the two-state simulation data (**Figure S4.3**) lack the complexity of the behaviors present in the dimer-scale 13-PF simulation data and the *in vitro* data (**Figures 4 G,H, 5 D-I, 6, 7 D-I**).

In conclusion, STADIA did not detect any clusters of up or down stutters in the two-state simulation data. Although STADIA did detect a few flat stutters, the locations of these artifactual flat stutters were not reproduced across different Data Acquisition Time Steps (see next page). These two-state model results contrast the robust detection of stutters in the dimer-scale 13-PF simulation data and the *in vitro* data (see **Supplemental Sections S2 & S3** for parameter sensitivity analyses testing robustness). Thus, comparison with the two-state simulation data demonstrates that the stutters observed in the dimer-scale 13-PF simulation data and the *in vitro* data are not artifacts produced by STADIA.

Additional discussion

Flat stutters: As discussed in the main text, STADIA identifies near-zero slope segments called flat stutters before performing the clustering step separately on the remaining positive and negative slope segments. In the two-state simulation data at 20 fps (0.05 s between data points), no flat stutters were identified. At 2 fps (0.5 s between data points), STADIA identified 26 flat stutters, of which 25 had a time duration of 0.5 s and one had a time duration of 1.5 s; these time durations total to 14 s, which is approximately 0.039% of the total 10-hour simulation time. At 1/3 fps (3 s between data points), STADIA identified 10 flat stutters, all with a time duration of 3 s, totaling to 30 s or approximately 0.083% of the total time. The segments identified as flat stutters occurred in the rare cases when a time step between two consecutive data points in the data with an imposed fixed frame rate happened to straddle a catastrophe or rescue from the original raw data in a way that produced a near-flat segment (one example in **Figure S4.3**, compare right panel of row D to right panels of the other rows). Furthermore, none of the flat stutters detected at 1/3 fps overlapped with any of the flat stutters detected at 2 fps.

Brief and sustained growth/shortening: Examination of time duration alone could create the appearance that the brief and sustained clusters of growth or shortening in the two-simulation data (**Figures S4.1, S4.2** in cases with k=2) are equivalent to the brief and sustained clusters identified in the dimer-scale 13-PF simulation data and the *in vitro* data (**Figure S1.8 B,D**). However, the brief and sustained clusters in the two-state simulation data are essentially indistinguishable in slope (fifth column of **Figures S4.1, S4.2**). In contrast, in the dimer-scale 13-PF simulation data and the *in vitro* data, the brief and sustained clusters have noticeably different distributions of slopes (**Figure S1.8 A,C**); furthermore, most segments in the brief growth/shortening clusters have steeper slopes than any segments in the sustained clusters, suggesting that the faster velocities are sustainable for long time periods (**Figure S1.8**). Thus, while the two-state model reasonably approximates the time duration differences between brief and sustained clusters, the two-state model's sampling of slopes from normal distributions fails to replicate the more complex distributions of slopes that are present in each of these clusters in the dimer-scale 13-PF simulation data and the *in vitro* data.

Negative slope segment feature plots: It is interesting to note that the 3-dimensional segment feature plots for the negative slope segments at long Data Acquisition Time Steps and long Minimum Segment Durations appear similar in the two-state simulation data (**Figure S4.2,** rows D,E, second column) and in the dimer-scale 13-PF simulation data (**Figure S3.9**, bottom tow rows). However, at higher temporal resolutions, the negative slope profiles for the two-state model (**Figure S4.2,** rows A-C, second column) are clearly different from the negative slope profiles for the dimer-scale 13-PF simulation data (**Figures S2.5, S3.7, S3.8,** and first four rows of **S3.9**) and the *in vitro* data (**Figure S2.6**). These observations demonstrate that performing data acquisition and analysis with long time steps can produce the appearance of some similarities between the two-state simulation data and the dimer-scale 13-PF simulation data. However, the positive slope profiles from the two-state model (**Figure S4.1,** second column) are consistently different from the positive slope profiles for the dimer-scale 13-PF simulation data (**Figures S2.5, S3.7, S3.8, S3.9**) and the *in vitro* data (**Figure S2.6**).

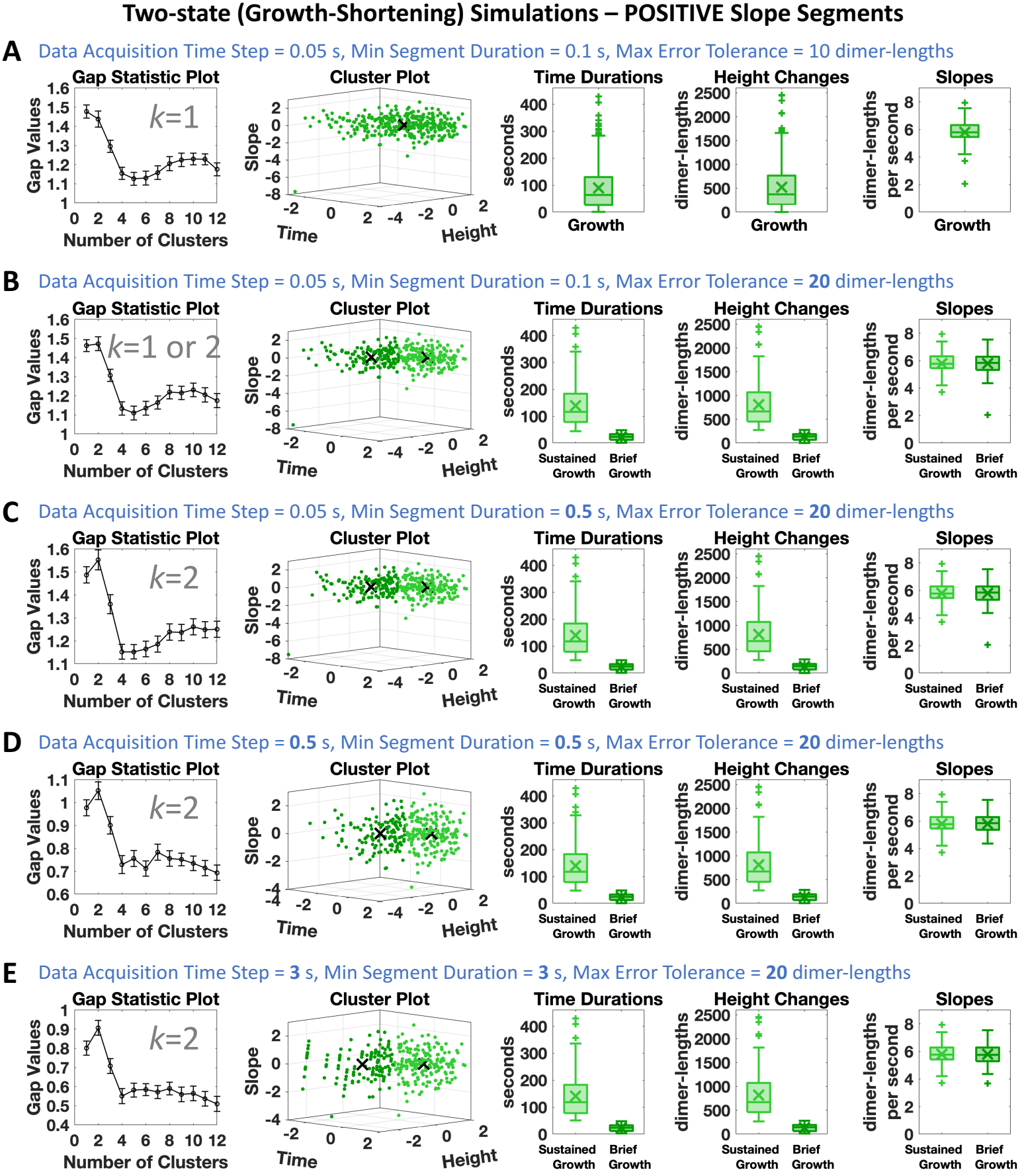

Figure S4.1. Negative Control: STADIA analysis of *positive* slope segments from the two-state (growth-shortening) model. From top (row A) to bottom (row E), the piecewise linear approximation to the original raw length-history data becomes coarser as the parameter values in the row headings are varied (values altered from the top row are in bold). In the resulting gap statistic plots, the first local maximum indicates either k=1 (row A) or k=2 (rows B,C,D,E). For the cases where k=2, the slopes of the two clusters are indistinguishable. No cluster with shallower slopes (i.e., no cluster of up stutters) is detected in the positive slope segments. In row B, the first local maximum at k=2 is not conclusively larger than the gap value at k=1 when considering the error bars; k=2 was chosen for use in the cluster profiles and box plots to demonstrate that even when allowing two clusters, the two clusters do not differ in slope. Please see **pages 40-43** for additional information and interpretations.

Two-state (Growth-Shortening) Simulations – NEGATIVE Slope Segments

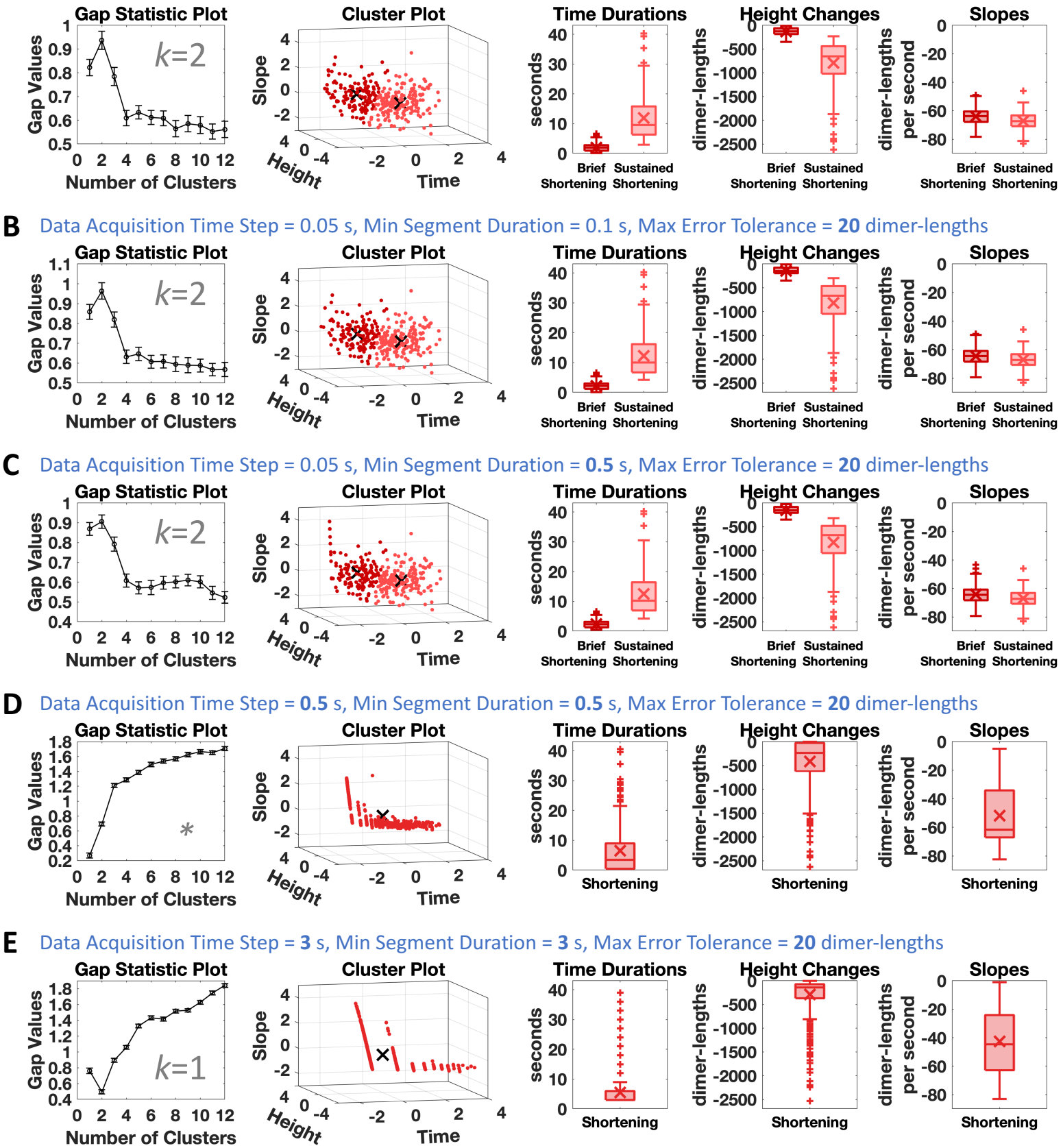

Figure S4.2. Negative Control: STADIA analysis of *negative* slope segments from a two-state (growth-shortening) model. The parameter values in the row headings are the same as in **Figure S4.1** (values altered from the top row are in bold). In the resulting gap statistic plots, the first local maximum indicates either k=1 (row E) or k=2 (rows A,B,C), or the gap statistic plot is generally increasing with no clear local maximum (*, row D, k=1 was used for displayed clustering and box plots). For the cases where k=2, the slopes of the two clusters are nearly indistinguishable. No cluster with shallower slopes (i.e., no cluster of down stutters) is detected in the negative slope segments. Please see **pages 40-43** for additional information and interpretations.

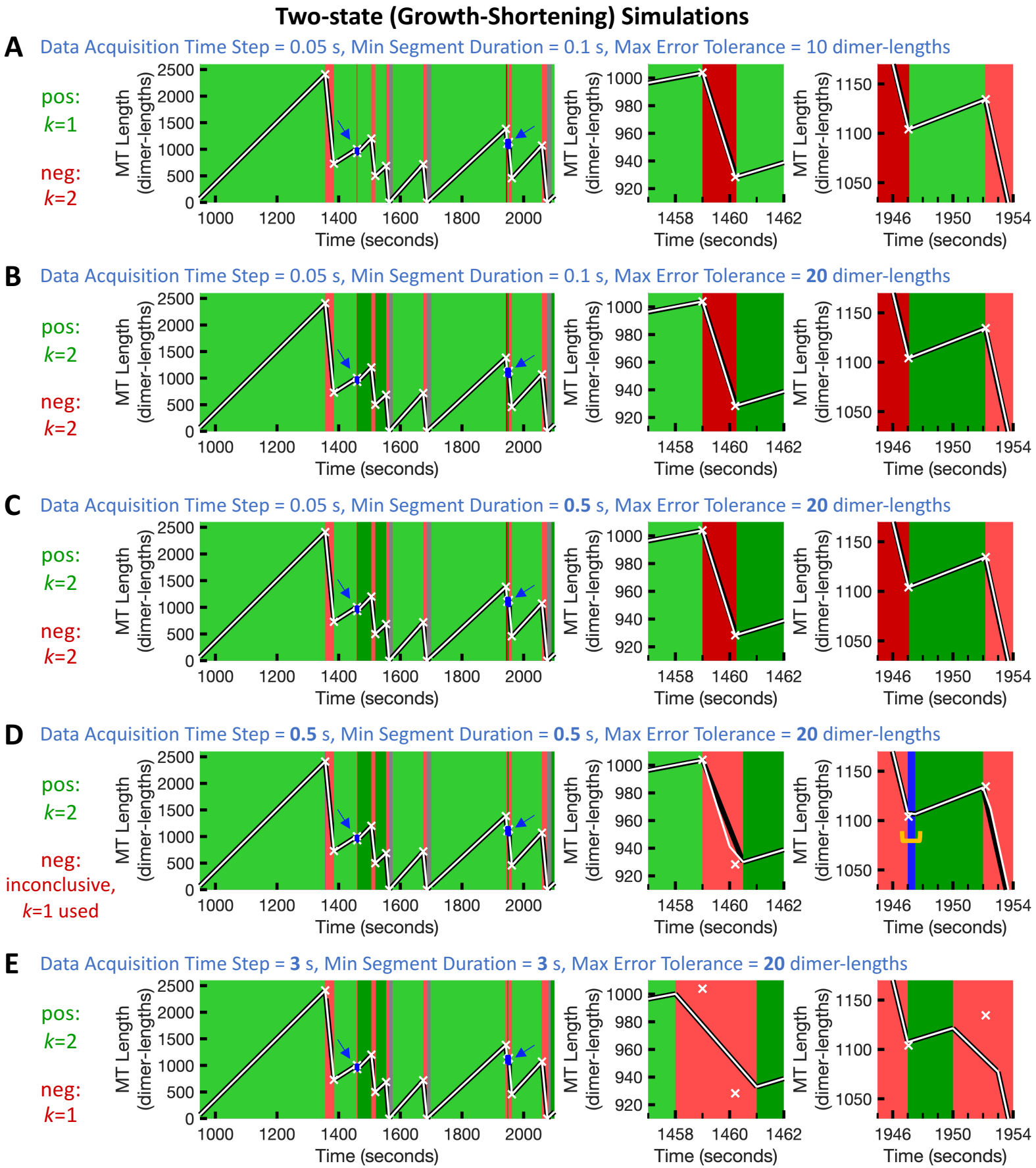

Figure S4.3. Negative Control: labeled length-history plots from STADIA analysis of two-state (growth-shortening) simulation data. The parameter values in the row headings are the same as in **Figures S4.1** and **S4.2** (values altered from the top row are in bold). The numbers of clusters (*k*-values) were determined from the gap statistic plots in **Figures S4.1** and **S4.2** The white x-symbols mark the exact points of the transitions (catastrophes, rescues, and complete depolymerizations to the seed) in the raw two-state simulation data (same points in all rows). The white lines show the length-history data inputted into STADIA after the indicated data acquisition rate was imposed. The black lines represent the STADIA piecewise linear approximation. The small blue rectangles (with the blue arrows) in the first column demarcate the regions shown in the zoomed-in plots in the second and third columns. The orange bracket in row D, third column, indicates a rare artifactual detection of a flat stutter. Please see **pages 40-43** for additional information and interpretations.